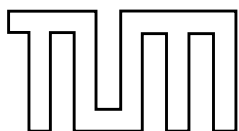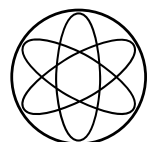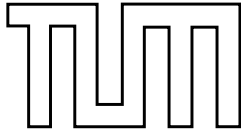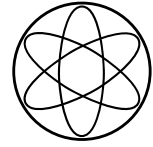# Phases of QCD

by

Simon Rößner

Technische Universität München

Technische Universität München

Physik Department
Institut für Theoretische Physik T39
Univ.-Prof. Dr. Wolfram Weise

Phases of QCD

Dipl.-Phys. (Univ.) Simon Rößner

Vollständiger Abdruck der von der Fakultät für Physik der Technischen Universität München zur Erlangung des akademischen Grades eines

Doktors der Naturwissenschaften (Dr. rer. nat.)

genehmigten Dissertation.

Vorsitzender: Univ.-Prof. Dr. Stephan Paul

Prüfer der Dissertation:

1.   Univ.-Prof. Dr. Wolfram Weise

2.   Univ.-Prof. Dr. Andrzej J. Buras

Die Dissertation wurde am 18.03.2009 bei der Technischen Universität München eingereicht und durch die Fakultät für Physik am 09.04.2009 angenommen.

Summary

Quantum Chromodynamics (QCD) is the theory of the strong interaction within the Standard Model of elementary particles. Today's research in this area dedicates substantial resources to numeric solutions of the QCD field equations and experimental programs exploring the phases of QCD. This thesis proceeds along a complementary line — that of modelling QCD, with the aim of identifying its dominant degrees of freedom. This is possible by minimally coupling effective potentials for the Polyakov loop to Nambu-Jona-Lasinio models using temporal background fields to model chiral symmetry breaking respecting colour confinement. The fermion sign problem resulting from the minimal coupling is addressed in this work establishing a novel, systematically ordered approach. The modifications to the approximative order parameter of colour confinement, the Polyakov loop, are in direct connection with the fermion sign problem. Furthermore an effective coupling of quark densities of different flavours is induced. This mechanism, most likely also present in QCD, produces finite contributions to flavour off diagonal susceptibilities. Susceptibilities are amongst the most promising physical quantities for the experimental exploration of the phase transition at high temperatures and densities.

Zusammenfassung

Die Quantenchromodynamik (QCD) ist die Eichtheorie der starken Wechselwirkung im Rahmen des Standardmodells der Elementarteilchen. Die aktuellen Forschung auf dem Gebiet verwendet beachtliche Ressourcen zur numerischen Lösung der QCD-Feldgleichungen und in experimentellen Programmen zur Untersuchung der Phasen der QCD. In dieser Doktorarbeit wird ein komplementärer Weg beschritten — die Modellierung der QCD mit dem Ziel, die dominanten Freiheitsgrade der QCD zu identifizieren. Durch die minimale Kopplung effektiver Potentiale für die Polyakov-Schleife an Nambu-Jona-Lasinio Modelle mittels zeitlicher Hintergrundfelder ist es möglich, die spontane chirale Symmetriebrechung zu modellieren und dabei Effekte des Farbconfinements zu berücksichtigen. Das aus der minimalen Kopplung resultierende "Fermion Sign Problem" (FSP) wird in dieser Arbeit mittels einer neuartigen, systematisch geordneten Methode behandelt. Die Modifikationen, die der approximative Ordnungsparameter für das Farbconfinement (die Polyakov-Schleife) erfährt, stehen in direkter Verbindung mit dem FSP. Desweiteren wird eine effektive Kopplung der Quarkdichten mit unterschiedlichen Flavours induziert. Dieser Mechanismus, der vermutlich auch in der QCD präsent ist, erzeugt Beiträge zu Flavour-abhängigen Suszeptibilitäten. Suszeptibilitäten zählen zu den vielversprechenden physikalischen Größen in der experimentellen Erforschung des Phasenübergangs bei hohen Temperaturen und Dichten.

Contents

Introduction

Modern physics classifies the interactions of particles into four groups: gravitation, electro-magnetic, weak and strong. Aside from the gravitational force, the remaining interactions of particles are described by a widely accepted theory called the Standard Model of particle physics. Within this Standard Model the strong interaction takes a special position, as it can be considered as an individual theory, which can be detached from the rest of the Standard Model. It was developed independently of the Standard Model and referred to as Quantum Chromodynamics (QCD). The definition of the strong forces via the Standard Model leads to the finding that there are quite some phenomena in our every day world that are governed by this fundamental interaction. The interaction of nucleons (neutrons and protons) and the formation of nuclei is governed by the strong force. But also the formation of nucleons themselves is driven by the strong force. In QCD nucleons are no fundamental particles but the outcome of the dynamics of QCD and its fundamental incrediences, which are quarks and gluons.

Interestingly the energies needed to break up the nucleon compound at high temperatures almost correspond to its rest mass. The remaining fragments (quarks and gluons) are highly relativistic possessing a rest mass of only a small fraction of the total available energy. The inverse process, the formation of nucleons from quarks, has to be seen as the origin of the vast majority of mass we are experiencing in our every day lives. This transition from quarks and gluons to hadrons happened shortly after the "Big Bang". For this type of problems it is not adequate to consider individual particles. The large number of individual degrees of freedom can only be discribed statistically. In such an ensemble of particles the focus has to shift to bulk properties, i.e. statistical properties of matter, supplying a description requiring only few relevant degrees of freedom.[1] Of course, it is in the end the microscopic interactions of the individual particles that determine the behaviour of bulk matter. All properties of bulk material can only depend analytically on microscopic degrees of freedom.

In the limit of infinitely many particles, changes of bulk properties may happen non-analytically. The instantaneous, non-analytic change of bulk properties is understood in terms of phase transitions. Control parameters that allow to distinguish two phases by their non-analytic behaviour are called order parameters. The qual-

---

[1] In classic approximation the particle energies follow a Boltzmann statistic, in quantum theory we find a Bose-Einstein distribution for bosons and a Fermi-Dirac distribution for fermions of the particle energies.

itative difference in the microscopic and macroscopic descriptions is related to the process of decoherence which happens on some unknown scale. This yet unsolved problem will not be subject to the discussion in this work. The connection of the bulk properties represented by an order parameter with a microscopic symmetry may grant important insight into the dynamics of the system. On microscopic scales it is the internal symmetries that distinguish two distinct thermodynamic phases, while at the macroscopic scale it is the thermal expectation value of the order parameter. The way how order parameters change across a phase transition line determines what we call the order of the phase transition. As mentioned above QCD is able to explain very different phenomena at different energy scales, which hints towards the presence of various phases.

This thesis uses a model approach to mimic the dynamics of QCD. One important application of this model, the so-called Polyakov loop extended Nambu and Jona-Lasino (PNJL) model, is the investigation of the phase transitions of QCD. Using such a model some outstanding phenomena generated by the dynamics of QCD can be followed in the regime of the phase transition.

Outline

Chapter 1 gives a brief introduction to Quantum Chromodynamics (QCD). We focus on those aspects of QCD which are most important for the thereafter presented work. These are chiral and flavour symmetries addressed in Sec. 1.1.1 and 1.1.2. Furthermore aspects of confinement, namely the $Z(3)$ centre-symmetry of $SU(3)_\mathrm{c}$, are discussed in Sec. 1.2.3. The general field theoretic treatment of finite temperatures and densities are in the focus of Sec. 1.2.1. Chapter 1 closes with a presentation of different ways of addressing QCD and an overview of the phase diagram in Secs. 1.3 and 1.4.

Chapter 2 approaches the centre of this thesis: models for the thermodynamics of QCD. After a short introduction to the topic of models (see Sec. 2.1) we concentrate on the foundations of the Polyakov loop extended Nambu and Jona-Lasinio (PNJL) model, introducing the Nambu and Jona-Lasinio (NJL) model and the Polyakov loop model in Secs. 2.2 and 2.3. Sec. 2.4 works out several interesting issues arising in the process of extending the NJL model by introducing Polyakov loop dynamics. Chapters 1 and 2 present a brief and compact sketch of important aspects of QCD. For further elaboration the reader is referred to the textbooks [TW, PS, LB].

The brief introduction and overview of QCD thermodynamics in chapters 1 and 2 is followed by a novel contribution to this field. First in Sec. 3.1 the model used, the PNJL model, is specified. Subsequently the aspects of confinement in the PNJL model are investigated. Both the influence of the modelled confinement on thermodynamic properties and on mesons in random phase approximation are studied on a quantitative basis. Unfortunately this implementation of confinement does not completely circumvent unphysical meson decays into quark-antiquark pairs. Nevertheless several model independent quantities of interest to the scientific community can be investigated without falling short. Most of these quantities are directly derived from the modelled equation of state (Sec. 3.3). On the one hand the results

may be used for predictions on fireball evolution (speed of sound) or the investigation of critical phenomena in the phase diagram of QCD (cumulants of the pressure with respect to various chemical potentials). On the other hand the PNJL model can be benchmarked comparing details of the equation of state with other calculations (e. g. QCD on the lattice). The extraction of the phase diagram of QCD in Sec. 3.4 requires further extrapolating steps. Some quantities like the position of the critical point can therefore only be investigated on a qualitative level. Quantitative results turn out to depend sensitively on the physical input used to adjust model parameters.

Without further input from QCD the PNJL model can be extended by isovector quantities (see Sec. 3.6). Some of the benchmarking using pressure and moments of the pressure is repeated using this generalised model. The calculations presented in this work do not include terms that break the symmetry of up- and down-quarks explicitly. Nevertheless the PNJL model exhibits non-vanishing isovector quantities, such as susceptibilties. This phenomenon which at first glance seems contradictory can be explained by the dynamics of Polyakov loop degrees of freedom. The presentation of the mechanism at work in the PNJL model closes this chapter.

Chapter 1

Quantum Chromodynamics

Quantum Chromodynamics (QCD) is considered to be the theory that correctly describes the nature of strongly interacting matter even beyond the energy regime accessible in today's experiments. Among others the observation of asymptotic freedom in high energy collisions of protons has most strongly supported that QCD has been accepted as the correct description of nature. In the low energy regime where the vacuum and its hadronic excitations have been studied experimentally it is the observed symmetries and symmetry breaking patterns that support QCD as the theory of the strong interaction. The different behaviour of matter at low and high energies leads one to expect that QCD has a rich phase structure. One of the main objectives of this thesis is to contribute to the exploration of the QCD phase structure.

The current chapter summarises those features of Quantum Chromodynamics (QCD) that are of mayor importance to the following discussions. For more detailed exposition of this theory we refer to other publications [AL73, PS, TW]. As modern quantum field theories like QCD are built on a framework of symmetries the introductory part of this thesis uses them as a guiding principle. The role of a symmetry in a quantum field theory is determined first of all by its nature which can be local or global. Local symmetries (also called gauge symmetries) take the most outstanding position in the symmetry framework (see Sec. 1.1). Global symmetries essential to QCD are the chiral symmetry discussed in Sec. 1.1.1 and the flavour symmetry discussed in Sec. 1.1.2. The centre symmetry of the gauge group turns out to be very useful in the discussion of the phase structure of QCD. Sec. 1.2.3 is dedicated to this sub-symmetry of the gauge symmetry.

The QCD Lagrangian density is given by

$$
\begin{aligned}
\mathcal{L}_{\text{QCD}} &= \mathcal{L}_{\text{quark}} &&+ \mathcal{L}_{\text{mass}} &&+ \mathcal{L}_{\text{glue}} \\
&= \bar{\psi}\,(i\gamma^\mu D_\mu)\,\psi &&- \bar{\psi}\,m\,\psi &&- \tfrac{1}{2}\text{tr}_{\text{c}}\,(G^{\mu\nu}G_{\mu\nu})\ .
\end{aligned}
\tag{1.1}
$$

Here ψ represent the quark fields which are fields in Dirac-, colour- and flavour space. An essential element is the covariant derivative

$$
D^\mu = \partial^\mu - i\,g\,A^\mu
\tag{1.2}
$$

as it couples the quark and gluon sectors of this Lagrangian. Here the fields $A^\mu = \sum_{a=1}^{N_c^2-1} t_a A_a^\mu$ are the gauge or gluon fields. Empirical data, e. g. for branching ratios,

determine $N_c = 3$. The $N_c^2 - 1 = 8$ fields A_a^μ give the contributions of each generator of the SU(3)$_c$ (colour) gauge group. From now on we would like to simplify notations by extending the Einstein summation convention to colour and flavour indices. The generators of the SU(3)$_c$-group t_a obey the commutation rule $[t_a,\, t_b] = i f_{abc}\, t_c$, where f_{abc} are the totally antisymmetric structure constants of SU(3)$_c$. We will use the representation named after Gell-Mann thoughout this work. Its explicit form can be found in many textbooks such as [PS, TW]. The presence of the mass term in the Lagrangian $\mathcal{L}_{\text{mass}}$ is essential for QCD dynamics as it is the only term breaking the chiral symmetry explicitly (see Sec. 1.1.1). Finally the quantity

$$G^{\mu\nu} = t_a\, G_a^{\mu\nu} = \frac{i}{g}\, [D^\mu,\, D^\nu] \tag{1.3}$$

is the field strength tensor generated by the gluon fields. As for non-Abelian symmetries the commutator of two generators do not vanish, $\mathcal{L}_{\text{glue}}$ introduces a self interaction of the gauge fields which is closely related to colour confinement.

1.1 Symmetries of QCD

The backbone of a modern quantum field theory is its gauge symmetry. In case of QCD we have to deal with SU(3)$_c$. By definition, a gauge symmetry is a local symmetry meaning that all symmetry transformations at each individual space-time point are independent. Gauge transformations of the quark and gluon fields can be written as

$$\psi \longrightarrow \tilde{\psi} = U(x)\psi \qquad A_\mu(x) \longrightarrow \tilde{A}_\mu(x) = U(x)\left(A_\mu(x) + \frac{i}{g}\right)U(x)^{-1}\ , \tag{1.4}$$

where $U(x)$ is an element of SU(3)$_c$ with an arbitrary space-time dependence. At finite temperatures this arbitrary space-time dependence will be limited due to the choice of boundary conditions (see Sec. 1.2).

1.1.1 Chiral symmetry

In the limit of vanishing quark masses, i. e. if $\mathcal{L}_{\text{mass}}$ in Eq. (1.1) is not present the Lagrangian density of QCD, $\mathcal{L}_{\text{QCD}}$ breaks up into two independent identical pieces. These two pieces can be obtained by separating right (left) handed quark fields ψ_R (ψ_L) where these chiral quark fields are defined by

$$\psi_{R/L} = \mathcal{P}_{R/L}\,\psi = \tfrac{1}{2}\left(\mathbb{1} \pm \gamma_5\right)\psi\ . \tag{1.5}$$

Therefore the QCD Lagrangian in the chiral limit features an $SU(N_f)_R \times SU(N_f)_L$ symmetry which can be recast into the form of a vector and an axial vector symmetry $SU(N_f)_V \times SU(N_f)_A$.

Finite quark masses break the symmetry of right and left handed quarks as the mass term $\mathcal{L}_{\text{mass}}$ in Eq. (1.1) mixes right and left handed quarks:

$$\bar{\psi}\, m\, \psi = \bar{\psi}_R\, m\, \psi_L + \bar{\psi}_L\, m\, \psi_R\ . \tag{1.6}$$

In nature it is observed however that the axial symmetry is broken while the vector symmetry remains almost unbroken. This is explained in the QCD framework by the appearance of spontaneous symmetry breaking (χSSB):

$$SU(N_{\text{f}})_{\text{R}} \times SU(N_{\text{f}})_{\text{L}} \xrightarrow{\chi\text{SSB}} SU(N_{\text{f}})_{\text{V}} \; . \tag{1.7}$$

Firstly spontaneous chiral symmetry breaking is discussed in the chiral limit, i. e. in the absence of explicit symmetry breaking mass terms in the QCD Lagrangian. If spontaneous chiral symmetry breaking does not occur we expect the vacuum to be "empty", meaning that there is no charge operator with a finite vacuum expectation value. As mentioned above the breaking of the axial symmetry is observed to be much stronger than the breaking of the vector symmetry. We define i-flavoured vector and axial vector current operators by

$$V_i^\mu = \bar\psi \, \gamma^\mu \tfrac{\lambda_i}{2} \, \psi \qquad\qquad \text{and} \qquad\qquad A_i^\mu = \bar\psi \, \gamma^\mu \gamma_5 \tfrac{\lambda_i}{2} \, \psi \; . \tag{1.8}$$

The vacuum expectation values of the vector and axial charge density correlation functions of the vacuum in the unbroken phase[1] should therefore vanish:

$$\langle 0 | V_i^{0\dagger} V_i^0 | 0 \rangle = \langle 0 | A_i^{0\dagger} A_i^0 | 0 \rangle = 0 \; . \tag{1.9}$$

It is observed in the meson spectra that the pseudoscalar and vector mesons appear at lower energies than their scalar and axialvector partners. In the discussed idealised chiral limit we conclude that in the spontaneously chiral broken phase

$$\langle \Omega | V_i^{0\dagger} V_i^0 | \Omega \rangle = 0 \qquad\qquad \text{whereas} \qquad\qquad \langle \Omega | A_i^{0\dagger} A_i^0 | \Omega \rangle \neq 0 \; , \tag{1.10}$$

which implies $A_i^0 | \Omega \rangle \neq 0$. This is the statement that the vacuum of spontaneously broken chiral symmetry now carries a non-zero axial charge density.[2] If the vacuum expectation value of $\left[A_i^\mu(x), \, A_j^\nu(y) \right]$ is evaluated one finds

$$\langle \Omega | \left[A_i^\mu(x), \, A_j^\nu(y) \right] | \Omega \rangle = -\tfrac{1}{4} g^{\mu\nu} \delta^4(x - y) \langle \Omega | \bar\psi \left\{ \lambda_i, \, \lambda_j \right\}_+ \psi | \Omega \rangle \; . \tag{1.11}$$

In the chiral limit this expectation value can only be non-zero once the anticommutator on the right hand side is diagonal. This implies that $i = j$. We conclude that a condensate of the form $\langle \bar\psi_i \psi_i \rangle \neq 0$ with i labelling all flavours is a necessary condition for a non-vanishing axial charge in the chiral limit.[3] The fact that the axial current does not annihilate the Nambu-Goldstone vacuum state $| \Omega \rangle$ implies the existence of a new particle. The operator $Q_i^{\text{A}} = \int \text{d}^3 x \, A_i^0(x)$, which generates such a particle, is the axial charge operator. The particles generated by the axial charge operator $Q_i^{\text{A}} | \Omega \rangle$ in the Nambu-Goldstone phase are called Goldstone bosons. In the chiral limit, i. e. in the absence of explicit symmetry breaking terms these

---

[1]The vacuum $|0\rangle$ in the unbroken phase is also called Wigner-Weyl phase or perturbative vacuum.

[2]The vacuum state $|\Omega\rangle$ implements the Nambu-Goldstone realization of the chiral symmetry.

[3]With finite current quark masses this conclusion is no longer necessary but sufficient if we allow for different values of $\langle \bar\psi_i \psi_i \rangle \neq 0$ for different flavours i.

bosons are necessarily massless. As the existence of the Goldstone boson state is part of the vacuum properties, it must not interfere with the Lorentz invariance. Thus the axial current operator A_i^μ is proportional to the only covariant quantity available which is the 4-momentum density of the Goldstone boson, and the mass of Goldstone bosons has to vanish $m_{\text{GB}}^2 = 0$.

Once chiral symmetry is explicitly broken by non-zero current quark masses equal for all flavours the divergence of the vector current still vanishes, while the divergence of the axial current does not. Using the Dirac equation we find

$$\partial_\mu V_i^\mu = \bar{\psi}\, i\overset{\leftrightarrow}{\slashed{\partial}}\tfrac{\lambda_i}{2}\,\psi \qquad = \bar{\psi}\,\tfrac{i}{2}m_q\,[\mathbb{1},\,\lambda_i]\,\psi \qquad\qquad\qquad = 0 \qquad (1.12)$$

$$\partial_\mu A_i^\mu = \bar{\psi}\, i\overset{\leftrightarrow}{\slashed{\partial}}\gamma_5\tfrac{\lambda_i}{2}\,\psi \qquad = \bar{\psi}\,\tfrac{i}{2}m_q\gamma_5\,\{\mathbb{1},\,\lambda_i\}_+\,\psi = i\,m_q\,\bar{\psi}\,\gamma_5\lambda_i\,\psi \qquad \neq 0\ . \qquad (1.13)$$

Now axial charge is carried not only by the vacuum ground state but also by quarks. As quark operators are involved in the construction of the axial charge operator Q_i^{A} Goldstone bosons can no longer be generated from the vacuum without generating massive quarks. The massless Goldstone boson field is being mixed with massive particle fields such that pure Goldstone bosons no longer exist. Amongst the pseudoscalar mesons it is primarily the (massive) pion that carries Goldstone boson character. Therefore the pion is usually referred to as the Goldstone boson of spontaneous chiral symmetry breaking in QCD. The Gell-Mann-Oakes-Renner relation [GMOR68] which allows to determine the pion mass to lowest order using the chiral expansion is discussed in the next section 1.1.2.

1.1.2 Flavour symmetry

To lowest order one can consider up, down and strange quarks as light quarks while charm, top and bottom are heavy. In the chiral limit as lowest order approximation, up, down and strange quark are considered massless, while the other three quarks are not considered at all, as they are too heavy to be excited. In this approximation the flavour symmetry $SU(3)_{\text{f}}$ is exact.[4] Quarks with different masses are able to explain the mass differences within the meson octet as explicit chiral symmetry breaking is now flavour dependent. The quark content of the meson states which are superimposed quark-antiquark states of different flavours determine the mass differences. The mechanism generating meson masses is demonstrated here only in the simplest case where the strange quark mass is finite and large compared to up and down quark mass, i. e. we reduce $SU(3)_{\text{f}}$ to $SU(2)_{\text{f}}$.

Finite but small up and down quark mass do modify the Goldstone boson state. Nevertheless the pion state still carries most of the Goldstone boson character. Let the pion state be normalised, such that $\langle\pi_a(p)|\pi_b(p')\rangle = 2\,E_p\delta_{ab}(2\pi)^3\delta^3(\vec{p}-\vec{p}')$. Then the Goldstone boson contribution to the pion state can be projected out using the state $A_a^\mu(x)|\Omega\rangle$ generated from the vacuum. As $A_a^\mu(x)|\Omega\rangle$ is a covariant quantity the matrix element $\langle\Omega|A_a^\mu(x)|\pi_b(p)\rangle$ has to be proportional to the pion momentum p^μ

---

[4]In nature one observes however a meson octet of similar masses while a single meson exists at higher energies. In the QCD framework this can be understood in the context of an anomalously broken global $U(1)_{\text{A}}$, which is part of the chiral $SU(3)_{\text{R}} \times SU(3)_{\text{L}}$ symmetry.

which is the only covariant structure available. Furthermore flavour and momentum conservation allows to define the strength of the matrix element, which is called pion decay constant f_π:

$$\langle \Omega | A_a^\mu(x) | \pi_b(p) \rangle = i \, f_\pi \, p^\mu \delta_{ab} e^{-ip \cdot x} \tag{1.14}$$

If we use Eq. (1.13) to evaluate the degree of non-conservation of the axial charge $Q_a^A = \int \mathrm{d}^3x \, A_a^0$ by taking the vacuum matrix element of the commutator $\left[Q_1^A, \, \partial_\mu A_a^\mu\right]$ we find a connection to the chiral condensate

$$\langle \Omega | \left[Q_1^A, \, \partial_\mu A_a^\mu\right] | \Omega \rangle = \frac{i}{2}(m_\mathrm{u} + m_\mathrm{d}) \langle \bar{u}u + \bar{d}d \rangle \ , \tag{1.15}$$

which can be used together with Eq. (1.14) to derive the Gell-Mann-Oakes-Renner relation (GMOR) [GMOR68]

$$m_\pi^2 = -\frac{1}{f_\pi^2} \frac{m_\mathrm{u} + m_\mathrm{d}}{2} \langle \bar{u}u + \bar{d}d \rangle \ , \tag{1.16}$$

which gives the lowest order dependence of the pion mass on the current quark masses. Note that while the pion mass m_π and the pion decay constant f_π are renormalised quantities, current quark masses and chiral condensates are scale dependent. This mechanism in combination with different current quark masses for up, down and strange quark, allows to explain the spectrum of the lightest mesons to astonishing accuracy.

1.2 QCD at finite temperatures

The standard approach to quantum field theories at finite temperatures and chemical potentials uses the statistical density matrix $\hat{\rho}$. The expectation values $\langle \phi | \hat{\rho} | \phi \rangle$ then give the relative probability that the system at a specific temperature and chemical potential finds itself in a given state $|\phi\rangle$. The normalisation factor is called grand canonical partition function $\mathcal{Z}$ and defined by $\mathcal{Z} = \mathrm{Tr} \, \hat{\rho}$, and the thermal expectation value of an operator $\hat{A}$ can be evaluated using

$$\langle A \rangle = \mathcal{Z}^{-1} \mathrm{Tr} \, \hat{A} \, \hat{\rho} \ . \tag{1.17}$$

The central piece in this formalism, the density matrix $\hat{\rho}$, can be accessed via the Hamiltonian $\hat{H}$ of the system:

$$\hat{\rho} = \exp\left[-\beta \left(\hat{H} - \mu \hat{N}\right)\right] \ , \tag{1.18}$$

where β is the inverse temperature and $\hat{N}$ is the particle number operator. In the first part of this section (Sec. 1.2.1) it will be outlined how the density matrix can be derived from the QCD Lagrangian (Sec. 1.1). The second part (Sec. 1.2.2) concentrates on the commonly used gauge, named after Polyakov, which is frequently used at finite tempertature. The final part of this section (Sec. 1.2.3) is dedicated to some important effects of the finite temperature treatment on the gauge symmetry. The finite temperature treatment imposes periodic boundary conditions for (gauge) bosons. This allows to separate the centre of the gauge group as a global symmetry.

1.2.1 Imaginary-time formalism

The partition function of QCD is given by

$$\mathcal{Z}_{\mathrm{QCD}} = \mathrm{Tr}\ e^{-\beta(\hat{H}-\mu\hat{N})}\ , \qquad (1.19)$$

where the trace is evaluated by summing over all possible quantum states. These states are characterised by the quark fields ψ and the gluon fields A_i: $|A_i,\,\psi\rangle$. In thermodynamic equilibrium these states are time independent. Due to the anti-commutation relation of fermions an integration over all quark fields ψ is an integration over a Grassmann variable, such that the trace can be written as $\int \mathcal{D}\psi\,\langle-\psi|\cdots|\psi\rangle$ in accordance with the identity operation which in this case can be expressed as $\int \mathcal{D}\psi|\psi\rangle\langle\psi|$ [LB]. Rewriting the trace we find

$$\mathcal{Z}_{\mathrm{QCD}} = \int \mathcal{D}A_i \int \mathcal{D}\psi\ \langle A_i,\,-\psi|e^{-\beta(\hat{H}-\mu\hat{N})}|A_i,\,\psi\rangle\ , \qquad (1.20)$$

where an integration over the gauge group is implied in the integration $\int \mathcal{D}A_i$. The index i in the gluon field A_i labels the three spatial components. The time component A_0 can be fixed by choice of a certain gauge. We choose the gauge such that $A_0 = 0$ (Weyl gauge). Furthermore finite temperatures and finite chemical potentials imply the presence of a heat bath which specifies an absolute rest frame which breaks the symmetry of space and time. Due to the reduced symmetry too many independent field variables are present. The redundant degrees of freedom can be removed by specifying spacelike manifolds on which Gauss' law must be satisfied. To write down Gauss' law we use the charge density and the colour electric fields, given in QCD as

$$\rho_a = \psi^\dagger \tfrac{\lambda_a}{2}\psi = -i\pi\tfrac{\lambda_a}{2}\psi \qquad \text{and} \qquad E_a^i = G_a^{0i} = \partial^0 A_a^i = -\Pi_a^{0i}\ , \qquad (1.21)$$

where π and Π_a^i refer to the canonic momenta corresponding to ψ and A_a^i. On the right hand side we exploited $A_0 = 0$ (i.e. the Weyl gauge) to evaluate the field strength tensor G_a^{0i}. Using these objects the projector $\mathcal{P}_{\mathrm{G}}$ enforcing Gauss' law $\mathcal{P}_{\mathrm{G}} = \delta(D_i E_a^i - \rho_a)$ on each individual point in space can be rewritten using Lagrange multipliers here noted as Γ^a:

$$\mathcal{P}_{\mathrm{G}} = \int \mathcal{D}\Gamma^a \exp\left[i \int \mathrm{d}^3x\ \Gamma^a \left(D_i E_a^i - \rho_a\right)\right] \qquad (1.22)$$

Now we use Trotter's formula[5] to split the density matrix and the projection operator enforcing Gauss' law on each space-like sheet ($\mathcal{P}_{\mathrm{G}}$) into n partitions equally spaced in inverse temperature. Here we use the idempotence of the projection operator and the fact that it commutes with the density matrix, or equivalently, with the Hamiltonian. Additionally we insert identity operators of the form $\int \mathcal{D}A_i\mathcal{D}\psi\ |A_i,\,\psi\rangle\langle A_i,\,\psi|$ and $\int \mathcal{D}\Pi_i\mathcal{D}\pi\ |\Pi_i,\,\pi\rangle\langle\Pi_i,\,\pi|$ in between each partition of the density matrix:

---

[5]Trotter's formula (or Lie product): $\lim_{n\to\infty}\left(e^{A/n}e^{B/n}\right)^n = e^{A+B}$

$$\mathcal{Z}_{\text{QCD}} = \lim_{n \to \infty} \int \mathcal{D}A_i \int \mathcal{D}\psi \ \langle A_i, \psi | e^{-\frac{\beta}{n}\left(\hat{H} - \mu\hat{N}\right)} \mathcal{P}_{\text{G}} \int \mathcal{D}\Pi^i \mathcal{D}\pi |\Pi^i, \pi\rangle \ \langle \Pi^i, \pi |$$
$$\times \int \mathcal{D}A_i' \int \mathcal{D}\psi' \ |A_i', \psi'\rangle \langle A_i', \psi'| e^{-\frac{\beta}{n}\left(\hat{H} - \mu\hat{N}\right)} \mathcal{P}_{\text{G}} \ \cdots \ |A_i, \psi\rangle \ . \quad (1.23)$$

Using $\langle \Pi^i, \pi | A_i, \psi \rangle = e^{i\,\Pi^i A_i} e^{i\,\pi\,\psi}$ and the representation of the projection operator (1.22) with the explicit definitions of charge density and colour electric fields (1.21), we perform the limit $n \to \infty$:

$$\mathcal{Z}_{\text{QCD}} = \int \mathcal{D}A_i^a \int \mathcal{D}\Gamma^a \int \mathcal{D}\Pi_a^i \int \mathcal{D}\psi \int \mathcal{D}\pi \ \exp \left[\int^{\beta} \mathrm{d}^4 x \left\{ i\Pi^i \partial_4 A_i^a + i\pi \partial_4 \psi \right. \right.$$
$$\left. \left. + i\Gamma^a \left(D_i \Pi_a^i - ig\pi \frac{\lambda_a}{2} \psi \right) - \mathcal{H} \right\} \right] \ . \quad (1.24)$$

Renaming Γ^a and π by A_4^a and $i\bar{\psi}\gamma_0$ allows to reconstruct the Lagrangian density applying a Legendre transform to the Hamiltonian density:

$$\mathcal{Z}_{\text{QCD}} = \int \mathcal{D}A_\mu \int \mathcal{D}\psi \int \mathcal{D}\bar{\psi} \ e^{-\int^{\beta} \mathrm{d}^4 x \, \mathcal{L}} \ , \quad (1.25)$$

where here and in Eq. (1.24) (anti-) periodic boundary conditions are implied for (quark) and boson fields, which are a leftover of the properties of the trace. Note that after introduction of the Euclidean time the metric applied to the Lagrangian density (1.1) is the Euclidean metric $diag(+1, +1, +1, +1)$.

Just as in the Minkowskian space-time one is free to choose the space-time basis. The usual Minkowskian space corresponds to an Euclidean space-time with a temporal extend reaching from 0 to β with (anti-)periodic boundary conditions. The other common basis is the momentum basis. In Minkowskian space, time is Fourier transformed just like the spatial directions. In Euclidean time, with its finite extent and boundary conditions, all fields can be expanded in terms of a Fourier series. Due to the boundary conditions the required frequencies differ for fermions and bosons:

$$\omega_n = \begin{cases} 2n\,\pi\,T & \text{for bosons} \\ (2n+1)\pi\,T & \text{for fermions} \end{cases} \ . \quad (1.26)$$

These are called Matsubara frequencies.

All the steps discussed above can be summarised in simple replacement rules. First of all the energy or zero component of the momentum, p_0, is replaced by the Matsubara frequencies $i\omega_n$. This produces a minus sign in the metric which allows to factor out an overall minus sign simplifying the metric to unity. The functional trace (integration over all direct or momentum space) needs to be modified as well:

$$\int \frac{\mathrm{d}^4 p}{(2\pi)^4}(\cdots) \longrightarrow i\,T \sum_n \int \frac{\mathrm{d}^3 p}{(2\pi)^3}(\cdots) \ , \quad (1.27)$$

where the summation runs over all Matsubara frequencies, fermionic or bosonic depending on the nature of the looping particle.

1.2.2 The Polyakov gauge

It is important to note that the integration over A_4 is necessary to remove ambiguities from the equations. In the finite temperature case these ambiguities appear upon breaking the Lorentz symmetry explicitly by the heat bath. The gauge of A_4 is not directly related to the original gauge field A_0 and the original gauge. Note that it is in general not possible to apply a simple gauge transformation to remove finite values of A_4, i.e. to enforce a Weyl gauge like condition in Euclidean space-time. The choice of gauge in Euclidean space-time is always related to the choice of the Euclidean time direction (the breaking of Lorentz symmetry by the heat bath). The so-called static gauge $\partial_4 A_4 = 0$ is in accordance with the common structure of space-time. Additionally A_4 as a generator of $SU(3)_\mathrm{c}$ may be diagonalised. This static, diagonal gauge is referred to as Polyakov gauge [tH81, FMT⁺98].

The fact that a Weyl gauge like condition in Euclidean space-time is incompatible with a canonic space-time structure has further consequences. A Wilson line which gives the relative gauge transformation between two space-time points can be defined using the exponential of a path ordered integral

$$W(x, y) = \mathcal{P} \exp \left[ig \int_x^y \mathrm{d}z_\mu A^\mu \right] \tag{1.28}$$

where the path of integration is arbitrary. In Euclidean space-time the path of integration may reach from the spatial position $\vec{x}$ at Euclidean time $\tau = 0$ to the same point $\vec{x}$ at $\tau = \beta$. Such a path may be interpreted as a closed loop that wraps around the Euclidean thermal torus and is referred to as Polyakov loop:

$$L(\vec{x}) = \mathcal{P} \exp \left[ig \int_0^\beta \mathrm{d}\tau A_4(\vec{x}) \right] \tag{1.29}$$

The fact that it is not possible to choose a gauge such that A_4 vanishes all along the thermal torus from $\tau = 0$ to β implies that a Polyakov loop cannot be changed to unity by simply applying an appropriate gauge. There is in general an overall transformation collected along the path of integration which cannot be made to vanish. As the Polyakov loop $L(\vec{x})$ is an element of $SU(3)_\mathrm{c}$ there are two gauge invariant quantities that can be derived from $L(\vec{x})$: the traces of $L(\vec{x})$ and $L^\dagger(\vec{x})$. The denomination of $L(\vec{x})$ and $L^\dagger(\vec{x})$ and the traces thereof is ambiguous. Also in this work we will refer to both $L(\vec{x})$ and $L^\dagger(\vec{x})$ as well as to the normalised colour traces of $L(\vec{x})$ and $L^\dagger(\vec{x})$ as the Polyakov loop. We define the normalised colour traces of $L(\vec{x})$ and $L^\dagger(\vec{x})$ as Φ and its complex conjugate Φ^* by

$$\Phi(\vec{x}) = \frac{1}{N_\mathrm{c}} \mathrm{tr_c}\, L(\vec{x}) \qquad\qquad \Phi^*(\vec{x}) = \frac{1}{N_\mathrm{c}} \mathrm{tr_c}\, L^\dagger(\vec{x})\ . \tag{1.30}$$

1.2.3 Confinement and $Z(3)$ center-symmetry of $SU(3)_\mathrm{c}$

To keep the familiar structure of Euclidean space-time one is restricted to periodic boson and antiperiodic fermion fields. The periodicity of the gauge boson fields however does not imply the same periodicity in the gauge transformation. We

have to require that the transformation operator $U(x)$ in Eq. (1.4) is such that the β-periodicity in Euclidean time of the gauge fields A_4 is preserved. In Eq. (1.4) a transformation $U(x)$ always appears in combination with its inverse. Thus the boundary condition for the transformation $U(x)$ can always be modified by an additional $SU(3)_c$ transformation, which commutes with all other $SU(3)_c$ transformations and its generators, namely the gluon fields. The boundary condition for a gauge transformation of the gauge sector of the Lagrangian therefore reads

$$U(x_4,\,\vec{x}) = z \cdot U(x_4 + \beta,\,\vec{x}) \quad \text{with} \quad z \in SU(3)_c \ni z\,Q = Q\,z, \ \forall \ Q \in SU(3)_c \ . \tag{1.31}$$

A group element z with the property that it commutes with all other group elements is by definition an element of the centre of the group. The centre group of $SU(N_c)$ is $Z(N_c)$ and is composed of the $SU(N_c)$ group elements

$$\mathbb{1}, \ \mathbb{1}\,e^{2\pi i/N_c}, \ \ldots, \ \mathbb{1}\,e^{2\pi i(N_c-1)/N_c} \tag{1.32}$$

in the most common representation. The centre symmetry allows to write down N_c equivalent finite temperature formulations of a $SU(N_c)$ gauge field theory corresponding to the N_c different realizations of the periodic boundary conditions for boson fields. Therefore the centre symmetry is not part of the gauge symmetry as it is equal for all space. The centre symmetry is a global symmetry generated by the finite temperature formulation. As the field equations of QCD are symmetric under centre symmetry transformations, there are two conceivable scenarios: the field configuration (vacuum state) may or may not share the centre symmetry. In a situation where it is only the quantum state that breaks a global symmetry of the field equations we refer to spontaneous symmetry breaking. One quantity that is able to measure whether the vacuum state breaks the centre symmetry is the Polyakov loop. Applying a gauge transformation such that the transformation matrix U at $\tau = \beta$ is twisted by an element of the centre group (not changing the boundary conditions in the gauge sector of the Lagrangian) leads to a transformation of the Polyakov loop:

$$\langle \Phi \rangle \rightarrow \langle z \cdot \Phi \rangle = e^{2\pi k i/N_c} \langle \Phi \rangle \quad k \in \mathbb{Z} \tag{1.33}$$

If $\langle \Phi \rangle$ equals $\langle z \cdot \Phi \rangle$ for arbitrary z taken from the centre of $SU(N_c)$ the centre symmetry is unbroken by the vacuum state. In this case we can immediately conclude from Eq. (1.33) that $\langle \Phi \rangle$ has to vanish as well as $\langle \Phi^* \rangle$.

$\langle \Phi \rangle = \langle \Phi^* \rangle = 0$ indeed has some important physical consequences. By its definition (1.30) the traced Polyakov loop Φ is related to a Wilson line (1.29) which wraps once around the Euclidean time torus. Wilson lines are the colour transformations needed to connect two points in space-time. In case of a Polyakov loop it is the connection of the same spatial position at different Euclidean times. I. e. the Polyakov loop connects a colour source at Euclidean time $\tau = 0$ with a colour sink at $\tau = \beta$. Given the periodicity in Euclidean time, source and sink are at equivalent positions. As the path integral together with its ficticious Euclidean time is used as a tool to evaluate the trace over all thermodynamic states we need to find the physical situation which belongs to this path integral. In fact the only isolated colour sources available in QCD are infinitely heavy quarks. The path integral used

to evaluate $\langle \mathrm{tr_c}\, L \rangle$ therefore is equivalent to the thermodynamic trace over all states in which there is one static quark at a fixed position in space:

$$\langle \mathrm{tr_c}\, L(\vec{x}) \rangle = \int \mathcal{D}A_\mu \int \mathcal{D}\psi \int \mathcal{D}\bar{\psi}\, e^{-S_{\mathrm{QCD}}}\, \mathrm{tr_c}\, L(\vec{x})$$

$$= \int \mathcal{D}A_i \int \mathcal{D}\psi \sum_{a=1}^{N_c} \langle A_i, -\psi | \bar{q}_a(\vec{x})\, \hat{\rho}\, q_a(\vec{x}) | A_i, \psi \rangle \qquad (1.34)$$

$$= \mathcal{Z}_{q(\vec{x})} = e^{-\beta\, F_{q(\vec{x})}}\ , \qquad (1.35)$$

where $\hat{\rho}$ is the density matrix of QCD, and the colour trace has been interpreted as an average over all colours. In the last line of Eq. (1.35) we conclude that the expectation value $\langle \mathrm{tr_c}\, L \rangle$ is equivalent to the canonical partition function of a thermodynamic system with exactly one quark at position $\vec{x}$ averaged over all colours. The partition function can be rewritten in terms of a free energy (1.35). Finally we find that $\langle \Phi \rangle = \langle \Phi^* \rangle = 0$ implies a vanishing partition function or an infinite free energy of a single static quark [Wei81, Wei82, Sve86]. All open colour sources are infinitely suppressed, i. e. colour is confined.

A situation at which $\langle \Phi \rangle$ vanishes can only occur in QCD with static quarks, i. e. in the limit of infinitely heavy quarks.[6] In this case of infinitely heavy quarks the Polyakov loop expectation value is an order parameter for confinement. According to lattice simulations using the gauge action only, the deconfinement phase transition is of first order [B+96]. The argument above that $\langle \Phi \rangle$ can only vanish once colour is confined was based on the existence of the centre-symmetry in the QCD action. The quark terms however spoil this symmetry, as gauge transformations for quarks only involve one unitary transformation operator $U(x)$. Therefore a change of the gauge transformation by an element of the centre of $SU(3)_c$ will not lead to the same transformed quark field:

$$\psi \longrightarrow \tilde{\psi} = U\,\psi \quad \neq \quad z \cdot U\,\psi\ . \qquad (1.36)$$

In QCD at finite temperature and finite quark masses the global $Z(3)$ centre symmetry of the Lagrangian is broken explicitly. Therefore any order parameter will always indicate that the symmetry is broken: $\langle \Phi \rangle \neq 0$. Strict colour confinement does not occur, implying a deconfinement crossover instead of first order phase transition. Physically this is not difficult to accept simply because an infinite free energy of course would allow to generate an arbitrary number of quarks carrying colour charges, screening the field of the original static colour charge. The fact that the free energy of a colour source is finite implies that colour confinement can only occur above a certain length scale. This observation is compatible with asymptotic freedom. At asymptotically high energies and short length scales we expect quarks (colour charges) to be free. In principle it is conceivable that there is a certain length scale above which QCD dynamics screens colour completely. In lattice QCD calculations an exponential screening has been observed. In Refs. [BBV98, DDGM03]

---

[6]In fact it is sufficient if the ratio of quark mass and temperature becomes infinite, which implies that at finite current quark masses QCD can confine colour at zero temperature.

the correlation lengths of the field strength tensors have been evaluated using an exponential ansatz. The typical correlation length scale is of the order of $0.2\,\mathrm{fm}$.[7]

1.3   Approaches to QCD

QCD shows very distinct behaviour at low energy, temperature and density compared to high energy and momentum scales. Due to the complexity of QCD the methods used to investigate QCD has become extremely diverse. This section only summarizes our present knowledge about QCD thermodynamics from lattice QCD and experiment.

1.3.1   QCD on the lattice

In Sec. 1.2.1 a method to evaluate thermal traces using path integrals was sketched. In principle these path integrals are infinite dimensional integrals. It is however possible to evaluate numeric approximations to these integrals, by discretizing space and Euclidean time. The infinite number of integrals is reduced to a finite number and can be approximated using Monte Carlo methods.

One of the first lattice calculations emphasizing the connection of chiral symmetry and confinement was conducted by Gocksch and Ogilvie [GO85]. Presently the main obstacle in the perfection of these calculations is lacking computing power. Optimisation for speed has to trade off between the number of lattice sites and the convergence improvements employed in the discretized action.

One major obstacle in finite density lattice QCD calculations is the so-called fermion sign problem. It appears at non-zero chemical potential and manifests itself in a complex eigenvalue spectrum of the Euclidian action. In principle this is no limitation to the applicability of the path integral formalism. It is easily shown that all physically accessible quantities remain real valued as they should. The convergence of the computational Monte Carlo methods however degrades and finally fails.

At present stage there are several approaches to circumvent these issues. One straight forward approach is to Taylor expand the effective action about $\mu = 0$ were the sign problem does not occur [C+08, GG08]. This method can be criticised for the fact that the radius of convergence remains unknown and is limited by the nearest singularity in the effective potential, which appears at the latest at a critical point. Instead of using Taylor series expansions it is also possible to use a Padé approximation to map regions with finite chemical potentials [Lom06]. In reweighing methods a statical ensemble is generated at $\mu = 0$ and applied to finite chemical potentials while changing the parameters, current quark mass(es) and coupling strength, such that physical quantities remain unchanged [AFKS06a, Eji08]. Here in addition the so-called overlap problem appears, which names the issue that the ensemble should be modified upon changing the chemical potential. Finally it is possible to exploit

---

[7]It is interesting to note that the correlation length scales of the field strength tensor correspond to the energy scale of the cutoff in the Nambu and Jona-Lasinio model presented in Sec. 2.2.
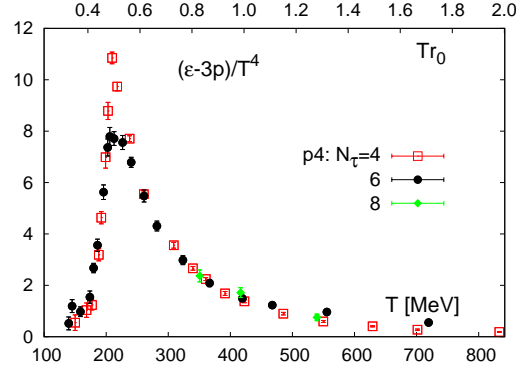
Figure 1.1: The trace anomaly $\theta_{\mu\mu}(T) = \epsilon - 3p$ in units of T^4 versus temperature as given in Ref. [C$^+$08] obtained from calculations on lattices with temporal extent $N_\mathrm{t} = 4$, 6, and 8.

the analytic properties of the effective action. The effective action is an analytic function with singularities at critical points which in principle can be analytically continued to imaginary chemical potential. At imaginary chemical potential the fermion sign problem does not occur. It is therefore much easier to evaluate the lowest order coefficients of a polynomial approximating the analytic effective potential. The extracted expansion coefficients can then be used to trace the analytic function back to real chemical potentials [dFP08]. As in the case for the Taylor series expansion the truncation of the approximating polynomial limits the range of applicability of this method.

Despite the diversity of calculations we pick only one representative to outline the major outcome of the finite temperature calculations. The primary quantity evaluated in thermodynamic lattice QCD calculation is the interaction measure, $\epsilon - 3p$, which is the trace of the relativistic energy-momentum-tensor (see Fig. 1.1). This interaction measure vanishes for ultrarelativistic non-interacting particle gases. Based on this quantity, energy density ϵ, pressure p and entropy density s are extracted from the data (see Fig. 1.2). Tracing these quantities along temperature reveals rapid changes around a characteristic transition temperature. As for finite volume and lattice spacing the effective potential cannot be singular, no true phase transitions can appear in lattice calculations. Only the scaling behaviour with changing lattice volume and lattice spacing can answer the question of the order of the phase transition. The current consensus is that there is no true phase transition at $\mu = 0$ [AEF$^+$06]. The rapid changes in energy density ϵ, pressure p and entropy density s therefore indicate a rapid crossover. For crossover transitions no true order parameters exist. This is why the crossover temperature cannot be fixed by a unique criterion. The pseudocritical temperature varies depending on the details of the lattice analysis and the chosen criterion. Values in the literature for $2 + 1$ flavours range from about $151\,\mathrm{MeV}$ [AFKS06b] to about $196\,\mathrm{MeV}$ [C$^+$06, C$^+$08]. Ambiguities in setting a scale on the lattice are part of the cause for these rather large variations.

Order parameters (or in case of crossover transitions: order parameter like quan-
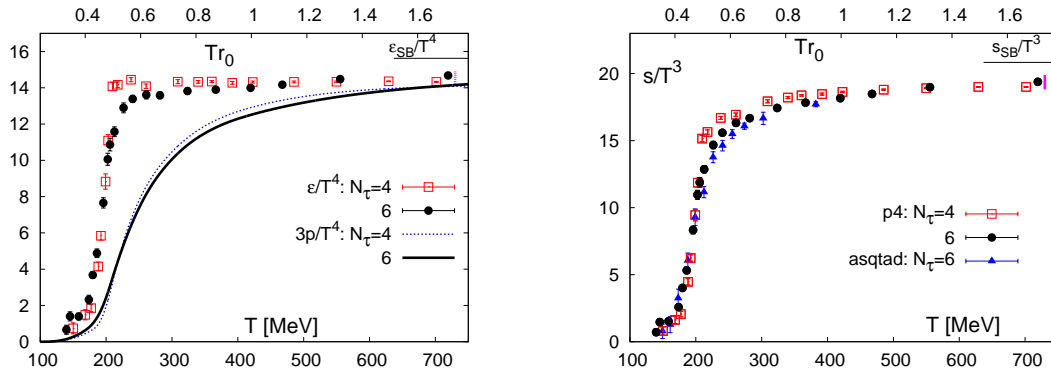
Figure 1.2:   Energy density and pressure (left) and entropy density (right) plotted as functions of the temperature as given in Ref. [C+08]. The shown results have been obtained from calculations on lattices with temporal extent $N_{\text{t}} = 4$ and 6. The small vertical bar in the left hand figure at high temperatures shows the estimate of the systematic uncertainty on these numbers that arises from the normalisation of the pressure at $T_0 = 100\,\text{MeV}$.

tities) are important indicators of the dynamics at finite temperatures. There are in fact two transitions located close together: the chiral and the deconfinement crossover (see Sec. 1.1 and Fig. 1.3). It is suspected that there is a dynamic mechanism at work in QCD that intertwines these two crossovers [GO85]. However there is no consensus on the question whether the transitions do happen exactly simultaneously or if there is a slight shift of the chiral transition to lower temperatures (see Fig. 1.4)

At zero density lattice QCD calculations provide strong indications that there is only a rapid crossover transition bordering the confined phase[8] with broken chiral symmetry. Model calculations using different approaches indicate that there exists a first order phase transition at low temperatures and high densities. Therefore a widely accepted scenario of the QCD phase diagram in the plane of temperature and chemical potential assumes the existence of a first order line starting on the μ-axis which ends in a critical point at finite T and μ. In Ref. [Ste06], where the phase diagram is discussed in detail, a substantial collection of model calculations supporting such a scenario are referenced. Using the current quark mass as an additional parameter the critical point may become tricritical once the light quark masses come to zero and the chiral crossover turns into a second order phase transition (see Sec. 1.4.2). However it is crucial how the strange quark and its mass as a parameter are treated in such approaches. For three degenerate light quarks the chiral phase transition is expected to be of first order in the chiral limit.[9] The order of the phase transition on the temperature axis (at $\mu = 0$) as a function of strange quark mass on the one and up and down quark mass on the other hand is often illustrated using the so-called Columbia plot [B+90] (see Fig. 1.7 in Sec. 1.4.2). Interestingly in this Columbia plot the physical realization of the current quark masses is located very

---

[8]The word phase is used here even though there is no phase transition in the strict sense.

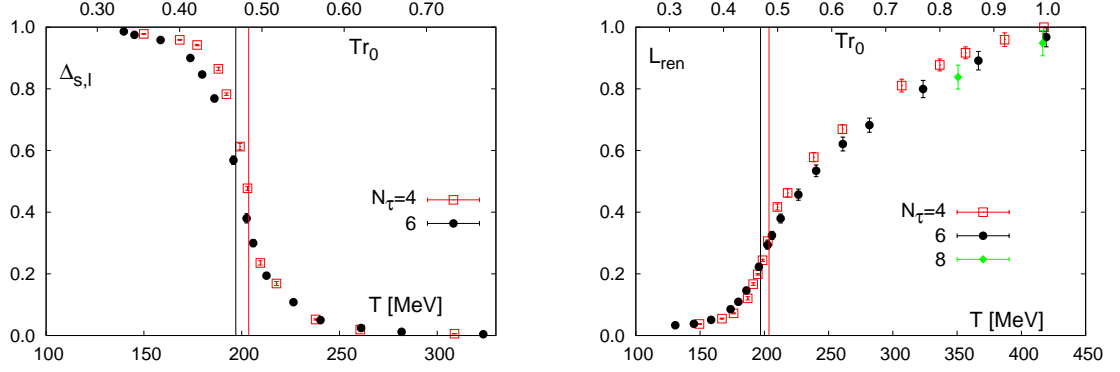[9]Pisarkski and Wilczek advocate such a first order transition line [PW84].

Figure 1.3: Renormalised Polyakov loop on lattices with temporal extent $N_t = 4$, 6 and 8 (left) and the normalised difference of light and strange quark chiral condensates defined in Ref. [C$^+$08]. The vertical lines show the location of the transition temperature determined in Ref. [C$^+$06] on lattices with temporal extent $N_t = 4$ (right line) and in this analysis for $N_t = 6$ (left line). The transition temperatures determined in terms of chiral condensate and Polyakov-loop almost coincide. [C$^+$08]
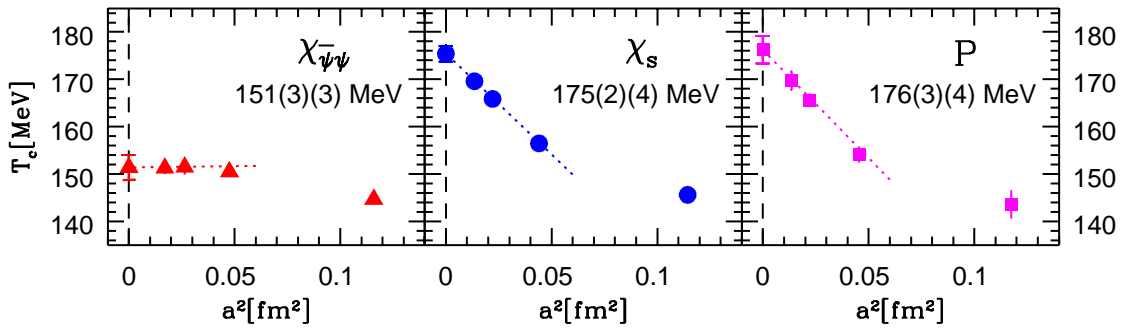

Figure 1.4: Continuum limit of the transition temperatures obtained from the renormalised chiral susceptibility $(m^2 \Delta \chi_{\bar{\psi}\psi}/T^4)$, strange quark number susceptibility (χ_s/T^2) and renormalised Polyakov-loop (P_R) as given in Ref. [AFKS06b]. The chiral and Polyakov-loop susceptibilities indicate different crossover transition temperatures.

close to the borderline of first order transition and crossover. In other words the question whether there is a first order phase transition or a crossover at $\mu = 0$ has not been settled yet (see discussions on Ref. [dFP08]). Away from the T and μ-axis even less is known about about the QCD phase diagram.

On the one hand lattice calculations need to produce more consistent results at $\mu = 0$ while experimental output on the other hand needs better interpretation. This requires understanding and insight into the dynamics during the evolution of the hot and dense matter produced in high energy collisions of heavy nuclei. Model calculations can then proceed to draw a picture of the QCD phases once they can make use of a solid data basis [Raj99, Alf03, Ste06].

1.3.2   Empirical insights into strongly interacting matter

The experiments concerning the issues discussed in this thesis have been performed mainly at the Relativistic Heavy Ion Collider (RHIC) at the Brookhaven National Laboratory (BNL) and at the Super Proton Syncrotron (SPS) at CERN. Future experiments may include a low energy run at RHIC dedicated to the search of the critical point, very highly energetic heavy-ion collisions at the LHC and the Compressed Barionic Matter (CBM) experiment at the planned FAIR facility next to GSI in Darmstadt. However, so far only few observables have been proposed and measured that do not require involved calculations for their interpretation in terms of the physics of strongly interacting matter.

The observation of the angular distribution of low energy particles has been interpreted in terms of hydrodynamic flow. This requires an extremely fast thermalization of large fractions of the fireball after a highly energetic nuclear collision leading to a thermal medium of particles with much lower energies than the initial centre of mass energy. Thermalization has become an accepted assumption also because measured particle ratios in the final state are in good agreement with thermal equilibrium statistics. The particle ratios allow to estimate the temperature at which the particles do no longer interact, the so-called freeze-out temperature [ABMS06] (see Fig. 1.5 in Sec. 1.4.1).

Particle abundances with different valence quark content show quark number scaling, i.e. abundances of particles only depend on the number of valence quarks independent of mass and other quantities [A+07a, A+07b]. The generation and thermalization of quarks therefore must have happened under conditions where light and strange quarks can be treated approximately equal. This indicates that shortly after thermalization the fireball was in a partonic, high temperature phase, a so-called quark-gluon plasma.

On the other hand high energetic particles are observed that did not equilibrate. These particles are interpreted as remnants of partonic collisions at very early times. Typically these so-called particle jets are observed in spatially anticorrelated pairs, carrying momenta in opposite directions. Comparing jets in heavy-ion collisions with jets in proton collisions leads to the observation that one of these paired jets is attenuated in the heavy-ion case. This phenomenon is referred to as jet suppression. The difference in the jet energies of a pair of jets in a heavy-ion collision is usually

explained by the asymmetry of the primary partonic collision. In general each jet of the same pair has to travel along paths of different lengths. The differences in their way through the thermalizing background of low energy particles leads to different attenuation of the two jets. The understanding of the in-medium effects leading to jet suppression require involved simulations of the fireball and its evolution.

Observables which can be interpreted without detailed modelling of the fireball are rare. On the one hand experimental corner stones are urgently needed to refine models and to benchmark lattice QCD calculations, on the other hand it is difficult to extract information from experimental data without sophisticated models describing the expansion of the fireball.

In the early stages of the fireball evolution the assumptions needed for the applicability of hydrodynamics seems to be sufficiently well fulfilled. Both ideal and viscous hydrodynamics have been used to describe such systems reproducing many features of the system [SH08, RR07]. At later stages of the evolution the assumptions needed for hydrodynamics become questionable. Here ultra-relativistic quantum molecular dynamics (UrQMD) codes have been applied to the fireball evolution [B$^+$99, B$^+$98]. At the present stage efforts are made to reduce the diversity of models and focus on the most promising approaches.

High energy probes like jets or dileptons originating in a highly energetic photon and their spatial correlations are expected to carry information about the very early collision and their journey through the medium. The difficulty in the interpretation of the obtained data is to de-convolute different interactions with the medium at different times from the process of generating these particles. On the other hand a multitude of interaction processes with the medium is accessible through such probes.

One of the methods to extract further information from heavy-ion collisions is the measurement of fluctuations. Particle abundances and ratios have revealed the high degree of thermalization of the fireball [ABMS06]. However, these measurements represent a snap-shot of the sphere of last interaction. This sphere of last interaction may show a dependence on the interactions involved. Typically different mesons dissolve in the thermal medium at different conditions depending on the binding strength of the quark-antiquark pair. Therefore the concept of a sphere of last interaction is a difficult concept to begin with. In contrast to this, fluctuations are able to give some insight into the evolution of the final state observed in the detector. Due to the fast evolution of the fireball, fluctuations generated in early stages may survive the ongoing interactions in the medium.[10]

One way to study fluctuations works on an event-by-event basis. If the used detectors would cover the total solid angle one could not expect fluctuations on an event-by-event basis of conserved charges. Due to the fact that the collision products are highly relativistic a large fraction of the particles leaves the detector in forward direction without being measured. The acceptance of the detector cuts out a window in phase space. If fluctuations are smaller than this window it is in principle possible to extract the correlation length (the size of the fluctuations) from the ensemble of

---

[10]Such analyses are analogous to the analysis of the cosmic microwave background to investigate the "Big Bang". Heavy-ion collisions are sometimes referred to as "little Big Bang".

individual events. Especially in the investigation of phase transitions, fluctuations are of major interest, as they are expected to be large near the critical point (second order phase transitions). In principle it is also possible to detect first order phase transitions using event-by-event fluctuations due to the fact that the fast expansion of the medium across first order phase transition will lead to spinodal instabilities. The typical size of these instabilities is a characteristic quantity which carries lots of information about the interactions in the fluid.

1.4 Phases of QCD

One of the central purposes of the models used in this work is to compute and predict a phase diagram which has as many features as possible in common with the "true" QCD phase diagram. The variables of such a phase diagram are chemical potentials and temperature. In a second step parameters of the theory of interest are varied. In the case of QCD these parameters are the current quark masses. In addition to the parameters of QCD, the quark masses, each model usually has several other constants such as interaction strengths. This opens up a variety of "theoretical" phase diagrams for qualitative and conceptual explorations.

To draw a phase diagram one needs some criterion to distinguish different regions in parameter space. The only solid criterion for a phase transition we know is the non-analyticity in some observable. This also implies a non-analyticity in the partition function. The partition function, however, is only accessible from the theory side. Strictly speaking such non-analycities can only appear in infinite systems. The border line between microscopic, quantum mechanical behaviour and classic, macroscopic behaviour is difficult to determine. This issue is connected to decoherence and the measurement process and shall not be discussed here. It is remarkable, however, that phase transitons as macroscopic phenomena are governed by changes on the microscopic scale.

Given an observable that displays non-analytic behaviour along some border line in parameter space, we can distinguish two different regions in parameter space. This border line defines a phase transition and the observable with its non-analytic behaviour is called order parameter. The choice of order parameter is generally not unique. It is possible to construct many different quantities that involve the same non-analyticity. In most cases it is however possible to associate a distinct microscopic symmetry with these equivalent order parameters. In this case the phase boundary separates areas where this symmetry is broken by quantum dynamics and areas where all occupied states share this symmetry. In cases where no microscopic symmetry is associated with the transition, phase transition lines may end in a so-called critical end point. As an ending transition line cannot separate two different regions in space, the existence of a critical end point implies that no microscopic symmetry is broken or restored when crossing the transition line. The most prominent example is the liquid-gas transition of ordinary substances like water.

As a first step in approaching these issues theoretically it is often usefull and possible to suppress terms in the Lagrangian density that break some symmetry explicitly. Having enforced the Lagrangian to be symmetric the derived thermody-

namic system may or may not share this symmetry. The symmetry of the Lagrangian is the precondition for the existence of a phase transition. In fact it may happen that this transition only happens at infinite or vanishing temperature or chemical potentials. Having constructed such a system it is then possible to study the vicinity of the symmetric Lagrangian by reintroducing a symmetry breaking term. As the symmetry is now broken everywhere in parameter space no non-analycities in the derived partition function can appear. In the limit of vanishing symmetry breaking the change in the order parameter remains sharp. Away from this limit the transition in this parameter becomes smoother. Due to this smooth and continous change it can no longer be consided an order parameter in the strict sense. In such cases the transition is referred to as a fast crossover transition and the order parameter is only approximate. As in the unbroken symmetry case it is possible to construct several equivalent order parameters. There are several quantities that exhibit a rapid crossover. However, now, considering the different approximate order parameters the exact position of the transition is not well defined. The uncertainties in its determination are of the order of the width of the peak in the susceptibility associated with an approximate order parameter.

1.4.1   QCD phase diagram at finite densities

In this section we concentrate on the physical phase diagram in the plane of temperature and chemical potential. Only in small regions of the QCD phase diagram a common consensus on the QCD phase structre has been achieved. The empirically well established points are the vacuum at zero temperature and zero chemical potential, and the saturation point of nuclear matter. Known from lattice QCD calculations allowing for some systematic uncertainties is the behaviour along the temperature axis at vanishing quark chemical potential. The fact that QCD produces a colour superconducting colour-flavour-locked (CFL) phase at asymptotically large chemical potential and low temperatures is based on theoretical arguments [ARW99]. Already at much lower chemical potentials we expect the baryon number density to become large, such that there is no space left in between the baryons. From this percolation argument we conclude that deconfinement should set in at large quark chemical potentials. The MIT bag model (see Sec. 2.1) predicts this to happen at about $0.4\,\text{GeV}$ in quark chemical potential. From the existence of nuclear matter with baryons (neutrons and protons) we know that the quark chemical potential at zero temperature for this to happen should definitely be above $M_\text{N}/3$. Whether this deconfining transition directly merges into a colour superfluid phase or a quark-gluon phase is not a settled issue. Some models like the MIT bag, the NJL model, the PNJL model, quark meson models [SPW07] and the random matrix model [HJS$^+$98] predict this transition to be of first order.

From the assumption that the phase transition is of first order on the chemical potential axis and of crossover type on the temperature axis, the existence of a critical point is inferred. This can be seen from an angle that associates the ending transition line with the chiral transition. The fact that we observe an ending transition line is owed to the explicit breaking of the chiral symmetry by non-zero

current quark masses in the QCD Lagrangian (see Sec. 1.1.1). From another angle the confinement-deconfinement transition may be considered to be at the origin of the ending transition line. Here the situation is similar, the corresponding symmetry (the Z(3) center of $SU(3)_c$) is explicitly broken by the presence of quarks with finite masses (see Sec. 1.2.3). Within the systematic errors and depending on which approximate order parameters are chosen, lattice QCD calculations indicate that the chiral and the deconfinement crossover transition are observed within a rather narrow corridor in the phase diagram. Yet, the existence and position of a critical end point is under intensive discussion.

In the t'Hooft limit[11] of large N_c it can be argued that chiral and deconfinement transitions remain completely separated [McL08]. In this limit the deconfinement transition should become independent of the quark chemical potential and remain at fixed temperature throughout the phase diagram. Chiral symmetry is broken once the Fermi sea of baryons fills up. This happens once $\mu_B > m_B$, where μ_B and m_B are baryon chemical potential and mass. At large chemical potentials and low temperatures matter is confined while chiral symmetry is spontaneously broken. This is in accordance with an argument by Gocksch and Ogilvie [GO85] who conclude that confinement implies chiral symmetry breaking. The author of Ref. [McL08] refers to this region of the (unphysical) phase diagram in the t'Hooft limit as quarkionic phase. Considering the possibility of the existence of this new quarkionic state of matter, one has to admit that there is no reason why chiral and deconfinement transitions have to coincide. Assuming that there is no first order phase transition on the temperature axis, which is supported by lattice QCD calculations, there still could exist separated first order phase transitions for chirality and confinement. Even though explicit symmetry breaking would prohibit the complete vanishing of the approximate order parameters (chiral condensate and Polyakov loop) they could still exhibit abrupt changes at different chemical potentials. Thus two critical end points are not ruled out. Even with only one order parameter several critical endpoints may appear which has been conjectured in Ref. [HTYB06]. It is also conceivable that distinct first order phase transitions for chirality and confinement surround an area in phase space. In principle a quarkionic phase could exist in such a bubble. However perfect confinement of this state of matter would be inhibited by the explicit symmetry breaking of the centre symmetry of $SU(N_c)$.[12]

On the experimental side scans of the phase diagram are proposed (e. g. the RHIC low energy run). New programs are also proposed, dedicated to the investigation of regions of high chemical potentials (e. g. CBM at the planned FAIR facility). It is very difficult, however, to construct an observable that represents a unique indicator for critical behaviour. So far statistical models are used to extract a lower bound for the deconfinement and chiral transition lines [BMRS04]. In Fig. 1.5 a graph taken from [BMRS04] is shown for orientation to indicate the lower bound of the actual phase transition. The distance from these freeze-out curves to

---

[11]$N_c \rightarrow \infty$, while $g^2 N_c$ remains finite.

[12]In the PNJL model calculations presented in this work (see Sec. 2.4) such a scenario cannot be realised as the Polyakov loop effective potential has been assumed to be independent of the quark chemical potential.
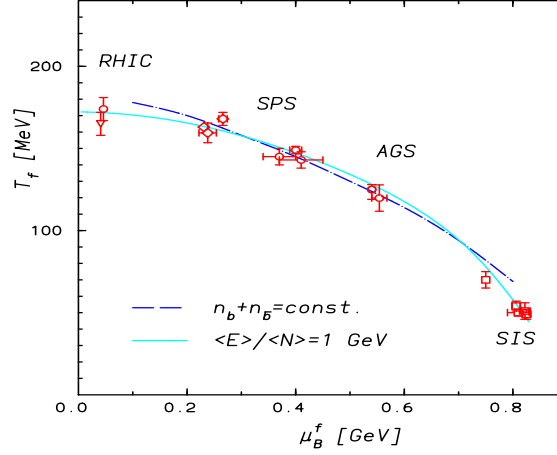
Figure 1.5: Reproduction of Fig. 28 in Ref. [BMRS04]. Comparision of two chemical freeze-out conditions: net baryon density $n_{\rm B} = 0.12\,{\rm fm}^3$ (dashed) and constant energy per particle $\simeq 1.0\,{\rm GeV}$ (solid).

the transition is an issue under debate. Detailed models are needed to extract more information on this issue (see discussion in Sec. 1.3.2). In theory it is foremost the lattice calculations that are expected to quantify the position of the critical end point. These calculations suffer, however, from the technical problems (sign problem, overlap problem etc.) discussed in Sec. 1.3.1.

1.4.2 Phase diagrams in "theory space"

An instructive extension to the phase diagram in the temperature chemical potential plane discussed in the previous section is the generalisation of this phase diagram using the physical parameters of QCD (the quark masses) as additional dimensions. In the temperature region below $1\,{\rm GeV}$ it is the up and down quark masses that are considered as parameters. The influence of the heavier quarks is assumed to be negligible. In this thesis, we focus on the two lightest quark flavours.

The two dimensional phase diagram discussed in Sec. 1.4.1 is extended by a third dimension, the mass of the two light quarks, up and down. The change of the current quark masses is of particular interest, first of all because the quark masses are the only parameter of QCD, and secondly because at the latest in the chiral limit (i. e. for vanishing up and down quark mass) the chiral phase transition has to switch from crossover to a true phase transition. In fact there is a new first order phase transition plane.[13] This plane appears in the region where the chiral

---

[13]A phase transition line in two dimensions can extend to an additional direction in a three dimensional parameter space. The line in two parameter dimensions is just a projection of a plane
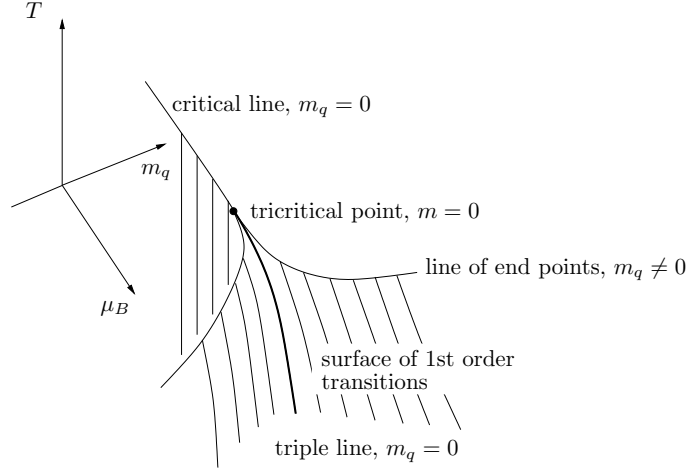
Figure 1.6: Reproduction of Fig. 4 in Ref. [Ste04]: A three-dimensional view (T, μ_B, m_q) of the QCD phase diagram near the tricritical point.

condensate $\langle \bar{\psi}\psi \rangle$ near $m_{\mathrm{q}} \equiv m_{\mathrm{u/d}} = 0$ is finite. At $m_{\mathrm{q}} = 0$ the chiral condensate switches sign which is the indication for non-analytic behaviour corresponding to a first order phase transition. Towards high temperatures the chiral condensate will drop to zero. The line delimiting the area where the chiral condensate is non-zero in the chiral limit, is a critical line. On this line bordering a first order phase transition plane the transition is of second order. Approaching the plane $m_{\mathrm{q}} = 0$ from finite quark mass the first order transition lines in the phase diagrams for temperature and chemical potential span a first order phase transition plane, too. Just as before this plane is bordered by a critical line of second order. The point where the three critical second order lines come together is a tricritical point. This tricritical point is discussed in more detail in Ref. [Ste04] and references therein. To illustrate this theoretical phase diagram in three dimensions, Fig. 4 of Ref. [Ste04] has been reproduced in Fig. 1.6.

Besides the extension of the QCD phase diagram in direction of the quark mass each model has intrinsic parameters which may be used to study aspects of QCD in terms of effective QCD parameters. As one example, QCD can be modelled in the low energy regime with gluons integrated out. The strengths of the remaining quark coupling constants can be used to extend the phase diagram in the plane of temperature and chemical potential. Such studies using Polyakov loop extended NJL models have been performed in Refs. [Fuk08b, Fuk08a]. In Ref. [Fuk08b] it is the strength of the t'Hooft coupling introduced to control the strength of the anomalous breaking of the axial $U(1)_A$ symmetry of QCD, that is used as an additional dimension in the phase diagram. In Ref. [Fuk08a] it is the effective four-quark vector coupling that is modelled. Interestingly these rather subtle changes produce large variations in the predicted phase diagrams. First of all this shall be taken as a warning, that modelling the QCD phase diagram is a very delicate issue, due to
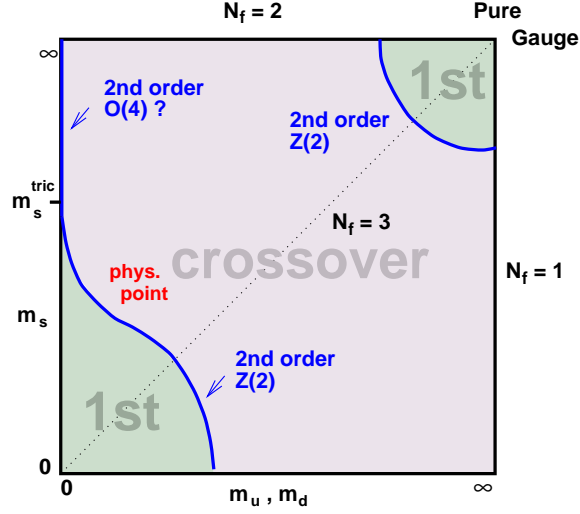
---

in three dimensions.

Figure 1.7: Columbia plot [B$^+$90] reproduced as shown in Fig. 1 in Ref. [dFP08]. The areas indicate the order of the phase transition at $\mu = 0$ as a function of the QCD parameters. At the scales below $1\,\text{GeV}$ only the light quark masses $m_\text{u} = m_\text{d} = 0$ and the strange quark mass $m_\text{s} = 0$ are of interest.

the high sensitivity of the order of phase transitions on small changes in an effective potential. Secondly Refs. [Fuk08b, Fuk08a] are credited here to give examples for the large variety of studies of the QCD phase diagram using models.

A further generalisation of the phase diagram is the so-called Columbia plot [B$^+$90]. In this plot the physical quantities accessible in experiments, temperature and chemical potential, are removed from the plot. Instead only the dependence on light and strange quark mass is plotted (see Fig. 1.7). The different areas in this figure indicate for which quark masses QCD would produce a first order, a second order or a crossover transition at $\mu = 0$. Sometimes the baryonic chemical potential is kept as third axis. The authors in Ref. [dFP08] claim that this generalised three dimensional Columbia plot indicates the non-existence of a critical point. Their line of reasoning starts from the observation that at $\mu = 0$ the physically realized quark masses lie in the crossover region. When expanding their lattice QCD results around $\mu = 0$ they observe a curvature of the plane separating quark mass values leading to crossover transitions and first order phase transitions that bends this separating plane away from the first order region. This would mean that even at higher chemical potentials no first order phase transition will set in removing the critical point from the phase diagram. The results are criticised for the fact that higher order terms could lead to a back-bending of the plane. When changing current quark masses in lattice QCD calculations lattice scales need re-adjustment. This re-adjustment, which is part of the renormalization procedure on the lattice, may influence the μ-expansion, such that the small curvature at vanishing μ changes sign. These issues are currently under discussion.

Chapter 2

Modelling QCD thermodynamics

The preceeding chapter has given a short overview of QCD. Solving QCD with its full complexity arising from the non-Abelian gauge symmetry is the task of numerical simulations on Euclidean space-time lattices. Such computations, however, do not give insights into a relevant physics question, namely to identify the most important degrees of freedom that govern the thermodynamics of QCD.

2.1 Simple models

One easy way to implement asymptotic freedom on the one hand and confinement on the other hand is achieved by the MIT bag model [CJJ+74, CJJT74, DJJK75]. In this model the two different phenomena are allowed to coexist by simply separating them in space. There are space regions where quarks and gluons exist in their deconfined realizations, and there are "bags" in which quarks and gluons are confined. The colour neutrality of the bags is not ensured by some dynamic mechanism as in QCD but merely postulated. To keep the quarks inside the bag and stop them from breaking up their colourless compound they are bound together by putting them in a cavity, the so-called bag. The ansatz for this bag is formulated covariantly by adding a constant term to the stress-energy tensor

$$T_{\text{in}}^{\mu\nu} = T_{\text{out}}^{\mu\nu} + g^{\mu\nu} B \ . \tag{2.1}$$

Here the stress-energy tensor $T^{\mu\nu}$ is defined in terms of the Lagrangian $\mathcal{L}$, the quark field q and the canonic 4-momentum π^μ of q by $T^{\mu\nu} = \pi^\mu \partial^\nu q - \delta^{\mu\nu} \mathcal{L}$. The pressure inside the bag is therefore reduced: $p_{\text{in}} = p_{\text{out}} - B$, while the energy density of the quarks inside the bag is increased: $\varepsilon_{\text{in}} = \varepsilon_{\text{out}} + B$. The size of the bag is then adjusted such that the total hadron energy made up by the quark localization energy and the contribution of the bag constant becomes minimal. This leads to a direct connection of the bag radius R_0 and the bag constant B: $R_0 \propto B^{1/4}$. Typical values for R_0 are $\lesssim 1\,\text{fm}$ and $B \approx (200\,\text{MeV})^4 \approx T_{\text{c}}^4$. This is equivalent to the statement that the mass of baryons and mesons is almost completely generated by the interaction energy and the large kinetic localization energy in the bag due to the uncertainty principle. The phase transition towards high temperatures and chemical potentials appears once temperatures and chemical potential reach the typical scale λ of the

bag constant, $B \approx \lambda^4$. Under these conditions the pressure of quarks inside a bag will surpass the pressure generated by the bags on the outside. The bags begin to vanish and the modelled hadronic confined phase makes way for deconfined quark matter. This implementation of the confinement-deconfinement phase transition in the bag model produces a first order phase transition, as entropy and density of the two phases differ in general.

As the bag model only knows inside and outside the bag, it is not able to produce quark properties in the transitional region of the confinement-deconfinement transition correctly. Quasiparticle models avoid this problem by turning to free quarks in the high temperature region. A simple approach is to adjust the dynamically generated mass of the quarks. This may be accomplished with the guidance from lattice QCD calculations. Using this pragmatic approach it is of no interest whether the quark mass generation is of perturbative origin or due to spontaneous (chiral) symmetry breaking.

More realistic approaches have been using perturbative techniques to find the effective quark mass above the transition temperature. Hard thermal loop (HTL) approximation is one of the main tools to perform such calculations [LB]. However these calculations are limited to the perturbative regime of QCD [PKS02, LH98]. It is an issue under debate down to what temperatures HTL approximation can be trusted. One way to extend the range of applicability and to improve the agreement with other approaches like lattice QCD calculations is to introduce factors modifying thermal distribution functions [SW01, TSW04]. Quasiparticle models have been applied to reproduce and predict many different quantities. Considering the studies of isovector quantities in Sec. 3.6 it is in order to refer to Ref. [BK08] presenting similar studies using a quasiparticle approach.

One can also think of the confinement-deconfinement transition as a percolation transition. The general concept of percolation is such that particles of a distinct size arrange in space arbitrarily according to some statistical distribution producing a given correlation function. Percolation appears once one cluster of particles is formed that dominates over all other clusters of particles. In case of the second percolation transitions this picture is inverted: it is not the particle clusters that percolate but the percolation of unoccupied, free space. Very simple percolation models for the confinement-deconfinement transition ask at which temperatures and chemical potentials percolation appears if space is filled up with free mesons and baryons. At zero chemical potential Ref. [CRS09] estimates the percolation temperature to be $T \approx 230 \, \text{MeV}$. When considering a hadron resonance gas this value decreases according to this reference to $T \approx 177 \, \text{MeV}$. The baryon critical chemical potential at zero temperature is estimated to be of the order of $\mu_B \approx 1.1 \, \text{GeV}$. In the context of such a percolation model a repulsive baryon interaction could explain the appearance of a critical endpoint [CRS09]. At low chemical potentials thermodynamics will be dominated by mesons that for the sake of their boson character like to cluster. Therefore the equation of state will not exhibit an inflection point allowing for only one minimum. At high chemical potentials and baryon densities the repulsive interaction could however be so important that this situation changes such that the equation of state becomes unstable and the system splits into two phases of distinct

density.

It is quite instructive to see that both bag model and percolation model produce rather similar transition temperatures and densities even though the origin of the induced phase transition is quite different. In the bag model the phase transition is governed by the interplay of bag constant, energy density and pressure. In a percolation model it is geometry and density that control the phases. Of course the assumed sizes of mesons and baryons is a crucial input value for the estimate in percolation models. In principle one can determine this size in terms of the baryon density or in terms of the range of colour correlations. In either case we end up with two very different transitions which correspond to the chiral and the deconfinement transitions. Percolation therefore provides an interesting way to relate particle sizes and correlation lengths to temperatures and densities. However this model is not able to explain the coincidence of chiral and deconfinement transitions nor give reasons for the absolute values of the length and energy scales involved.

2.2   The Nambu and Jona-Lasinio (NJL) model

The Nambu and Jona-Lasinio (NJL) model was first proposed as a model to describe nucleons and mesons [NJL61a, NJL61b], while the elementary particles of the model were interpreted as baryons having fermionic character. The mesons as bosons are created in this original version of the NJL model by a fermion-antifermion ladder in random phase approximation (RPA). Once the quark hypothesis had settled in the scientific community the NJL model seemed to be unsuited to describe strong interaction phenomenology and was abandoned. It was much later that the NJL model was revived and its elementary fermions were reinterpreted as quarks [HK84, Vol84]. The one feature of the NJL model that remains in both interpretations of the fermions is that the fermions are implemented chirally symmetric. The chiral symmetry of the underlying Lagrangian is the interface to the Lagrangian of QCD. What makes the NJL model so valuable for the intermediate energy range where QCD starts to become non-perturbative is spontaneous chiral symmetry breaking (see Sec. 2.2.1). Spontaneous symmetry breaking implies the existence of Goldstone bosons discussed in Sec. 2.2.2.

2.2.1   Quarks and mesons

Nambu and Jona-Lasinio models (in $N_{\mathrm{f}} = 2$ flavours) are based on Lagrangian densities of the form

$$\mathcal{L} = \mathcal{L}_{\mathrm{chiral}} + \mathcal{L}_{\mathrm{mass}} + \mathcal{L}_{\mathrm{I}} + \mathcal{L}_{\mathrm{I}}^{\mathrm{det}} \ . \tag{2.2}$$

The chiral part of the free Lagrangian $\mathcal{L}_{\mathrm{chiral}}$ is just the kinetic term for the fermions in the model and is equivalent to the corresponding part in the QCD-Lagrangian: $\mathcal{L}_{\mathrm{chiral}} = \bar{\psi}\, \slashed{\partial}\, \psi = \bar{\psi}\, (i\gamma_{\mu}\partial^{\mu})\, \psi$. Just as in QCD it is the mass term $\mathcal{L}_{\mathrm{mass}} = \bar{\psi}_{\mathrm{L}}\, m_0\, \psi_{\mathrm{R}} + \bar{\psi}_{\mathrm{R}}\, m_0\, \psi_{\mathrm{L}}$ that mixes fermion fields with right- and left-handed chirality (1.5). Thus $\mathcal{L}_{\mathrm{mass}}$ breaks the chiral symmetry explicitly. These two analogous terms in the NJL and the QCD Lagrangian motivated the interpretation of the NJL model as a model

for QCD. By construction the first interaction term $\mathcal{L}_{\mathrm{I}}$ shall only represent four-quark interaction terms of the form $\frac{1}{2}G_\Gamma \left(\bar{\psi}\, \Gamma\, \psi \right)^2$, where Γ is a structure in Dirac, flavour and colour space.[1] In the case used here to model QCD, Γ is set to $\gamma_\mu t_a$, where the t_a are the generators of $SU(3)_{\mathrm{c}}$ with implied summation over repeated indices μ and a. Such an interaction is motivated by one gluon exchange where the gluon is integrated out and contracted to a point. For momentum scales below the inverse correlation length of the field strength tensor this simplification can be justified. Lattice QCD results predict values of the order of $(0.2\,\mathrm{fm})^{-1} \approx 1\,\mathrm{GeV}$ for this inverse correlation length (see Sec. 1.2.3) which lies above typical NJL 3-momentum cutoffs.

The four-quark interaction terms have great impact on the realization of the chiral symmetry. The symmetries of interest are the flavour symmetries of QCD: $\mathcal{G} = U(N_{\mathrm{f}})_{\mathrm{R}} \times U(N_{\mathrm{f}})_{\mathrm{L}} = SU(N_{\mathrm{f}})_{\mathrm{V}} \times SU(N_{\mathrm{f}})_{\mathrm{A}} \times U(1)_{\mathrm{V}} \times U(1)_{\mathrm{A}}$. The interaction terms should be chosen such that the symmetry pattern of QCD is reproduced. A vector colour-current interaction term with $\Gamma = t_a \gamma^\mu$ (implying summation over μ and a) is indeed invariant under $\mathcal{G}$.

The last part of the Lagrangian as it is given in Eq. (2.2) only comprises maximally flavour mixing terms while explicitly avoiding to mix chiralities[2]. Maximal flavour mixing terms avoid breaking parts of the flavour symmetry other than $U(1)_{\mathrm{A}}$. Named after t'Hooft these terms are important in modelling the anomalous breaking of $U(1)_{\mathrm{A}}$ in QCD. The maximal mixing of flavour is achieved by a total anti-symmetrisation in flavour space which can be enforced using the determinant in flavour space $\det_{\mathrm{f}}$:

$$\mathcal{L}_{\mathrm{I}}^{\mathrm{det}} = K \left(\det{}_{\mathrm{f}} \left[\bar{\psi}(\mathbb{1} + \gamma_5)\psi \right] + \det{}_{\mathrm{f}} \left[\bar{\psi}(\mathbb{1} - \gamma_5)\psi \right] \right) \ . \tag{2.3}$$

In $N_{\mathrm{f}} = 2$ flavours this term looks rather simple: $\mathcal{L}_{\mathrm{I}}^{\mathrm{det}} = \frac{1}{2}K[(\bar{\psi}\psi)^2 + (\bar{\psi}i\gamma_5\vec{\tau}\psi)^2 - (\bar{\psi}i\gamma_5\psi)^2 - (\bar{\psi}\vec{\tau}\psi)^2]$.

Due to the local character of the interaction terms, a Fierz rearrangement of the fermion fields in the covariant four-quark colour current interaction does not change the general form of the interaction. A Fierz rearrangement interchanges direct and exchange terms, i.e. transforms Hartree to Fock terms and vice versa. Adding the Fierz transformed interaction Lagrangian to the original Lagrangian does not change the character of the interaction in Hartree or Hartree-Fock approximation.

The Fierz rearrangement of a colour current interaction can be found in the Appendix of Ref. [Bub05] or similar review articles. As long as we are interested in the model only on mean field level, it is legitimate to neglect all terms which do not lead to non-vanishing mean fields. In this work the approximation is taken somewhat further neglecting terms with non-significant condensation. The Lagrangian used for the actual modelling of QCD first of all contains chiral $SU(2)_{\mathrm{R}} \times SU(2)_{\mathrm{L}}$ invariant interaction terms already implemented by Nambu and

---

[1]The original NJL model used two structures $\Gamma = \mathbb{1}$, and $\Gamma = i\gamma_5\vec{\tau}$. The first one is essential to create spontaneous chiral symmetry breaking, the second one is responsable for the proper generation of mesons in the RPA formalism.

[2]Keeping right and left handed quarks separated is achieved here by adding two individual terms, explicitly making use of projection operators on right and left chirality $\mathcal{P}_{\mathrm{L/R}} = \frac{1}{2}(\mathbb{1} \pm \gamma_5)$

Jona-Lasinio [NJL61a, NJL61b]:

$$\mathcal{L}_{\mathrm{I}} = \frac{G}{2} \left[\left(\bar{\psi}\psi \right)^2 + \left(\bar{\psi} i \gamma_5 \vec{\tau} \psi \right)^2 \right] \ . \tag{2.4}$$

This interaction term is in fact already $U(1)_{\mathrm{A}}$ breaking such that an additional determinant interaction term is not needed.[3] For the general discussion of the NJL model in this chapter no additional interaction terms are included. However this will be done in Chapt. 3 to take into account degrees of freedom important at high quark chemical potentials.

At mean field level the only effects that contribute to quark dynamics other than the terms bilinear in the quark fields are effects generated by a shift of some vacuum expectation value. The shift in a vacuum expectation value appears whenever the vacuum spontaneously breaks a symmetry of the Lagrangian density. In the NJL calculation with $N_{\mathrm{f}} = 2$ flavours such a shift of vacuum expectation values can be accounted for using a Hubbard-Stratonovic transformation. This transformation removes the four-quark interaction terms by introducing an auxiliary boson field. Free quarks in the NJL model corresponding to free quarks in QCD turn into quasiparticles when transformed. The quark quasiparticle hypothesis can only hold in a certain energy range. The transformation of the quark fields therefore limits the range of applicability of the NJL model to scales where deconfinement has set in while perturbative effects are still dominated by first order chiral effects.

In a Hubbard-Stratonovic transformation one uses the fact that the integral

$$\int \mathrm{d}\phi_a \exp \left[-\frac{G}{2} \left(\bar{\psi} \Gamma_a \psi - \phi_a \right)^2 \right] = \mathcal{N} \tag{2.5}$$

evaluates to a constant $\mathcal{N}$. Therefore this integral can be multiplied with the partition function without changing physics. At the same time this method introduces the auxiliary field ϕ_a, which should be integrated out. An appropriate choice of G however allows to remove all four-quark interaction terms leaving only the terms bilinear in $\bar{\psi}$ and ψ. It is the bilinear coupling term of the quarks to the new auxiliary field that modifies the quarks from free (NJL) quarks to constituent quarks as quasiparticles. It is said that constituent quarks move in a background field. Background fields are a specific way to describe the properties of a vacuum state which breaks a symmetry of the Lagrangian. The perturbative vacuum combined with an auxiliary boson field can account for different vacuum states. In this sense the auxiliary boson field is part of the vacuum description and not a degree of freedom of the Lagrangian. The integration over the auxiliary field weighted thermodynamically allows to construct an approximation to the proper vacuum state.

A significant further approximation can be performed if the thermodynamic weight is well localised around one field configuration. In mean field approximation only this most important field configuration is used to approximate the weighted integral. Four-quark coupling channels with small coupling strengths inducing only

---

[3]In $N_{\mathrm{f}} = 2$ there is in fact no meson mode which could be used to anchor physical input for an additional $U(1)_{\mathrm{A}}$ breaking strength.

small quark-antiquark or quark-quark correlations may safely be neglected, as additional variations in these channels usually do not improve the mean field approximation significantly. This is the case if the potential is already very close to minimal, i. e. if the curvature of the potential and the field values are small. The configuration with maximal weight satisfies the so-called mean field or gap equation, which is the necessary condition for the minimisation of $\mathcal{S}_{\mathrm{E}}(\phi_a)$:

$$\left.\frac{\partial \mathcal{S}_{\mathrm{E}}(\phi_a)}{\partial \phi_a}\right|_{\phi_a=\phi_{a,\,\mathrm{MF}}} = 0 \ . \tag{2.6}$$

After bosonisation and optimisation only bilinear terms in the fermion fields remain, such that the fermion fields can be integrated out. The calculus of Grassmann variables [LB] allows to write

$$\int \mathcal{D}\psi \int \mathcal{D}\bar{\psi} \ e^{-\bar{\psi}\left(\beta S^{-1}\right)\psi} = \det\left[\beta S^{-1}\right] \ . \tag{2.7}$$

Using the relation $\log \det = \mathrm{tr} \log$ the determinant can be evaluated. We can now evaluate the effective action (with respect to the fermion fields):

$$\mathcal{S}_{\mathrm{eff}}(\phi_a) = -\log \mathcal{Z} = \log \int \mathcal{D}\psi \int \mathcal{D}\bar{\psi} \ e^{-\mathcal{S}_{\mathrm{E}}(\phi_a)}$$

$$= -\log \widetilde{\det}\left[\beta S^{-1}(\phi_a)\right] + \frac{\phi_a^2}{2G} = -\widetilde{\mathrm{Tr}} \log\left[\beta S^{-1}(\phi_a)\right] + \frac{\phi_a^2}{2G} \ , \tag{2.8}$$

where all quantities still depend on the vacuum configuration parametrised by ϕ_a. Applying mean field approximation this is the effective action realized by a vacuum that may develop a non-zero expectation value of ϕ_a.

Another way of finding how a NJL quark effectively propagates in the vacuum (i. e. to find the correct quasiparticle) is to apply recursive equations that have to be solved self consistently. The propagator of the quasiparticle quark is derived from the bare NJL-quark using a Dyson Schwinger equation

$$\tag{2.9}$$

where the thick lines depict full quark quasiparticle propagators, while thin lines are bare quark propagators. Multiplication from the left with an inverse bare and from the right with an inverse quasiparticle propagator plus some algebraic rearrangement allows to rewrite this as

$$\Sigma = G\,\Gamma\,\widetilde{\mathrm{Tr}}\left[S\,\Gamma\right] \qquad \text{with} \qquad S^{-1} = \slashed{p} - m_0 - \Sigma \ , \tag{2.10}$$

where S^{-1} denotes the quasiparticle propagator and Γ is the Dirac, colour and flavour structure in the four-quark coupling channel. For $\Sigma = \Gamma\,\phi_a$ the two formulations of the gap equations (2.9) and the minimisation of Eq. (2.8) are equivalent, if all Γ are chosen orthogonal $(\mathrm{tr}\left[\Gamma\,\tilde{\Gamma}\right] = 0)$[4].

---

[4]If all mean fields can be assigned with distinct and unique sets of quantum numbers this orthogonality is granted.

The trace $\widetilde{\mathrm{Tr}}$ is understood as a trace over all space: functional space, Dirac, colour and flavour. The functional trace at finite temperature transforms to an infinite summation over Matsubara frequencies[5] and integration over momentum space:

$$\widetilde{\mathrm{Tr}}[\cdots]_{T\neq 0} = T \sum_{\omega_n} \int \frac{\mathrm{d}^3 p}{(2\pi)^3} \cdots \qquad\qquad \widetilde{\mathrm{Tr}}[\cdots]_{T=0} = \int \frac{\mathrm{d}^4 p}{(2\pi)^4} \cdots \qquad (2.11)$$

In the NJL model the summation and integration over one quark loop is not convergent. The usual way to deal with this in a quantum field theory is the renormalisation proceedure. In principle this could be done in the NJL model as well. This would imply that the coupling strength and regularisation scale are no independent quantities but connected by the constraint of a physical observable that the model would have to match at some scale. It turns out, however, that there are too many physical observables and other relevant quantities to be reproduced: pion mass, pion decay constant, chiral condensate and constituent quark mass ($M \approx \frac{1}{3} M_{\mathrm{N}}$). Even though the current quark mass is another parameter that can be used to match the model to nature the problem remains overdetermined. It is not possible to reproduce all physical quantities while keeping the degree of freedom in the regularisation scale. From another point of view the problem is that QCD and the NJL model do not show the same scale dependence. If the pion decay constant as a physical observable[6] is kept at its physical value, the chiral condensate as a scale dependent quantity shows different scale dependence in NJL model and in QCD. Therefore we do not allow the NJL parameters to run. Instead the regularisation scale is fixed and treated as an ordinary model parameter. The NJL model is regularised not renormalised.

With these considerations in mind the quantities used to fix the NJL parameters have to be evaluated in the model framework. The physical entities that have to be reproduced are the pion decay constant, the pion mass and the chiral condensate at some low energy scale. The simplest way to couple meson fields to quarks is a piece in the Lagrangian of the form [Kle92]:

$$\mathcal{L}_{\pi qq} \propto g_{\pi qq} \, \bar{\psi} \left(\gamma_5 \vec{\tau} \cdot \vec{\pi} \right) \psi \ , \qquad (2.12)$$

with the pion to quark coupling strength $g_{\pi qq}$ and $\vec{\tau} \cdot \vec{\pi} = \tau^1 \pi^1 + \tau^2 \pi^2 + \tau^3 \pi^3 = \tau^+ \pi^+ + \tau^3 \pi^0 + \tau^- \pi^-$. Here π^+, π^- and π^0 are meson (pion) field operators. Using the bosonisation proceedure in the four-quark coupling channel $\left(\bar{\psi} \, \gamma_5 \, \tau_a \, \psi \right)^2$ as shown above, such a term is indeed produced. The meson (pion) fields are introduced in a Hubbard-Stratonovic transformation introducing a self interaction term for each meson (pion) field of the form $\frac{\vec{\pi}^2}{2G}$. As there are no isospin breaking terms, vacuum expectation values in the pion channel vanish for $\mu_{\mathrm{I}} \leq m_\pi$. There are two ways to derive the meson (pion) propagator: the first one uses a recursive formulation of quark loops, the other one is a direct derivation from the quark effective action (2.8).

---

[5]The Matsubara frequencies for fermions (bosons) are $\omega_n = (2n+1)\pi T$ ($\omega_n = 2n\pi T$) with $n \in \mathbb{Z}$.

[6]The pion decay constant being a low energy limit is necessarily scale invariant.

Further details on the evaluation of the pion propagator can be found in App. A.1 or in various reviews on the NJL model [KLVW90, VLKW90, VW91, Kle92, Bub05]. Only the final result is quoted here.

$$m_\pi^2 = \frac{m_0}{M} \frac{1}{2\,G\,N_{\rm c}\,N_{\rm f}\,I_2(m_\pi^2)} \qquad\qquad f_\pi^2 = 4\,N_{\rm c}\,M^2\,I_2(0) \; , \qquad (2.13)$$

where we have defined the integral I_2 in the zero-temperature[7] case by

$$I_2(q) = -i \int \frac{{\rm d}^4 p}{(2\pi)^4} \frac{1}{\left[(p+\frac{q}{2})^2 - M^2\right]\left[(p-\frac{q}{2})^2 - M^2\right]} \qquad (2.14)$$

The derivation of the Gell-Mann-Oakes-Renner (GMOR) [GMOR68] relation and the Goldberger-Treiman relation are reproduced in the Appendix (see App. A.1 and Refs. [KLVW90, VLKW90, VW91, Kle92, Bub05]).

2.2.2 Meson properties in the NJL model

Using the formulae given in Sec. 2.2.1 it is possible to vary the parameters of the NJL model (m_0, G and Λ) such that physical quantities are reproduced. Of primary importance are pion mass m_π and pion decay constant f_π as they are scheme invariant quantities. But also the constituent quark mass $M \approx \frac{1}{3}M_{\rm N}$ and the chiral condensate $\langle\bar{\psi}\psi\rangle$ should be reproduced as accurate as possible. Due to the overdetermination of this problem it will only be possible to find a parameter set which reproduces these quantities to a certain accuracy. The standard parameters used here are the ones given in Tab. 2.1 and Ref. [RTW06]. If these parameters are used to evaluate the pion mass m_π and the pion decay constant f_π as function of temperature (at $\mu = 0$) the behaviour shown in Fig. 2.1 is found. In the phase of broken chiral symmetry we find a light pion and a heavy sigma boson. Above threshold temperature the pion becomes lighter than two constituent quarks, kinematically allowing for a decay of the pion into two quarks. In the NJL case we find $T_{\rm thr} \approx 187\,{\rm MeV} \gtrsim T_{\rm c} \approx 177\,{\rm MeV}$, where $T_{\rm c}$ is defined as the crossover temperature of the chiral phase transition using the quark mass susceptibility as indicator for the transition.[8] The NJL model always ensures $m_\sigma^2 = m_\pi^2 + M^2$ enforcing that at any time the decay of the sigma mode into a quark-antiquark pair is kinematically allowed.

2.3 The Polyakov loop model

The Polyakov loop model is motivated by the observation that the Polyakov loop defined in Eq. (1.29) can be used as an order parameter for confinement [Pol78, Sus79, SY82]. In Refs. [Pol78, Sus79, SY82, Sve86] the Polyakov loop is used to build an effective model for $SU(3)_{\rm c}$ gauge theories. At higher temperatures we

---

[7]At finite temperature I_2 is transformed to $I_2(q) = \sum_n \int^\Lambda \frac{{\rm d}^3 p}{(2\pi)^3} \frac{1}{[\omega_n^2 + \vec{p}^2 + M^2][(\omega_n - \omega)^2 + (\vec{p} - \vec{q})^2 + M^2]}$.

[8]Interestingly the relation $T_{\rm thr} \gtrless T_{\rm c}$ is inverted in the PNJL model described in Sec. 2.4.
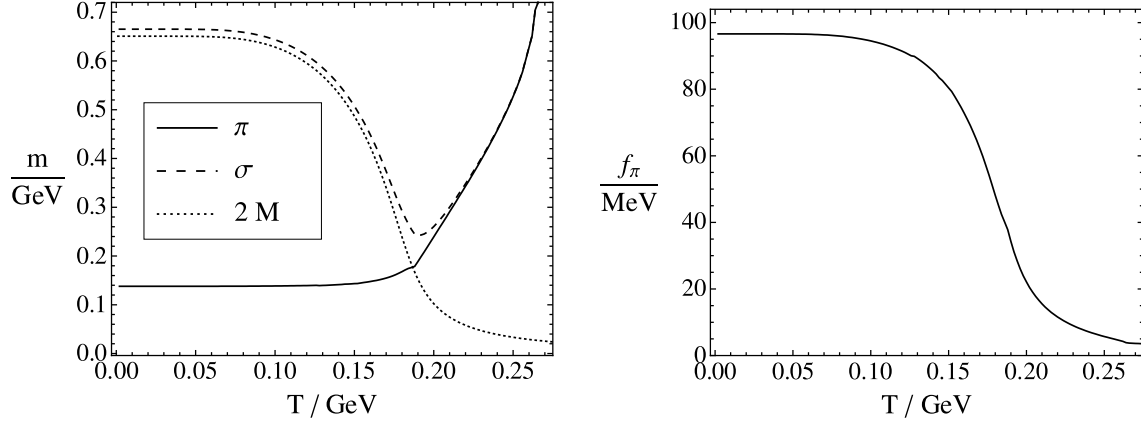
Figure 2.1: The pion mass (solid, left) and the pion decay constant (right) as functions of temperature at vanishing chemical potential. The standard set of NJL model parameters was used to evaluate the pion properties. On the left the pion mass is compared to the sigma meson mass (dashed) and twice the constituent quark mass (dotted). The decay of pions into a quark pair at low temperature is only kinematically forbidden; at temperatures above $T_{\mathrm{thr}} \approx 187\,\mathrm{MeV} \gtrapprox T_{\mathrm{c}} \approx 177\,\mathrm{MeV}$ this decay channel is coming on shell.

Λ [GeV]	G $\left[\mathrm{GeV}^{-2}\right]$	m_0 [MeV]
0.651	10.08	5.5

$\left\|\langle \bar{u}u \rangle\right\|^{\frac{1}{3}}$ [GeV]	f_π [MeV]	m_π [MeV]
0.251	94.0	140.5

Table 2.1: NJL model parameters (top) reproducing the physical quantities (bottom), resulting in a constituent quark mass of $M = 0.325\,\mathrm{GeV}$ ($N_{\mathrm{f}} = 2$ and $N_{\mathrm{c}} = 3$) [RTW06].

expect that all gauge degrees of freedom are excited equally. In this temperature regime other degrees of freedom are needed to describe the system exhaustively.

It has been outlined in Sec. 1.2.3 that the Polyakov loop can be used as order parameter of confinement, with $\langle\Phi^*\rangle = \langle\Phi\rangle = 0$ implying confinement. The quantitative information in $\langle\Phi^*\rangle > 0$ and $\langle\Phi\rangle > 0$ can be used to describe the vicinity of the phase transition.[9] Around the transition a so-called strong coupling expansion can approximate the system with Polyakov loop degrees of freedom only [Pol78, Sus79]. The strong coupling expansion is based on large (diverging) field strength correlation lengths. In this approximation the temporal extend of Euclidean space-time may be considered small. Large field strength correlation lengths imply slowly changing gauge fields. This only allows for large (but almost constant) gauge field values in Euclidean time direction, resulting in non-trivial values of the Polyakov loops.[10] Pure gluonic systems do not appear in nature. Therefore one has to rely on the results of lattice calculations [B+96, KKPZ02]. As these calculations without quarks do not face the difficulty of approximating the fermion determinant they are believed to be very accurate and reliable. The calculations indicate that the deconfinement transition in the absence of quarks is of first order and appears at $T_0 = 270\,\text{MeV}$. The available lattice data only constrain the potential at temperatures around and above the transition temperature T_0. At low temperatures, where the Polyakov loop vanishes, predictions on the loop susceptibilities strongly rely on the functional form of the potential. The single minimum at $\Phi = 0$ in the effective potential plotted in Fig. (2.3) is independent of the steepness of the potential.

The quickest way to arrive at an effective potential is to start immediately with an ansatz for the functional form of the effective potential adjusting its parameters to physics input in Ginzburg-Landau manner. In such a potential all terms in agreement with the realized symmetries have to be considered. In the present case of a pure gluonic system this is the center of the gauge group. The effective potential has to be a polynomial in $\Phi^*\Phi$, Φ^{*3} and Φ^3. A minimal polynomial has to comprise at least terms up to fourth order to allow for a first order phase transition.[11] Each term is assigned a temperature[12] dependent prefactor. Considering the fact that Φ^* and Φ are traces of $SU(3)_\text{c}$ matrices implies restrictions on the functional form of the potential. The group volume of $SU(3)_\text{c}$ results in a term in the potential of the form $\log\left[J(\Phi,\Phi^*)\right]$, where $J(\Phi,\Phi^*) = 1 - 6\Phi^*\Phi + 4\left(\Phi^{*3} + \Phi^3\right) - 3\left(\Phi^*\Phi\right)^2$ [Fuk04]. As this term already incorporates fourth order terms, it is sufficient to add a second

---

[9]This statement is true, if the Polyakov loop degrees of freedom are a complete set of order parameters. This is the case once there is no other symmetry which is broken alongside the $Z(3)$-center symmetry of $SU(3)_\text{c}$, i.e. if we are dealing with a single transition and not with several transitions that accidentally coincide.

[10]Large values of the spatial gauge fields would imply strong spatial colour correlations, which have not been observed. As Euclidean time is a ficticious functional dependence, introduced only to respect the the quantum character of the theory, large gauge fields do not result in physically observable colour correlations.

[11]An effective potential leading to a first order phase transition has to produce at least two degenerate local minima. A more detailed discussion of the effect of these terms can be found in Ref. [Sve86].

[12]In presence of quarks temperature and chemical potential dependence are required.

order term with a temperature dependent strength to induce a first order phase transition. A second order term ($\Phi^*\Phi$) is the leading order in a strong coupling expansion.

As the group volume is fixed the prefactor of $\log\left[J(\Phi, \Phi^*)\right]$ has to follow the temperature dependence $\propto T$. The simplest approach for the modelled $\Phi^*\Phi$-dependence is a polynomial ansatz. Using such an ansatz it is possible to adjust the parameters such that lattice data are reproduced to astonishing accuracy. This has been done in Ref. [RRW07b], from where we adopt the form of the Polyakov loop effective potential:

$$\frac{\mathcal{U}(\Phi, T)}{T^4} = -\tfrac{1}{2}a(T)\,\Phi^*\Phi + b(T)\,\ln\left[1 - 6\,\Phi^*\Phi + 4\left(\Phi^{*3} + \Phi^3\right) - 3\left(\Phi^*\Phi\right)^2\right]\;, \quad (2.15)$$

where the prefactors are given by

$$a(T) = a_0 + a_1\left(\tfrac{T_0}{T}\right) + a_2\left(\tfrac{T_0}{T}\right)^2 \qquad \text{and} \qquad b(T) = b_3\left(\tfrac{T_0}{T}\right)^3. \qquad (2.16)$$

In Ref. [RRW07b] the values for these coefficients have been adjusted to reproduce lattice data [B$^+$96, KKPZ02] (see Tab. 2.2 with error estimates given in Ref. [RRW07b]).

As can be seen from Fig. 2.4 the Polyakov loop model is able to reproduce lattice data for pressure, entropy density and energy density [B$^+$96] as well as lattice data [KKPZ02] for the expectation value of the Polyakov loop (Fig. 2.5). While adjusting the parameters several constraints were imposed in Ref. [RRW07b].[13] The $Z(3)$-center symmetry of the Polyakov loop effective potential and the $SU(3)_{\rm c}$ volume constraints are illustrated in Fig. 2.2 [RHRW08].

Of course this ansatz is limited in its applicabiltity to a finite temperature range. The argument that the Polyakov loop (as an order parameter for deconfinement) is well-suited to describe gluon dynamics is only true close the deconfinement phase transition. At high temperatures one expects all gluonic degrees of freedom to contribute equally to the thermodynamic properties of the system. The reason why the Polyakov loop model works so well even at high temperatures remains unknown. In this work all conclusions are restricted to the temperature range well below the NJL cutoff. Other forms of the potential which are strictly derived from strong coupling expansions [Fuk04, HF04] do not reproduce the Stefan-Boltzmann limit. However in the temperature region of interest (well below the NJL cutoff) the models in Ref. [Fuk04, HF04] and Ref. [RRW07b] do not differ significantly.

2.4 The Polyakov loop extended NJL model

In the effort to model the thermodynamics of QCD two main features of QCD have to be implemented. On the one hand the chiral properties of QCD have to

---

[13]In Ref. [RRW07b] it was made sure that a first order phase transition appears at $T = T_0$. This leads to a constraint which can be frased numerically by the relation $b_3 = -0.108\,(a_0 + a_1 + a_2)$. Additionally the potential was required to reproduce the Stefan-Boltzmann limit which is enforced by $a_0 = \frac{16\pi^2}{45}$.

a_0	a_1	a_2	b_3
$\frac{16\pi^2}{45} \approx 3.51$	-2.47	15.2	-1.75
—	$6\,\%$	$3\,\%$	$2\,\%$

Table 2.2: The parameters used in Ref. [RRW07b] which reproduce [B$^+$96, KKPZ02] lattice data for Polyakov loop and the equation of state. Requiring a first order phase transition at $T = T_0$ leads to the constraint $b_3 = -0.108\,(a_0 + a_1 + a_2)$. a_0 is fixed by virtue the Stefan-Boltzmann limit.
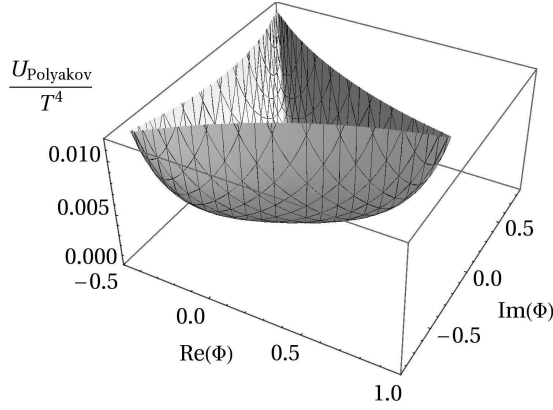

Figure 2.2: The Polyakov loop potential $\mathcal{U}(\Phi, \Phi^*, T)/T^4$ plotted in the complex plane of Φ at $T = T_0 = 0.27\,\mathrm{GeV}$ [RHRW08].
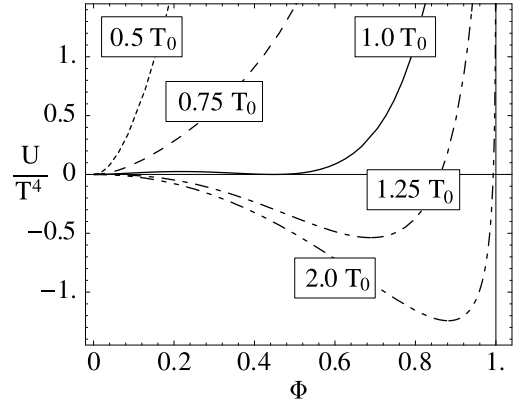
Figure 2.3: Resulting effective potential (2.15) that drives spontaneous Z(3) symmetry breakdown at $T = T_0$.
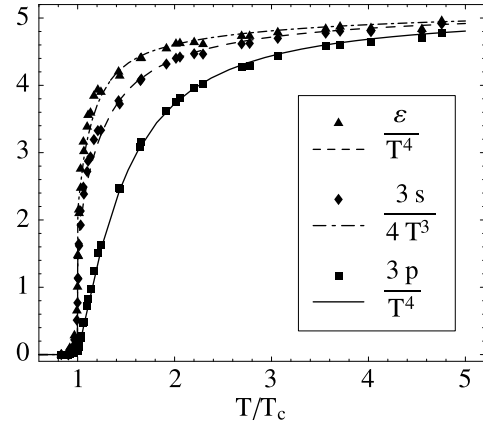
Figure 2.4: Fit to scaled pressure, entropy density and energy density as functions of the temperature in the pure gauge sector, compared to the corresponding lattice data taken from Ref. [B$^+$96].
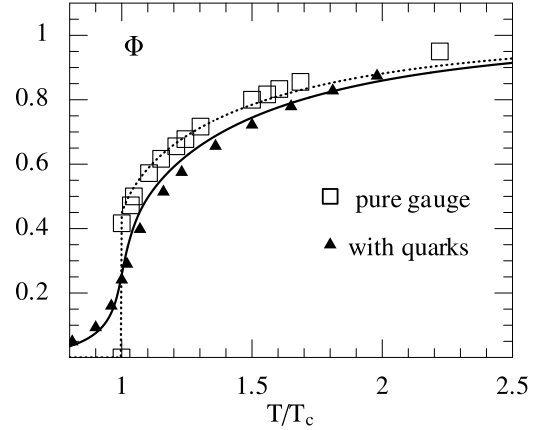
Figure 2.5: The Polyakov loop evaluated in the Polyakov loop model (dotted line) and the PNJL model (solid line) is compared to lattice results for the pure gauge sector [KKPZ02] (empty symbols) and to lattice results incuding dynamical quarks [KZ05] (full symbols).

be respected, on the other hand aspects of confinement have to be included. In quasiparticle models [TSW04] confinement can be accounted for by an additional factor controlling the thermodynamic multiplicity of quarks. Such a mechanism suppresses the thermodynamic weight of free quarks in regions where quarks should feel the onset of confinement. The QCD situation can also be approached from the Polyakov loop side. Here QCD is approximated by implementing the explicit Z(3) breaking effects of dynamic quarks[14]. Starting from the interpretation of the Polyakov loop as the partition function of a static quark, the free energy of a quark is influenced by a finite quark chemical potential. This point of view leads to the formal substitution rules $\Phi \to e^{\mu/T}\Phi$ and $\Phi^* \to e^{-\mu/T}\Phi^*$. Now it is the Polyakov loop that obtains a control factor, namely the quark fugacity, enhancing or suppressing its influence on the properties of the system. This approach has been chosen in Ref. [DPZ05] to study matrix models of SU(N) gauge theories. The ansatz presented here balances these two ways by joining a quark model (the NJL model) and a Polyakov loop model [MO96, MOM04].

2.4.1 Coupling Polyakov loops to quarks: the PNJL model

As the NJL model and the Polyakov loop model shall be unified, the total effective action of the new composite model shall comprise both individual actions. The simple summation of the two actions however does not produce any interaction between the degrees of freedom. In QCD quarks are coupled to the gluonic sector of the Lagrangian via the minimal gauge-covariant substitution which is the principle to be adopted here. Even though the gluons have been integrated out in the NJL model the partial derivative ∂^μ can still be substituted by a covariant derivative $D^\mu = \partial^\mu + iA^\mu$ connecting the quarks to an additional gluon field. In the definition of the covariant derivative D^μ the QCD coupling constant g has been absorbed into the gauge field A^μ. On the other hand the Polyakov loop defined in Eqs. (1.29) and (1.30) is a gauge link which establishes the connection around the Euclidean time torus. For simplicity the spatial dependence of the Polyakov loop is neglected such that the Polyakov loop can be parametrised in Polyakov gauge by only two real degrees of freedom. On the one hand we are dealing with Φ^* and Φ, on the other hand Φ^* and Φ can be parametrised by the zero momentum gauge fields in Euclidean time direction $A_4^{(3)}$ and $A_4^{(8)}$. A_4 has two components, $A_4^{(3)}$ and $A_4^{(8)}$, corresponding to the two diagonal SU(3) generators λ_3 and λ_8 in Gell-Mann representation. The simplified Polyakov loop is defined by

$$\Phi = \frac{1}{N_c} \exp\left[\frac{i}{T}\left(A_4^{(3)}t_3 + A_4^{(8)}t_8\right)\right] = \frac{1}{N_c}\exp\left[i\left(\phi_3\lambda_3 + \phi_8\lambda_8\right)\right] , \qquad (2.17)$$

where we use the definition $\phi_3 = A_4^{(3)}/(2\,T)$ and $\phi_8 = A_4^{(8)}/(2\,T)$. With this approximation of the Polyakov loop the minimal substitution has to be carried out in the temporal directions with diagonal colour representations. Using the Matsubara formalism we find a substitution rule of the form $\omega_n \to \omega_n + A_4$ with $A_4 = A_4^{(3)}t_3 + A_4^{(8)}t_8$.

---

[14]In contrast to infinitely heavy, static quarks, dynamic quarks with finite quark mass break the Z(3) symmetry.

This proceedure results in the PNJL action

$$\mathcal{S}_{\text{PNJL}} = \frac{V}{T}\mathcal{U}\left(\Phi,\,\Phi^*,\,T\right) - \frac{V}{2}\sum_n\int\frac{\mathrm{d}^3p}{(2\pi)^3}\text{Tr}\ln\left[\beta\tilde{S}^{-1}\right]\Big|_{\omega_n\to\omega_n+A_4} + \mathcal{V}\,, \quad (2.18)$$

where $\tilde{S}^{-1}$ is the inverse quasiparticle quark propagator and $\mathcal{V}$ is the potential in the boson fields produced during bosonization. In the quasiparticle quark propagator both the Matsubara frequency ω_n and the quark chemical potential μ appear as prefactors of the Dirac structure γ_0: $\tilde{S}^{-1} = \cdots i\gamma_0\omega_n + \gamma_0\mu\cdots$, such that a shift in ω_n by A_4 can be reinterpreted as a shift of the quark chemical potential μ by $-iA_4$. It is therefore possible to use the effective action derived in the NJL model for the Polyakov-loop extended NJL model by formally shifting the chemical potential:

$$\mathcal{S}_{\text{PNJL}} = \frac{V}{T}\mathcal{U}\left(\Phi,\,\Phi^*,\,T\right)\,+\,\mathcal{S}_{\text{NJL}}\big|_{\mu\to\mu-iA_4}\,. \quad (2.19)$$

Of course the substitution $\mu\to\mu-iA_4$ is different for each colour as $A_4 = A_4^{(3)}t_3 + A_4^{(8)}t_8$ is a quantity with non-trivial colour structure.

2.4.2 The fermion sign problem in the PNJL model

The action of the NJL model $\mathcal{S}_{\text{NJL}}$ is by construction an analytic function in μ_a, where μ_a is the chemical potential for quarks with colour a. For real values of the quark chemical potentials the action $\mathcal{S}_{\text{NJL}}$ is real valued. The analyticity of $\mathcal{S}_{\text{NJL}}$ in μ_a implies that once we choose $\mu_a\in\mathbb{C}$ we cannot expect $\mathcal{S}_{\text{NJL}}$ to remain real. The variations of μ_a in the complex plane are constraint by the fact that $A_4 = A_4^{(3)}t_3 + A_4^{(8)}t_8$, where A_4 can only vary in two real degrees of freedom. There is no reason why this constraint could prevent the potential $\mathcal{S}_{\text{NJL}}$ from assuming complex values. Nevertheless, complex values of the action $\mathcal{S}_{\text{PNJL}}$ do not imply unphysical behaviour as $\mathcal{S}_{\text{PNJL}}$ is only an effective action with respect to the quarks which have been integrated out after bosonization. The auxiliary boson fields introduced by bosonization have not been integrated out at this stage. The analytic properties of $\mathcal{S}_{\text{PNJL}}$ require that inversion of the sign of A_4 (complex conjugation of $\tilde{\mu} = \mu - iA$) leads to the complex conjugate of the effective action $\mathcal{S}_{\text{PNJL}}$.[15] If the gauge fields $A_4^{(3)}$ and $A_4^{(8)}$ are integrated out one can find another set of values of $A_4^{(3)}$ and $A_4^{(8)}$ for which the action is exactly the complex conjugate of the original value. It is therefore possible to construct an explicitly real integrand.

The situation in lattice QCD calculations is very similar to this one: In lattice QCD calculations the fermions are integrated out analytically, while the integration over the gauge fields is performed using Monte Carlo methods. Once the quark chemical potential becomes finite the lattice action becomes complex. In lattice QCD this problem is referred to as the fermion sign problem. The fermion sign problem also arises in the PNJL model, where it can be addressed with less effort. One possible approach not applicable to lattice QCD calculations will be discussed

---

[15] $\mathcal{S} = \sum_n a_n x^n \Rightarrow \sum_n a_n x^{*n} = \mathcal{S}^*$ with $a_n\in\mathbb{R}$.

in detail in the following section. For the time being we establish a zeroth order approximation suppressing the fermion sign problem. This lowest order approximation retains the identification of the action with the pressure: $p = -\frac{T}{V}\mathcal{S}_{\mathrm{bos}}$, where $\mathcal{S}_{\mathrm{bos}}$ is the effective action[16] after bosonization. One straight forward way to define a mean field thermodynamic potential Ω_{MF} and a mean field action $\mathcal{S}_{\mathrm{MF}}$ is to truncate imaginary parts

$$\Omega_{\mathrm{MF}} = \frac{T}{V}\mathcal{S}_{\mathrm{MF}} = \mathrm{Re}[\Omega_0] = \frac{T}{V}\,\mathrm{Re}[\mathcal{S}_{\mathrm{bos}}] \ . \tag{2.20}$$

Of course this truncation of the imaginary parts is a rather crude approximation. In the present model the Polyakov loop potential is a polynomial in Φ^* and Φ with real coefficients. Dropping its imaginary part makes this potential insensitive to changes of $\mathrm{Im}\,\Phi = \frac{1}{2}(\Phi - \Phi^*)$ around $\mathrm{Im}\,\Phi = 0$ as $\frac{\partial\Omega_0}{\partial\,\mathrm{Im}\,\Phi} \in i\,\mathbb{R}$ at $\mathrm{Im}\,\Phi = 0$. The lowest order (mean field) approximation will therefore not be able to describe $\mathrm{Im}\,\Phi = \frac{1}{2}(\Phi - \Phi^*)$ properly. The description of the real part of Φ, $\mathrm{Re}\,\Phi = \frac{1}{2}(\Phi^* + \Phi)$, should not be affected significantly by this approximation.

When determining solutions to the mean field equations the fields must only be varied such that the field configuration allows for a physical interpretation at all times. In particular real fields must not assume complex values with non-zero imaginary part. In order to always comply with $A_4^{(3)}$, $A_4^{(8)} \in \mathbb{R}$ we define the mean field equations using only the real part of the thermodynamic potential

$$\frac{\partial\,\Omega_{\mathrm{MF}}}{\partial\,(\sigma, \Delta, \phi_3, \phi_8)} = \frac{\partial\,\mathrm{Re}[\Omega_0]}{\partial\,(\sigma, \Delta, \phi_3, \phi_8)} = 0 \ . \tag{2.21}$$

A complex mean field action would result in complex mean field equations which determine two real degrees of freedom, an imaginary and a real part possibly leading to unphysical mean field solutions. The presented approach of "quenching" the complex action and limiting it to its real part avoids such difficulties. Treating the truncated imaginary parts as perturbations the leading order approximation can be refined systematically by a systematic series of perturbative corrections. This approach is presented in the following section.

2.4.3 Perturbative approach to the PNJL sign problem

In the previous section the notion of mean fields as it is used in this work has been defined. The mean field equations (2.21) in this definition only determine the stationary point of the real part of the potential, which is the lowest order approximation of thermodynamic expectation values. Eq. (2.21) maximises the modulus of the thermodynamic weight. The imaginary part of the gradient in Eq. (2.21) and higher order terms in a Taylor expansion of the thermodynamic potential are not considered in lowest order, i.e. in mean field approximation.

Before working out details of a systematic perturbative series we assure that complex values of the action $\mathcal{S}_{\mathrm{PNJL}}$ as such are not unphysical. The quantities

---

[16]$\mathcal{S}_{\mathrm{bos}}$ is an effective action with respect to quarks, but a standard action with respect to the auxiliary boson fields (see Sec. 2.4.3).

that have to remain real at all times are firstly the Lagrangian (together with the Hamiltonian) and secondly the effective action (equivalent to the thermodynamic potential). While Lagrangian and Hamiltonian only figure bare fields, the effective action is the result of integrating out *all* bare fields. The action that we are considering is neither of these two, as only the fermion fields (the quark quasiparticles) have been integrated out while auxiliary boson fields, which have been introduced through bosonization, still figure explicitly in this action. Integrating over the gauge boson fields leads to a subtle cancellation of all imaginary parts. The gauge boson fields responsable for the complex values of the action are those in Euclidean time direction.[17] If the temporal gauge boson fields are set to zero, the action as function of chemical potential is real valued. In this case the quark propagator is hermitian such that the determinant transforms into its complex conjugate under hermitian conjugation of the argument. Thus the action at vanishing gauge fields is an analytic function in μ with real valued expansion coefficients. In the quark quasiparticle propagator both temporal gauge fields A_4 and chemical potential μ appear as prefactors of the Dirac structure γ_0. The action at finite gauge fields A_4 can be derived from the action at vanishing fields by the substitution $\mu \to \mu - iA_4$. For simplicity colour indices have been omitted here. In principle this substitution would have to be carried out for each colour separately. The properties of the action (analyticity with real expansion coefficients) guarantees that $\mathcal{S}(A_4) = \mathcal{S}^*(-A_4)$. Using this property the integration over the gauge field A_4 can be transformed in the following way:

$$\int \mathrm{d}A_4 \, e^{-\mathcal{S}(A_4)} = \int \mathrm{d}A_4 \, e^{-\mathcal{S}^*(-A_4)} = \int \mathrm{d}(-A_4) \, e^{-\mathcal{S}^*(A_4)} = \int \mathrm{d}A_4 \, e^{-\mathcal{S}^*(A_4)} \quad (2.22)$$

$$\Rightarrow \int \mathrm{d}A_4 \, e^{-\mathcal{S}(A_4)} = \frac{1}{2} \int \mathrm{d}A_4 \, e^{-\mathcal{S}(A_4)} + e^{-\mathcal{S}^*(A_4)} = \int \mathrm{d}A_4 \, \mathrm{Re}\big[e^{-\mathcal{S}(A_4)}\big] \, , \quad (2.23)$$

where we have exploited the fact that the SU(3) integration measure $\mathrm{d}A_4$ is invariant under sign changes of A_4. For the evaluation of thermal expectation values the considered quantities have to be split into even and odd contributions in their A_4 dependence. Even contributions are weighted thermodynamically with $\mathrm{Re}\big[e^{-\mathcal{S}(A_4)}\big] = \cosh[\mathcal{S}(A_4)]$, while odd contributions are weighted with $\mathrm{Im}\big[e^{-\mathcal{S}(A_4)}\big] = -\sinh[\mathcal{S}(A_4)]$.

In general it is not possible to integrate out the gauge fields A_4 due to technical difficulties. An approach which allows to perform approximations to the integrals over A_4 is perturbation theory. The action is split into two parts: "free" parts that can be integrated out and "perturbative" parts (interactions). For the free part we restrict ourselved to the gaussian approximation, i. e. only the zeroth and second order terms of a Taylor expansion of the action are considered. This Taylor series of the action $\mathcal{S}_{\mathrm{PNJL}}$ is an expansion in the fields about their mean field values. Eq. (2.21) is the necessary condition for the maximisation of the modulus of the thermodynamic weight $\big|e^{-\mathcal{S}_{\mathrm{E}}}\big|$.[18] The most important corrections to mean field are generated by

---

[17]In spatial direction the minimal substitution $\vec{p} \to \vec{p} + \vec{A}$ does not cause complex values of the action as it is a real shift of the spatial momenta.

[18]In analogy to the procedure in Minkowskian space-time one might argue that the complex

the first order Taylor coefficient. By construction of the mean field approximation the real part of the first order term vanishes. Being imaginary valued this term may formally be treated like a source term, which allows to apply the calculus of generating functions. In contrast to this formalism the generating function is evaluated at finite values of the source. Further corrections can be calculated using higher order derivatives (third order and higher). In the name of conciseness of this model such corrections have been omitted. These corrections only lead to small changes which are not able to change physics qualitatively. The technical details of this derivation of correction terms are summarised in Appendix B. The central result including next-to-leading order is

$$\Omega = \Omega_{\mathrm{MF}} - \frac{1}{2} \left(\frac{\partial \Omega_0}{\partial \theta} \right)^T \cdot \left[\frac{\partial^2 \Omega_0}{\partial \theta^2} \right]^{-1} \cdot \frac{\partial \Omega_0}{\partial \theta} \Bigg|_{\theta = \theta_{\mathrm{MF}}} , \qquad (2.24)$$

starting from the (complex) Ω_0, with Ω_{MF} and θ_{MF} defined by Eq. (2.21). The gradients $\partial \Omega_0 / \partial \theta$ are understood with the set of field variables $\theta = (\theta_i)$ arranged in vector form. $\partial^2 \Omega_0 / \partial \theta^2$ represents the Hessian matrix $(\partial^2 \Omega_0 / \partial \theta_i \partial \theta_j)$. The correction term in (2.24) is evaluated at the mean field configuration: $\theta = \theta_{\mathrm{MF}}$. Note that this term respects contributions generated by non-vanishing imaginary parts of Ω_0. Up to second order the corrected potential Ω is a real quantity by construction. The thermal expectation value $\langle f \rangle$ of a physical quantity f is calculated according to

$$\langle f \rangle = f(\theta_{\mathrm{MF}}) - \left(\frac{\partial \Omega_0}{\partial \theta} \right)^T \cdot \left[\frac{\partial^2 \Omega_0}{\partial \theta^2} \right]^{-1} \cdot \frac{\partial f}{\partial \theta} \Bigg|_{\theta = \theta_{\mathrm{MF}}} . \qquad (2.25)$$

2.4.4 Perturbative corrections and mean field equations

A useful consistency check, performed here only to lowest order, is to verify that the thermal expectation values are now closer to the properties of an order parameter than the mean field result. In other words: we examine whether the thermodynamic potential Ω is a Landau effective action minimised with respect to $\langle \sigma \rangle$, $\langle \Delta \rangle$, $\langle \Phi \rangle$, $\langle \Phi^* \rangle$ using Eq. (2.25) for the expectation values. The analysis below is done for the lowest order terms, $\alpha = 0$ and $\beta = 0, 1$. We start from the form also used for the numerical calculations, presented below Eq. (2.24), and differentiate with respect to the expectation values $\langle \theta \rangle = (\langle \sigma \rangle, \langle \Delta \rangle, \langle \Phi \rangle, \langle \Phi^* \rangle)^T$. To orders $\alpha = 0$ and $\beta = 0, 1$ we find that $\langle \theta \rangle = \theta_0 + \delta \theta$, where $\delta \theta$ is given by

$$\delta \theta_i = \frac{1}{2} \left(\left[\frac{\partial^2 \Omega_{\mathrm{MF}}}{\partial \theta^2} \right]^{-1} \cdot \frac{\partial \Omega_{\mathrm{MF}}}{\partial \theta} \Bigg|_{\theta = \theta_{\mathrm{MF}}} \right)_i \qquad (2.26)$$

---

phase needs to become stationary. Taking the thermodynamic limit one observes that the field configuration in stationary phase approximation is favoured over other configurations proportional to $\frac{V}{T}$, while the absolute value is enhanced over other configurations exponentially, i.e. $\propto \exp\left[\frac{V}{T} \right]$.

(which is Eq. (2.25) with $f(\theta) = \theta_i$). After some calculation we arrive at the lowest order term in β

$$
\begin{aligned}
\left.\frac{\partial \Omega}{\partial \theta_i}\right|_{\theta=\langle\theta\rangle} &= \frac{9}{8} \sum_{jk} \left[\frac{\partial^3 \Omega_{\mathrm{MF}}}{\partial^3 \theta}\right]_{ijk} \left(\left[\frac{\partial^2 \Omega_{\mathrm{MF}}}{\partial \theta^2}\right]^{-1} \cdot \frac{\partial \Omega_{\mathrm{MF}}}{\partial \theta}\right)_j \\
&\quad \left.\left(\left[\frac{\partial^2 \Omega_{\mathrm{MF}}}{\partial \theta^2}\right]^{-1} \cdot \frac{\partial \Omega_{\mathrm{MF}}}{\partial \theta}\right)_k \right|_{\theta=\theta_{\mathrm{MF}}} \cdots + \text{ higher orders, } \quad (2.27)
\end{aligned}
$$

which is of order $\beta = 2$, i. e. the self consistency equations are satisfied to the order we have been working in. As a consequence the corrections necessary to account for the fermion sign problem do not modify the mean field equations. A backward reaction on the mean field equations does not occur at this level of the approximation.

2.4.5 Self consistency and saddle point approximation

Another way to approximate a complex integral over an exponential is the so-called saddle point approximation. In this approximation the analyticity of the integrand is exploited. For analytic integrands an integration along a contour in the complex plane may be deformed without changing the value of the integral. The deformation used in saddle point approximation deflects this contour to the path of steepest descent[19]. Using this approximation it is possible to approximate an integral of the form $\int e^{-f(z)}\mathrm{d}z$ up to gaussian (second) order. This approximation incorporates first order terms which may not vanish on the real axis where the original path of integration is located. The approach chosen here is to implement these non-vanishing terms perturbatively. In a first step higher order terms are neglected. We restrict ourselves to the case of a gaussian action which can be expanded in the fields around mean field solutions defined by

$$
\left.\frac{\partial \operatorname{Re}\mathcal{S}[\phi]}{\partial \phi}\right|_{\phi=\phi_{\mathrm{MF}}} = 0 \tag{2.28}
$$

and around the saddle point defined by

$$
\left.\frac{\partial \mathcal{S}[\phi]}{\partial \phi}\right|_{\phi=\phi_{\mathrm{SP}}} = 0 \quad \Longleftrightarrow \quad \left.\frac{\partial \operatorname{Re}\mathcal{S}[\phi]}{\partial \phi}\right|_{\phi=\phi_{\mathrm{SP}}} = \left.\frac{\partial \operatorname{Im}\mathcal{S}[\phi]}{\partial \phi}\right|_{\phi=\phi_{\mathrm{SP}}} = 0 \; . \tag{2.29}
$$

These expansions are of the form

$$
\begin{aligned}
\mathcal{S}[\phi] &= \mathcal{S}_{\mathrm{MF}} \quad + \mathcal{S}_{\mathrm{MF}}^{(1)}(\phi - \phi_{\mathrm{MF}}) \quad + \frac{1}{2}\mathcal{S}_{\mathrm{MF}}^{(2)}(\phi - \phi_{\mathrm{MF}})^2 \text{ and} \\
\mathcal{S}[\phi] &= \mathcal{S}_{\mathrm{SP}} \qquad\qquad\qquad\qquad\quad + \frac{1}{2}\mathcal{S}_{\mathrm{SP}}^{(2)}(\phi - \phi_{\mathrm{SP}})^2 \; ,
\end{aligned} \tag{2.30}
$$

where $\mathcal{S}_{\mathrm{MF}} = \mathcal{S}[\phi_{\mathrm{MF}}]$ and $\mathcal{S}_{\mathrm{SP}} = \mathcal{S}[\phi_{\mathrm{SP}}]$. The upper index in $\mathcal{S}^{(n)}$ labels the nth derivative with respect to the fields ϕ: $\mathcal{S}^{(n)} = (\partial^n \mathcal{S})/(\partial \phi)^n$. We can now calculate

---

[19]The path of steepest descent minimises the absolute value of the integrand all along the contour.

the action at the saddle point $\mathcal{S}_{\text{SP}}$ in terms of the expansion coefficients about the mean fields

$$\mathcal{S}_{\text{SP}} = \mathcal{S}_{\text{MF}} + \mathcal{S}_{\text{MF}}^{(1)}(\phi_{\text{SP}} - \phi_{\text{MF}}) + \frac{1}{2}\mathcal{S}_{\text{MF}}^{(2)}(\phi_{\text{SP}} - \phi_{\text{MF}})^2 \; . \tag{2.31}$$

We find the difference $\phi_{\text{SP}} - \phi_{\text{MF}}$ by virtue of Eq. (2.29)

$$\phi_{\text{SP}} - \phi_{\text{MF}} = -\left[\mathcal{S}_{\text{MF}}^{(2)}\right]^{-1}\mathcal{S}_{\text{MF}}^{(1)} \; , \tag{2.32}$$

where $\mathcal{S}_{\text{MF}}^{(1)}$ is purely imaginary due to Eq. (2.28). Inserting Eq. (2.32) in Eq. (2.31) yields

$$\mathcal{S}_{\text{SP}} = \mathcal{S}_{\text{MF}} - \frac{1}{2}\mathcal{S}_{\text{MF}}^{(1)}\left[\mathcal{S}_{\text{MF}}^{(2)}\right]^{-1}\mathcal{S}_{\text{MF}}^{(1)} \; , \tag{2.33}$$

which is equivalent to Eq. (2.24). On top of the gaussian approximation higher order terms in a Taylor expansion of $\mathcal{S}[\phi]$ in terms of ϕ can be respected establishing an additional perturbative series. Such a series can be performed about both the saddle point and the mean field configuration. However, due to the different expansion points the coefficients are different.

Once the integration variables ϕ_3 and ϕ_8 are not constraint to real (physical) values, but are chosen along a contour in the complex plane Γ, they can no longer be considered as physical fields. Instead they have to be seen as a mere reparametrisation of $\langle\Phi\rangle$ and $\langle\Phi^*\rangle$ (note the brackets $\langle\cdots\rangle$). Saddle point approximation immediately jumps from bare fields to thermodynamic expectation values due to

$$\begin{aligned}\langle\phi\rangle &= \frac{1}{\mathcal{N}}\int_\Gamma \mathcal{D}\phi \; \phi \, e^{-\mathcal{S}[\phi]} \quad\approx\quad \frac{1}{\mathcal{N}}\int_\Gamma \mathcal{D}\phi \; \phi \, e^{-\mathcal{S}_{\text{SP}} - \frac{1}{2}\mathcal{S}_{\text{SP}}^{(2)}(\phi - \phi_{\text{SP}})^2} \\ &= \frac{1}{\mathcal{N}}\int_\Gamma \mathcal{D}\phi \; \phi \, e^{-\mathcal{S}_{\text{MF}} + \frac{1}{2}\mathcal{S}_{\text{MF}}^{(2)}(\phi_{\text{SP}} - \phi_{\text{MF}})^2 - \frac{1}{2}\mathcal{S}_{\text{SP}}^{(2)}(\phi - \phi_{\text{SP}})^2} \; = \; \phi_{\text{SP}} \; .\end{aligned} \tag{2.34}$$

Therefore this approximation does not allow to separate the bare fields from the perturbative corrections.

In general the direct connection $\Phi = \Phi(\phi_3, \phi_8)$ of the two parametrisations, (ϕ_3, ϕ_8) on the one hand and (Φ, Φ^*) on the other hand, is lost once we step away from mean field and calculate thermodynamic expectation values: $\langle\Phi\rangle \neq \Phi(\langle\phi_3\rangle, \langle\phi_8\rangle)$. This observation is crucial when comparing the present method of approximation to schemes in previous publications [RTW06, SFR07, GMMR06, MMR07, ZL07]. In these publications the fields ϕ_3, ϕ_8 have been abandoned in favour of Φ, Φ^* before doing mean field approximation. This implies that $\langle\Phi\rangle$ and $\langle\Phi^*\rangle$ (and *not* Φ, Φ^*) are treated as independent mean field degrees of freedom. The minimisation of Ω_0 is then performed requiring that $\langle\Phi\rangle$ and $\langle\Phi^*\rangle$ are real quantities. In such approximation schemes it is not possible to find a way back to the (real) quantities ϕ_3, ϕ_8: $\langle\Phi\rangle$ and $\langle\Phi^*\rangle$ already comprise fluctuations of ϕ_3, $\phi_8 \in \mathbb{R}$. In other words, the definition of the lowest order approximation (which is usually referred to as mean field approximation) is different in Refs. [RTW06, SFR07, GMMR06, MMR07, ZL07] and this work. The definition of the lowest order (mean field) approximation in this work allows to strictly separate contributions originating in constant and fluctuating parts of the fields.

Chapter 3

Applications of the PNJL model

After the previous chapters have given guidance to the centre of this work the current chapter will concentrate on numeric results. Already on the mean field level the PNJL model shows a variety of most interesting and striking results [RRTW07, RRW07b, RRW07a, Fuk04, SFR07, GMMR06, ZL07, H$^+$07, AAG$^+$08]. Perhaps the most outstanding one is how chiral and Polyakov loop dynamics cooperate to produce crossover transitions. These two crossover transitions end up (at zero chemical potential) in a narrow overlapping range of temperatures (see Fig. 3.1). In isolation, the pure gauge Polyakov loop sector and the NJL sector in the chiral limit show first and second order phase transitions with critical temperatures far separated, as demonstrated by the dashed and dash-double dotted lines in Fig. 3.1. When entangled in the PNJL model, these transitions (with non-zero quark masses) move together to form a joint crossover pattern. The joint transition pattern has first been proposed by Gocksch and Ogilvie in Ref. [GO85]. Lattice calculations do not give a completely unanimous answer to the relation of these two crossovers. Within the tolerance of systematic uncertainties of those lattice calculations and in view of the model character of the PNJL calculations it can be stated that there is agreement.

After having convinced ourselves that the PNJL model has incorporated the correct degrees of freedom to model the dynamics of QCD, the realization of confinement in the PNJL model will be studied in greater detail in Sec. 3.2. This section will first illuminate the modifications of the Fermi-Dirac distribution function of the quark quasiparticles due to the presence of confinement in its PNJL realization. Further important issues studied are the properties of the vacuum implementing spontaneous chiral symmetry breaking, in particular the properties of the lightest mesons which are governed by the properties of the Nambu-Goldstone modes.

The following sections of this chapter concentrate on the equation of state (Sec. 3.3), the QCD phase diagram in the temperature and chemical potential plane (Sec. 3.4), the Polyakov loop degrees of freedom $\langle \Phi^* \rangle$ and $\langle \Phi \rangle$ at finite chemical potentials beyond mean field approximation (Sec. 3.5) and isovector degrees of freedom (Sec. 3.6). In Sec. 3.7 the qualitative behaviour of $\langle \Phi^* \rangle - \langle \Phi \rangle$ is compared to isovector degrees of freedom. The similar behaviour suggests a mechanism that is most likely also at work in full QCD.
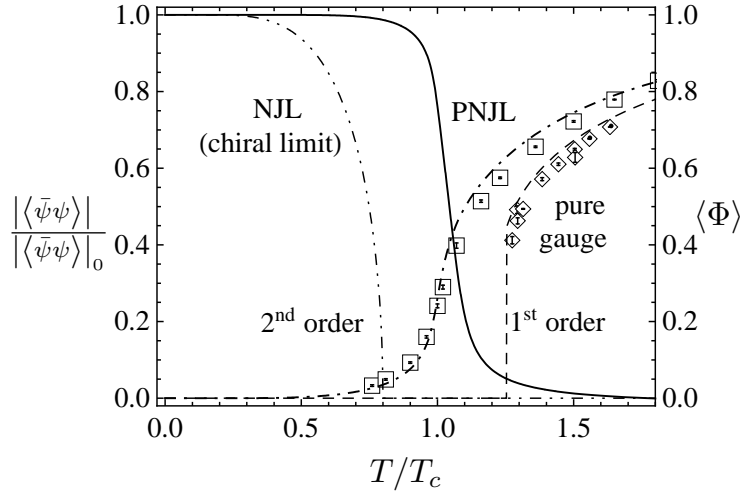
Figure 3.1: Chiral condensate normalised to its value at temperature $T = 0$ (dash-double-dotted line) in the NJL model with massless quarks, and Polyakov loop $\langle \Phi \rangle$ in the pure gauge model (dashed line). The PNJL model (with non-zero quark masses) shows dynamical entanglement of the chiral (solid line) and Polyakov loop (dash-dotted line) crossover transitions. For comparison lattice data for the Polyakov loop in pure gauge and full QCD (including quarks) are also shown [KZ05] .

3.1   Thermodynamic potential and mean field equations

An alternative way to derive the PNJL Euclidean action is via the Hamiltonian which in thermal field theory is the principal quantity determining the thermodynamics of a system as explained in Sec.1.2.1. The Euclidean action of the two-flavour PNJL model including diquark degrees of freedom [RRW07b, RHRW08] written down in terms of the fermionic Hamiltonian density reads

$$
\mathcal{S}_{\mathrm{PNJL}}(\psi, \psi^{\dagger}, \phi) = \int_{0}^{\beta = T^{-1}} \mathrm{d}\tau \int \mathrm{d}^3 x \left[\psi^{\dagger} \partial_{\tau} \psi + \mathcal{H}(\psi, \psi^{\dagger}, \phi) \right] + \delta \mathcal{S}_E(\phi, T) \quad (3.1)
$$

with the fermionic Hamiltonian in Euclidean space[1]:

$$
\mathcal{H} = -i\psi^{\dagger} \left(\vec{\alpha} \cdot \vec{\nabla} + \gamma_4\, m_0 - A_4 \right) \psi + \mathcal{V}(\psi, \psi^{\dagger}) \;, \quad (3.2)
$$

where ψ is the $N_{\mathrm{f}} = 2$ doublet quark field and $m_0 = \mathrm{diag}(m_u, m_d)$ is the quark mass matrix. The quarks move in a background colour gauge field A_4 discussed above Eq. (2.17). The matrix valued, constant field A_4 relates to the (traced) Polyakov loop as in Eq. (1.29). The two fields $A_4^{(3)}$ and $A_4^{(8)}$ are a parametrisation of the diagonal elements of SU(3)$_{\mathrm{c}}$. The piece $\delta \mathcal{S}_{\mathrm{E}} = \frac{V}{T} \mathcal{U}$ of the action (3.1) carries information about the gluon dynamics presented in Sec. 2.3 using the parameter choice of Refs. [RRTW07, RRW07b] quoted in Tab. 2.2.

---

[1]$\vec{\alpha} = \gamma_0\, \vec{\gamma}$ and $\gamma_4 = i\gamma_0$ in terms of the standard Dirac γ matrices.

The NJL interaction term $\mathcal{V}$ in Eq. (3.2) includes chiral $\mathrm{SU(2)_L \times SU(2)_R}$ invariant four-point couplings of the quarks acting in pseudoscalar-isovector/scalar-isoscalar quark-antiquark and scalar diquark channels:

$$\mathcal{V} = -\frac{G}{2}\left[\left(\bar\psi\psi\right)^2 + \left(\bar\psi\, i\gamma_5\vec\tau\,\psi\right)^2\right] - \frac{H}{2}\left[\left(\bar\psi\,\mathcal{C}\gamma_5\tau_2\lambda_2\,\bar\psi^T\right)\left(\psi^T\gamma_5\tau_2\lambda_2\mathcal{C}\,\psi\right)\right]\ ,\qquad (3.3)$$

where $\mathcal{C}$ is the charge conjugation operator. These interaction terms in Eq. (3.3) are obtained from a local colour current-current interaction between quarks,

$$\mathcal{L}_\mathrm{int} = -G_\mathrm{c}(\bar\psi\gamma_\mu t^a\psi)(\bar\psi\gamma^\mu t^a\psi)\ ,$$

by a Fierz transformation which relates the coupling strengths G and H as $G = \frac{4}{3}H$ which we choose not to alter. Additional terms generated by the Fierz transformation are of no importance in the present context and will be omitted.

To evaluate the thermodynamic properties of the model the quark degrees of freedom are integrated out. New auxiliary fields are introduced by bosonisation, absorbing quark-antiquark and quark-quark (antiquark-antiquark) correlations. These are a scalar-pseudoscalar field $(\sigma, \vec\pi)$ and a diquark (antidiquark) field $\Delta\ (\Delta^*)$. The resulting thermodynamic potential then reads

$$\Omega_0 = \frac{T}{V}\,\mathcal{S}_\mathrm{bos} = \mathcal{U}\left(\Phi,\,\Phi^*,\,T\right) + \frac{\sigma^2}{2G} + \frac{\Delta^*\Delta}{2H}$$
$$-\frac{T}{2}\sum_n\int\frac{\mathrm{d}^3 p}{(2\pi)^3}\mathrm{Tr}\ln\left[\beta\tilde{S}^{-1}\left(i\omega_n,\vec p\right)\right]\ ,\quad (3.4)$$

where the Matsubara sum runs over $\omega_n = (2n+1)\pi\,T$ reproducing antiperiodic boundary conditions in the Euclidean time direction. The inverse Nambu-Gor'kov propagator $\tilde{S}^{-1}$ in Eq. (3.4) is defined by

$$\tilde{S}^{-1}\left(i\omega_n,\vec p\right) = \begin{pmatrix} \slashed{p} - m + \gamma_0\left(\mu - iA_4\right) & \Delta\gamma_5\tau_2\lambda_2 \\ -\Delta^*\gamma_5\tau_2\lambda_2 & \slashed{p} - m - \gamma_0\left(\mu - iA_4\right) \end{pmatrix}\qquad (3.5)$$

$$\text{with}\quad \slashed{p} = i\gamma_0\,\omega_n - \vec\gamma\cdot\vec p\ .\qquad (3.6)$$

The mass of the quark-quasiparticles is given as in the standard NJL model by the gap equation $m = m_0 - \sigma = m_0 - G\langle\bar\psi\psi\rangle$. The Matsubara sum is evaluated analytically. The quasiparticle energies emerging in this procedure are related to the solutions of $\det\left[\tilde{S}^{-1}(p_0)\right] = 0$. The thermodynamic potential then reads

$$\Omega_0 = \mathcal{U}\left(\Phi,\,\Phi^*,\,T\right) + \frac{\sigma^2}{2G} + \frac{\Delta^*\Delta}{2H}$$
$$-2N_f\int\frac{\mathrm{d}^3 p}{(2\pi)^3}\sum_j\left\{T\ln\left[1 + e^{-E_j/T}\right] + \frac{1}{2}\Delta E_j\right\}\ ,\quad (3.7)$$

with six distinct quasiparticle energies

$$E_{1,2} = \varepsilon(\vec p) \pm \tilde\mu_b\ ,$$
$$E_{3,4} = \sqrt{(\varepsilon(\vec p) + \tilde\mu_r)^2 + |\Delta|^2} \pm i\,T\,\phi_3\ ,$$
$$E_{5,6} = \sqrt{(\varepsilon(\vec p) - \tilde\mu_r)^2 + |\Delta|^2} \pm i\,T\,\phi_3\ ,\qquad (3.8)$$

where $\varepsilon(\vec{p}) = \sqrt{\vec{p}^2 + m^2}$, $\tilde{\mu}_b = \mu + 2i\,T\,\frac{\phi_8}{\sqrt{3}}$ and $\tilde{\mu}_r = \mu - i\,T\,\frac{\phi_8}{\sqrt{3}}$. The energy difference ΔE_j is defined as the difference of the quasiparticle energy and the energy of a free fermion, $\varepsilon_0 = \sqrt{\vec{p}^2 + m_0^2}$: $\Delta E_j = E_j - \varepsilon_0 \pm \mu$. The form of the bosonised action, Eq. (3.7), does not allow to factor out the Polyakov loop fields Φ and Φ^*, as it was done in Ref. [RTW06]. Instead we keep the form of Eq. (3.7) using ϕ_3 and ϕ_8 with ϕ_3, $\phi_8 \in \mathbb{R}$.[2] The mean field equations (2.21) with the current choice of degrees of freedom are four equations determining the set of fields $(\sigma, \Delta, \phi_3, \phi_8)$. The hereby neglected imaginary part of this derivative will be taken into account using the proceedure outlined in Sec. 2.4.3 and App. B.

3.2 Realization of confinement

While the NJL model is unable to model the effects of confinement present in QCD the Polyakov loop extended version of the NJL model shows promising results. The implications of the Polyakov loop effective potential present in the PNJL model are discussed in detail in this section. The first subsection concentrates on the quark quasiparticle properties produced by the PNJL model. Next we focus on the lightest mesons, the Goldstone modes of spontaneous chiral symmetry breaking, which are accessible in this model using the random phase approximation (RPA). We close with the discussion of spectral functions of the lightest mesons which are the most sensitive benchmark in the comparison to QCD.

3.2.1 Modified Fermi-Dirac distribution

Using the PNJL model without explicit inclusion of diquarks it is shown in Ref. [H+07] that the coupling of the NJL model to the Polyakov loop effective potential can be accounted for by substituting the standard Fermi-Dirac distribution $f^{\pm}(E)$, by a modified distribution function $f_{\Phi}^{\pm}(E)$. The Polyakov loop modified distribution function $f_{\Phi}^{\pm}(E)$ merges to a standard Fermi-Dirac distribution $f^{\pm}(E)$ in the case of perfect deconfinement ($\Phi = \Phi^* = 1$), while it becomes a Fermi-Dirac distribution $f(3E)|_{\mu=0}$ once the Polyakov loop indicates confinement ($\Phi = \Phi^* = 0$):.

$$f^{\pm}(E) \rightarrow f_{\Phi}^{\pm}(E) = \frac{\Phi^* e^{-\frac{E\mp\mu}{T}} + 2\,\Phi e^{-2\frac{E\mp\mu}{T}} + e^{-3\frac{E\mp\mu}{T}}}{1 + 3\,\Phi^* e^{-\frac{E\mp\mu}{T}} + 3\,\Phi e^{-2\frac{E\mp\mu}{T}} + e^{-3\frac{E\mp\mu}{T}}} \tag{3.9}$$

$$f_{\Phi}^{\pm}(E) \xrightarrow{\Phi\rightarrow 0} \frac{1}{1 + e^{+3\frac{E\mp\mu}{T}}} \qquad\qquad f_{\Phi}^{\pm}(E) \xrightarrow{\Phi\rightarrow 1} \frac{1}{1 + e^{\frac{E\mp\mu}{T}}} \tag{3.10}$$

The behaviour for intermediate values of the Polyakov loop shows some interpolation between the extreme cases ($\Phi = \Phi^* = 0$ and $\Phi = \Phi^* = 1$) which have been

---

[2]As the parameter space of ϕ_3 and ϕ_8 is periodic there are different parameter sets representing the same physics. We use the (triangular shaped) domain $\{(\phi_8 \geqq -\frac{\pi}{\sqrt{3}}) \wedge (\phi_8 \leqq \sqrt{3}(\phi_3 + \frac{2\pi}{3})) \wedge (\phi_8 \leqq \sqrt{3}(-\phi_3 + \frac{2\pi}{3}))\}$. Note that the periodic domain of L and $L^{\dagger}$ is 3!-times larger than the domains for Φ and Φ^* (or equivalently ϕ_3 and ϕ_8) due to the trace's invariance under unitary transformations of L.
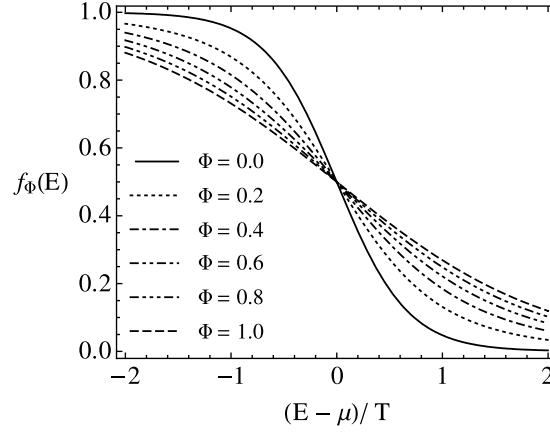
Figure 3.2: The Polyakov loop modified Fermi-Dirac distribution of quark quasiparticles. Fixing the Polyakov loop to specific values (here from $\Phi = 0.0$ to 1.0 in 0.2 steps) shows that the quark distribution function remains centered at the same energy, its slope however is getting steeper.

illustrated in Fig. 3.2. The limiting case of deconfinement $(f_\Phi^\pm(E) \xrightarrow{\Phi \to 1} 1/(1+e^{\frac{E \mp \mu}{T}}))$ reproduces the standard Fermi-Dirac distribution as expected. The confinement case can be interpreted as follows. One can argue that the thermodynamically active quasiparticles are three quark compounds with three times the energy of one quark quasiparticle [SFR08]. This interpretation is quite intuitive as baryons, which are the correct QCD degrees of freedom at low temperatures, contain three valence quarks. The chemical potential relevant for such compounds is three times the quark chemical potential μ approving the identification of the Baryon chemical potential μ_{B} with three times the quark chemical potential.

3.2.2 Meson spectral functions

Meson propagators can be evaluated in the PNJL model in the very same fashion as in the NJL model (see App. A.1). With a propagator of a meson at hand the spectral functions can be evaluated

$$\rho_{\mathrm{M}}(\omega,\, \vec{q};\, T) = \frac{G \operatorname{Im} \Pi_{\mathrm{M}}(\omega,\, \vec{q};\, T)}{(1 - G \operatorname{Re} \Pi_{\mathrm{M}})^2 + (G \operatorname{Im} \Pi_{\mathrm{M}})^2} \tag{3.11}$$

with the inverse meson propagator $\tilde{S}_{\mathrm{M}} = (1 - G\Pi)$ and with the thermal quark-antiquark polarisation function

$$\Pi_{\mathrm{M}}(\omega,\vec{q};\, T) = T \sum_{\omega_n} \int \frac{\mathrm{d}^3 p}{(2\pi)^3} \operatorname{Tr} \left[\Gamma_{\mathrm{M}} \tilde{S}(i\omega_n + \mu, \vec{p}) \Gamma_{\mathrm{M}} \tilde{S}(i(\omega_n - \omega) + \mu, \vec{p} - \vec{q}) \right] \,,$$
$$\tag{3.12}$$

where the sum is taken over the Matsubara frequencies $\omega_n = (2n + 1)\pi T$. Here Γ_{M} is a Dirac, flavour and colour representation of a meson current labelled M. Further details of the evaluation of real and imaginary part of the quark-antiquark
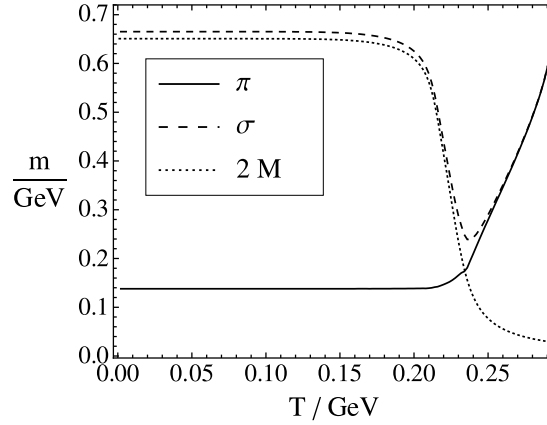
Figure 3.3: The mass of the pion evaluated in RPA in the PNJL framework [RHRW08]. At vanishing temperature all three colours decouple in the PNJL model reproducing the NJL meson mass spectrum. The transition to the chirally unbroken phase sets in at higher temperatures than in the NJL case (compare Fig. 2.1) and occurs more rapidly. At temperatures of $\approx 1.1\,T_\mathrm{c}$ the pion mass exceeds twice the constituent quark mass. Already at $T \approx 1.3\,T_\mathrm{c}$ the meson masses surpass the NJL cutoff scale.

polarisation function Π_M are given in App. A.2. In this work we only focus on the pseudoscalar isovector channel (i.e. pionic excitations) and the scalar isoscalar channel. $\tilde{S}(i\omega_n, \vec{p}) = -\frac{m + \not{p}}{\omega_n^2 + p^2 + m^2}$ denotes the quark quasiparticle propagator with $\not{p} = i\omega_n\gamma_0 - \vec{\gamma}\cdot\vec{p}$. The spectral function of pion and sigma are illustrated in Fig. 3.4. The left panel of Fig. 3.4 is evaluated at threshold temperature (i.e. at the temperature at which the pion exceeds the mass of two constituent quarks, see Fig. 3.3). The peak in the pion spectral function indicates this situation at which an on-shell pion can interact resonantly with a quark-antiquark pair. The fact that the spectral function of the sigma is quite distinct from the pion spectral function and shifted to higher ω values indicates chiral symmetry breaking. At temperatures above threshold (right panel of Fig. 3.4) these two spectral functions merge into one indicating the restoration of the chiral symmetry. The situation at very low temperatures shall not be shown here in detail, as the PNJL model which uses quark degrees of freedom is not expected to give correct results, as at low temperatures all quark degrees of freedom have to disappear due to confinement.[3]

3.3   The Equation of State

This section concentrates on the equation of state evaluated in the PNJL model at temperatures around the crossover transition. The principle quantity in the PNJL model is the thermodynamic potential which is related to the pressure (3.17). The

---

[3]In fact by performing an explicit calculation it can be seen that the pion spectral function does not vanish. This indicates that even at low temperatures pion and sigma do decay into quarks. As discussed in Sec. 3.2 the confinement implemented in the PNJL model only has an impact on the quark distribution functions leading to good approximations in thermodynamic calculations.
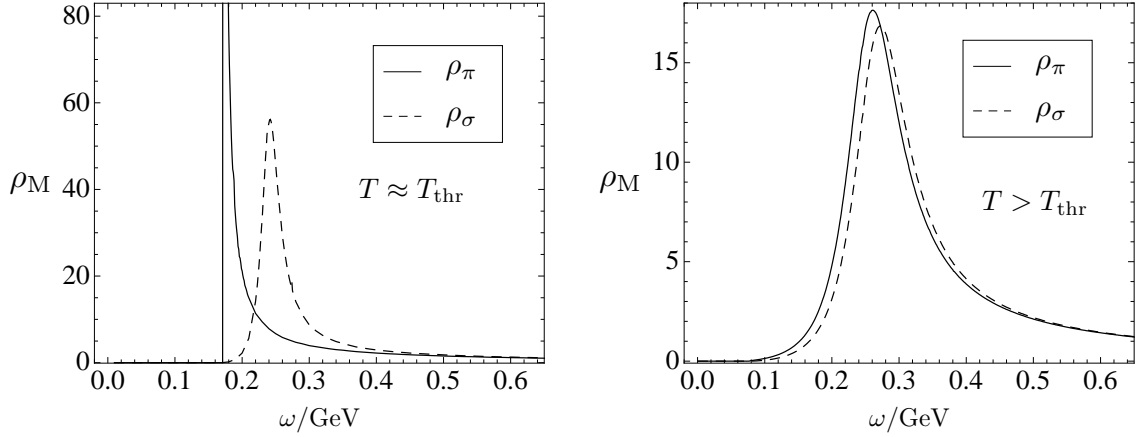
Figure 3.4: The spectral functions $\rho_{\mathrm{M}} = \frac{G\,\mathrm{Im}\,\Pi_{\mathrm{M}}}{(1 - G\,\mathrm{Re}\,\Pi_{\mathrm{M}})^2 + (G\,\mathrm{Im}\,\Pi_{\mathrm{M}})^2}$ taken at $\vec{q} = \vec{0}$ for pion and sigma at $T \approx T_{\mathrm{thr}}$ (left) and at $T > T_{\mathrm{thr}}$ (right).
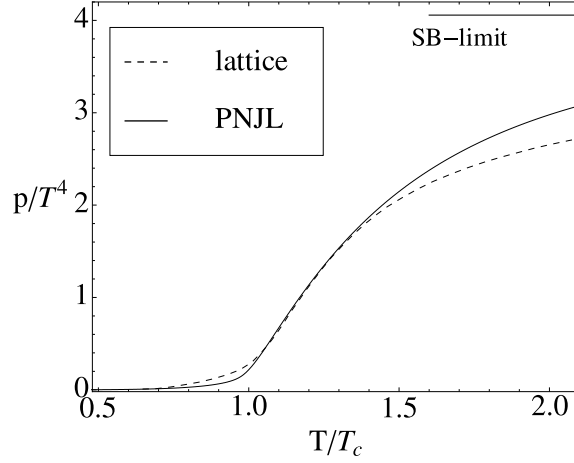
Figure 3.5: In the temperature range suited for calculations in the PNJL model the pressure (solid) shows agreement with lattice data in $N_{\mathrm{f}} = 2$ [KLP00] within systematic errors of the two approaches.

pressure at vanishing quark chemical potential is plotted in comparison with lattice QCD data in Fig. 3.5.

In the course of this section several quantities derived from here are compared with lattice QCD calculations. Lattice QCD starts at the so-called interaction measure $\varepsilon - 3p$ which is related to the pressure as follows

$$\frac{\varepsilon - 3p}{T^4} = T \frac{\partial}{\partial T} \frac{p(T)}{T^4} \ . \tag{3.13}$$

A comparison of this quantity and of the moments of the pressure as a function of quark chemical potential is presented in Sec. 3.3.2. The moments of the pressure as a function of quark chemical potential represents a sensitive benchmark of the PNJL model in comparison with lattice QCD. The cumulant ratios derived from this quantities are related to the quark number fluctuations across the deconfinement and chiral crossovers, and may be a valuable handle in the experimental search for the

critical point (see Sec. 3.3.4). In view of the effort to model the fireball evolution in heavy-ion collisions the speed of sound is a central quantity. It is presented in Sec. 3.3.5.

3.3.1 Estimating mesonic pressure contributions

The calculation presented in Fig. 3.5 only included fluctuations beyond mean field of space-time independent fields. Especially at temperatures below the crossover temperature the resonant interaction of instable mesons with the quark sea above T_c produces an additional pressure contribution. This contribution is not part of the quark pressure previously calculated in Hartree-Fock approximation. The meson decay products form rings of RPA chains. Such kind of pressure contributions are investigated in Ref. [HKZV94] and calculated performing the ring sum. However, below T_c the NJL model does not handle the mesonic degrees of freedom properly. In the hadronic phase the coupling of mesonic modes to the quark-antiquark continuum is suppressed by confinement, whereas the meson spectral function ρ_M (see Sec. 3.2.2) receives contributions from decays into $q\bar{q}$ even below T_c. This unphysical feature persists [H+07] in the PNJL generalisation of the NJL approach. Moreover, the non-renormalisability of the NJL model requires to introduce further subtractions when following the lines of Ref. [HKZV94]. To avoid such arbitrariness and unphysical features we ignore the decay of meson modes into $q\bar{q}$-pairs altogether when calculating an estimate for the meson contributions to the pressure

$$\delta\Omega = \nu \int \frac{\mathrm{d}^3 q}{(2\pi)^3} \, T \ln(1 - e^{-E_q/T}) + B(T) \;, \tag{3.14}$$

where ν is the statistical weight of the corresponding meson species, $E_q = \left(\vec{q}^2 + m_{\mathrm{pole}}^2(T)\right)^{1/2}$ with $m_{\mathrm{pole}}(T)$ the temperature dependent pion and sigma pole mass determined by $1 - G \operatorname{Re}\Pi = 0$. Furthermore $B(T)$ is an appropriately chosen vacuum energy constant ensuring thermodynamic consistency. $B(T)$ is fixed such that the temperature dependence of the pole mass $m_{\mathrm{pole}}(T)$ is compensated on differentiating Ω with respect to the temperature T. This implies that the inclusion of $B(T)$ ensures that $\partial\Omega/\partial m_{\mathrm{pole}}|_T = 0$.

In Fig. 3.6 the calculated pressure of $\pi^{0,\pm}$ and sigma modes are compared with the quark Hartree-Fock pressure and the result for the overall pressure of Hartree-Fock plus RPA is plotted. For comparison the pressure of a Bose gas with three internal degrees of freedom is indicated by the thin solid line. Below the crossover temperature T_c one can clearly identify the pion gas contribution resulting from the RPA calculations. Once the meson masses reach the scale of the NJL cutoff Λ the used approximation breaks down. The inversion of the scale hierarchy appears at temperatures of about $1.3\,T_c$.

For larger current quark masses the meson gas contributions and correlations are reduced. This effect is illustrated by Fig. 3.7 where the pressure of the PNJL model is plotted using an increased current quark mass leading to an unphysically heavy pion. Thus for heavy pions the agreement with lattice data observed in a previous publication [RRW07b] remains.
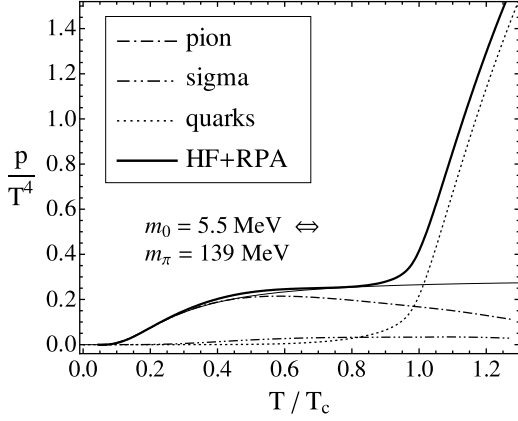
Figure 3.6: The pressure contribution originating from pion modes, sigma modes and from quarks in Hartree-Fock approximation (dotted). The thin solid line represents the pressure of a gas of bosons with three internal degrees of freedom and a constant mass $m = m_\pi(T = 0)$.
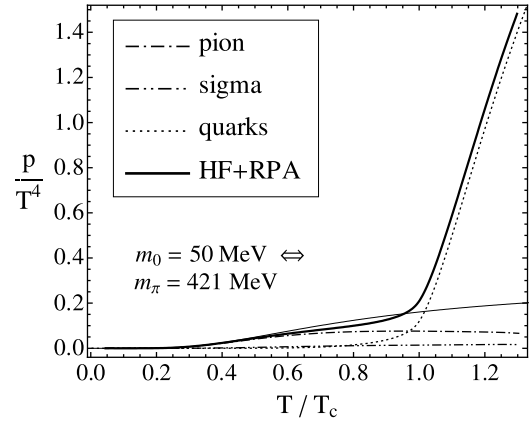
Figure 3.7: Same as Fig. 3.6, but with higher current quark mass $m_0 = 50\,\mathrm{MeV} \Rightarrow m_\pi = 421\,\mathrm{MeV}$ (compared to $m_0 = 5.5\,\mathrm{MeV} \Rightarrow m_\pi = 139\,\mathrm{MeV}$ in Fig. 3.6). The pressure of the boson gas (thin solid line) was now plotted using the heavier pion mass.

The approach discussed in the remainder of this thesis does not include RPA correction. Such RPA approaches allow to address meson properties and correlation lengths. Near phase transitions correlation lengths may diverge modifying mean field critical exponents. Correlation lengths cannot be addressed with spatially and temporally constant fields used in the remaining parts of this work. The corrections implemented in the following sections only release constraints imposed on degrees of freedom which are already part of the mean field PNJL model. Thus there are no backward reactions on the mean field equations. Due to the non-renormalisability of the local PNJL model the implementation of $1/N_c$ corrections is a very delicate issue. Additional regularisation prescriptions suppressing infinities appearing in the higher loop integrals cannot be motivated within the PNJL framework. One way to avoid this uncontrolled influence of further regularisation is the non-local generalisation of the PNJL model [BBRV08, AAG$^+$08, HRCW09]. Such approaches are beyond the scope of this work. The calculations in Refs. [BBRV08, AAG$^+$08, HRCW09] however show that the contribution of meson loops generated in resonant interaction with quark-antiquark states are small. Thus estimating the meson pressure by only taking into account pole contributions, as it has been done here, is a good approximation.

3.3.2   Moments of the pressure

One benchmark for the PNJL model is its surprising capability of reproducing the trends of lattice QCD calculations.[4] One way to handle the fermion sign problem in lattice QCD is to expand the calculated pressure about $\mu = 0$ in a Taylor series.

---

[4]Note however the discussion concerning the dependence on quark masses in Ref. [RRW07a].
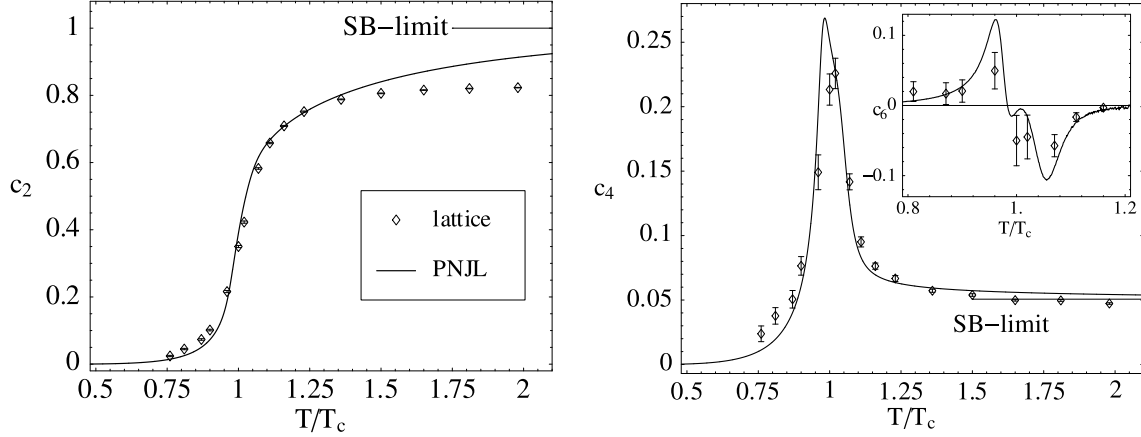
Figure 3.8:   The moments of the pressure with respect to $\frac{\mu}{T}$ as defined in Eq. (3.15). c_2 is shown in the left panel, c_4 is displayed to the right where c_6 is shown in the inset. The data deduced from lattice computations are taken from [A^{+}05].

Such an expansion is given in Ref. [A^{+}05]:

$$\frac{p(T,\mu)}{T^4} = \sum_{n=0}^{\infty} c_n(T) \left(\frac{\mu}{T}\right)^n \qquad \text{with} \qquad c_n(T) = \frac{1}{n!} \frac{\partial^n (p(T,\mu)/T^4)}{\partial(\mu/T)^n}\bigg|_{\mu=0} \qquad (3.15)$$

with even n as the situation is charge conjugation invariant. Specifically:

$$\begin{aligned}
c_2 &= \frac{1}{2!} \frac{\partial^2 (p/T^4)}{\partial(\mu/T)^2}\bigg|_{\mu=0}, \quad c_4 = \frac{1}{4!} \frac{\partial^4 (p/T^4)}{\partial(\mu/T)^4}\bigg|_{\mu=0}, \\
c_6 &= \frac{1}{6!} \frac{\partial^6 (p/T^4)}{\partial(\mu/T)^6}\bigg|_{\mu=0}, \quad c_8 = \frac{1}{8!} \frac{\partial^8 (p/T^4)}{\partial(\mu/T)^8}\bigg|_{\mu=0}.
\end{aligned} \qquad (3.16)$$

The pressure in the PNJL model is evaluated by subtracting the divergent vacuum contributions of the thermodynamic potential:

$$p = -\left(\Omega - \Omega(T=0)\right) \qquad (3.17)$$

Results for c_2, c_4 and c_6 are shown in Fig. 3.8. In comparison with the plots for c_n presented in Ref. [RRW07b] at the mean field level the moments c_n show slightly more structure. The rise in c_2 is somewhat sharper, the peak in c_4 is about 5 % higher. In summary the corrections induced by the more carefull treatment of $\langle \Phi^* - \Phi \rangle$ around its mean field values are small. Pionic fluctuations tend to be more important. In presently available lattice results [A^{+}05], these latter effects are however suppressed by the relatively large pion masses (see also the discussion in Sec. 3.3.1 including Figs. 3.6 and 3.7).

The PNJL results for the interaction or conformal measure $\varepsilon - 3p$ are illustrated in Fig. 3.10. The total interaction measure normalised to T^4 is split into quark and Polyakov loop parts. Note the sensitive balance between quark quasiparticle and Polyakov loop contributions to $\varepsilon - 3p$ close to T_c. In pure gauge QCD (or with infinitely heavy quarks) the Polyakov loop interaction measure is positive throughout. The presence of light quarks and their dynamical coupling to the Polyakov

loop changes their pattern significantly. The Polyakov loop part of the pressure itself, that determines the dashed curve in Fig. 3.10, is found to be consistent with calculations reported in Ref. [Fuk08b]. For orientation, the total PNJL interaction measure (with $N_{\mathrm{f}} = 2$) is shown in Fig. 3.10 along with recent $N_{\mathrm{f}} = 2 + 1$ lattice QCD results [Kar08].

3.3.3   Chiral and Polyakov loop susceptibilities

A susceptibility χ_g involving a quantity g is defined by

$$\chi_g^2 = V \ \langle (g - \langle g \rangle)^2 \rangle = V \left(\langle g^2 \rangle - \langle g \rangle^2 \right) \ . \tag{3.18}$$

Susceptibilities of special interest in the present context are the ones related to the dynamical quark mass, $m = m_0 - \sigma$, and to the Polyakov loop. They are expressed in terms of the inverse matrix of the second derivatives of the full thermodynamic potential Ω:

$$\chi_M^2 = V \left(\langle m^2 \rangle - \langle m \rangle^2 \right) = T \left[\frac{\partial^2 \Omega}{\partial \theta_i \partial \theta_j} \right]^{-1}_{m, m} \tag{3.19}$$

$$\chi_\Phi^2 = V \left(\langle \Phi^2 \rangle - \langle \Phi \rangle^2 \right) = T \left[\frac{\partial^2 \Omega}{\partial \theta_i \partial \theta_j} \right]^{-1}_{\Phi, \Phi} \tag{3.20}$$

$$\chi_{\mathrm{Re}\,\Phi}^2 = \frac{T}{4} \left[\frac{\partial^2 \Omega}{\partial \theta_i \partial \theta_j} \right]^{-1}_{\Phi, \Phi} + \frac{T}{2} \left[\frac{\partial^2 \Omega}{\partial \theta_i \partial \theta_j} \right]^{-1}_{\Phi, \Phi^*} + \frac{T}{4} \left[\frac{\partial^2 \Omega}{\partial \theta_i \partial \theta_j} \right]^{-1}_{\Phi^*, \Phi^*} \ . \tag{3.21}$$

These susceptibilities are calculated using the graph rules given in Tab. B.2 of the appendix which lead to the following explicit form:

$$\chi_g^2 = T \left(\frac{\partial g}{\partial \theta} \right)^T \cdot \left[\frac{\partial^2 \Omega_0}{\partial \theta^2} \right]^{-1} \cdot \frac{\partial g}{\partial \theta} \Bigg|_{\theta = \theta_{\mathrm{MF}}}$$

$$- 2 T \left(\frac{\partial g}{\partial \theta} \right)^T \cdot \left[\frac{\partial^2 \Omega_0}{\partial \theta^2} \right]^{-1} \cdot \frac{\partial^2 g}{\partial \theta^2} \cdot \left[\frac{\partial^2 \Omega_0}{\partial \theta^2} \right]^{-1} \cdot \frac{\partial \Omega_0}{\partial \theta} \Bigg|_{\theta = \theta_{\mathrm{MF}}}$$

$$+ T \sum_{i,j,k} \frac{\partial^3 \Omega_0}{\partial \theta_i \partial \theta_j \partial \theta_k} \left(\left[\frac{\partial^2 \Omega_0}{\partial \theta^2} \right]^{-1} \cdot \frac{\partial g}{\partial \theta} \right)_i \left(\left[\frac{\partial^2 \Omega_0}{\partial \theta^2} \right]^{-1} \cdot \frac{\partial g}{\partial \theta} \right)_j$$

$$\times \left(\left[\frac{\partial^2 \Omega_0}{\partial \theta^2} \right]^{-1} \cdot \frac{\partial \Omega_0}{\partial \theta} \right)_k \Bigg|_{\theta = \theta_{\mathrm{MF}}} \ . \tag{3.22}$$

Here g stands for m or Φ, respectively. The first term in Eq. (3.22) is the susceptibility of the gaussian theory whereas the other terms are interpreted as corrections.

The definition of susceptibilities in Eq. (3.18) gives a statistical interpretation of the susceptibility χ_g. It is the measure for the typical size of deviations of the quantity g from its mean value. Large χ_g indicate large deviations form the expectation value $\langle g \rangle$ which can be explained on the basis of a Ginzburg-Landau model

in terms of a small curvature of the effective potential around $\langle g \rangle$. In a Ginzburg-Landau analysis a vanishing curvature of the effective potential is characteristic for a second order phase transition, while a first order transition even requires a sign change of the curvature of the effective potential creating an instability and a split of the system in two phases. As the sign change of the curvature in a system with first order phase transition does not happen at the expectation value of $\langle g \rangle$ we do not observe large susceptibilities in thermodynamic equilibrium. At a second order phase transition the system lingers, however, exactly at the position of the effective potential where the curvature vanishes. This leads to diverging susceptibilities at second order phase transitions. At some distance to second order phase transitions we expect the divergence to become finite. In mean field calculations[5] one finds the critical exponent $\gamma = 1$ for the quark number susceptibility. I.e. approaching the phase transition the susceptibility will diverge according to a $(T - T_c)^{-1}$-law. It is however a very delicate issue along which path such a singularity is approached. In general there are two directions that have to be distinguished: the temperature-like and the magnetic field-like direction. The given mean field scaling law refers to a temperature-like approach to the critical point. According to Ref. [HI03] approaching the critical point on a trajectory asymptotically not parallel to the temperature direction results in the critical exponent $-2/3$.

Similar relations can be established in mean field calculations considering the vicinity of the tricritical point using the current quark mass as one direction in the phase diagram of our model [HI03]. Here the quark number susceptibility diverges with a $m_0^{-2/5}$ power law, where m_0 is the current quark mass. Nevertheless, as the current quark mass in nature is of course fixed, we expect that susceptibilities are enhanced near the second order phase transition at vanishing current quark mass, i.e. near the chiral limit. Unfortunately it is not guaranteed that the physical quark mass is still close enough to the second order transition such that this enhancement is significant. The size of the critical region has been investigated numerically in an NJL model in Ref. [HI03]. It is concluded that the tricritical point in the QCD phase diagram at $m_0 = 0$ is located sufficiently close to physically realized quark masses to dominate the pseudo-critical behaviour along the chiral crossover. The size of the prefactor of the divergences is a model (theory) dependent quantity. The region where the divergent part of a quantity dominates over the regular part is usually called critical region. The presented model calculation (in agreement with others [SFR08]) predict that QCD with physical quark masses is still inside the critical region of QCD in the chiral limit. The proximity of the second order phase transition and the tricritical point at $m_0 = 0$ also influences which direction in the T, μ and m_0 parameter space is temperature-like and which one is magnetic field-like. These issues may complicate the extraction of critical exponents and influence shape and size of the critical region. The direction orthogonal to the ending first order phase transition region typically exhibits temperature-like scaling behaviour, while

---

[5]If spatial fluctuations are respected along the divergence of the susceptibilities, the correlation length diverges. This changes the effective size of the system simultaneously, leading to modifications of the mean field critical exponents. These changes are model (theory) dependent. Using this highly non-trivial effect allows to categorise models (theories) by a universality class.

the directions parallel to the first order phase transition manifold behave magnetic field-like. Considering the different critical exponents leads to a flattening of the critical region in temperature-like direction if the threshold of irregular domination over regular contributions is increased.

The critical behaviour of susceptibilities may be exploited to locate the chiral crossover transition experimentally. The extraction of susceptibilities from heavy-ion collisions is difficult, however. One of the main difficulties in the extraction of thermodynamic quantities from heavy-ion collisions is the fact that thermodynamics is an equilibrium description of nature, whereas the experimental situation is highly dynamic. Together with the divergence of the susceptibilities we expect correlation lengths to diverge. Thus size and limited timescales in the dynamic evolution of two colliding nuclei smoothens all divergences and peaks which are present in thermal equilibrum. Even though the fireball expansion is highly dynamic local thermodynamic equilibration has proven to be a good assumption. The successful description of the fireball evolution by hydrodynamic calculations is an indication towards local equilibration. The elementary processes that lead to very short equilibration times is not known yet. The inhomogeneity of the fireball brings about that heavy-ion collisions probe rather large areas in the QCD phase diagram at the same time. To de-convolute the experimental prerequisites from the theoretical phase diagram requires very detailed understanding of the processes involved in the fireball expansion and the experimental setup. We are facing a "chicken or the egg" dilemma here: the analysis of experimental data require accurate description of the processes involved, which at the moment is hard to achieve due to the poor quality of experimental input. This vicious circle can only be broken in an iterative interplay of experiment and theory refining theory and experiment successively. Therefore all additional experimental data collected (even when collected with outdated machines) will help refining our understanding in this iterative process.

To measure susceptibilities in heavy-ion collisions one has to come back to the definition in Eq. (3.18). Having available a large piece of bulk matter the measurement of a fluctuation requires to define a test volume, in which a certain quantity e. g. quark number is measured. Ideally this test volume is much larger than the size of the fluctuations. From an ensemble of independent measurements at different times and (or) in different equivalent subvolumes susceptibilities can then be extracted. One way to do this in heavy-ion collisions is to take various successive collisions as statistical ensemble. The finite acceptance of every detector defines a fixed window in phase space. The measured value e. g. for the quark number is then subject to the statistical properties of the system. This approach to measure fluctuations on the so-called event-by-event basis [BJK00, SRS99, BH99, Koc08] suffers from a varying and limited number of nucleons participating in successive collisions due to changing impact parameters. I. e. the systems we are probing is neither very large nor are they equivalent. Therefore, in a first step all events have to be binned according to the number of participants[6] to define an ensemble of equivalent systems. To increase the test volume large detector acceptances are required in addition. The

---

[6]The number of participants is the number of nucleons that actually participate in primary collisions. The trajectories of these nucleons cross the intersection area of the two colliding nuclei.

phase space volume cut out by the acceptance involves limitations in direct and momentum space. These two issues can in principle be solved by large statistics and careful detector analysis. A more principle problem poses the proper separation of scales. It is difficult to fulfil the prerequisite that the system size is much larger that the test volume which again has to be much larger than the fluctuations (the correlation length). Estimates are that the correlation length is of the order of $2\,\mathrm{fm}$ which is substantially smaller that the system size [Koc08] such that two colliding nuclei produce a sufficiently large system for this investigation. Finally one relies on the fact that the interactions in the hadronic final state are small, such that correlations which have piled up crossing the phase transition are not washed out during the final stages of the evolution of the collision. In Ref. [Koc08] high collision energies and large detector acceptances are mentioned as prerequisites for this final requirement to be fulfilled. Despite all those difficulties quite some experimental data on fluctuations has been collected. However, according to Ref. [Wes08], the data currently available is not conclusive.

At present the direct extraction of susceptibilities from the QCD Lagrangian can only be accomplished with numeric lattice QCD calculations. To avoid the highly complex problems involved we switch to PNJL model calculation. One of the reasons for doing this is the possibility to implement small current quark masses in the model frame work. Rather large current quark masses often applied in lattice QCD calculations are expected to dampen the signatures of the crossover imprinted in susceptibilities. In Fig. 3.9 the chiral and the Polyakov loop susceptibilities as functions of temperature at vanishing quark chemical potential (left panel) are compared to the temperature derivatives of the constituent quark mass and the Polyakov loop (right panel). While the chiral susceptibility to the left of Fig. 3.9 only shows a single peak structure the temperature derivative of the constituent quark mass to the right exhibits a widened peak, indicating the influence of both chiral symmetry breaking and Polyakov loop induced confining effects. This indicates that the constituent quark mass plays a major role in the correct implementation of thermodynamics in the PNJL model; after all the PNJL model is a (quark-) quasiparticle model.

If we consider the behaviour of χ_M, $\chi_{\mathrm{Re}\,\Phi}$ and χ_Φ at $T \to 0$ we find that $\chi_{\mathrm{Re}\,\Phi}$ is finite, while χ_M and χ_Φ vanish. This can be explained by the fact that $(\mathrm{Re}\,\Phi)^2 = \frac{1}{4}(\Phi^2 + 2\,|\Phi|^2 + \Phi^{*2})$ contains a U(1)-symmetric term $|\Phi|$. As the U(1) symmetry incorporates the $Z(3)$ centre of SU(3)$_\mathrm{c}$ this term does not have to vanish once the $Z(3)$ symmetry is fully restored at $T = 0$.[7] The width of the peak in the temperature derivative of the dynamical quark mass $m = m_0 - \sigma$ suggests that this crossover is influenced by the crossover of the Polyakov loop.

The PNJL model predicts rather articulately structured susceptibilities at vanishing chemical potentials using physical quark masses. This is an indication for the proximity of the critical behaviour in the chiral limit. The presented calculation implementing Polyakov loop dynamics is in agreement with the investigation in Ref. [HI03] using an NJL model without Polyakov loop which predicts the model implementing physical quark masses to be located in the critical region of the tri-

---

[7]The author thanks Chihiro Sasaki for pointing this out to him.
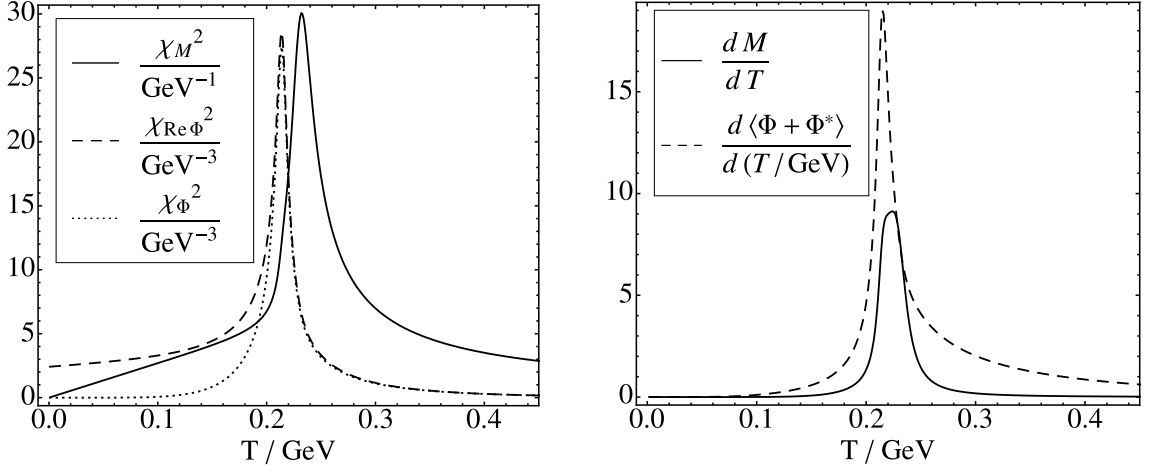
Figure 3.9: The chiral susceptibility χ_M (left panel solid line) and the Polyakov loop susceptibilities $\chi_{\mathrm{Re}\,\Phi}$ (left panel dashed line) and χ_Φ (left panel dotted line) plotted as functions of temperature at vanishing quark chemical potential. These susceptibilities defined by Eqs. (3.19, 3.20, 3.21) and evaluated using Eq. (3.22) are compared here to the derivative of the constituent quark mass (right panel solid line) and the expectation value of the real part of the Polyakov loop (right panel dashed line) with respect to temperature. [RHRW08]

critical point in the chiral limit. Thus fluctuation are in principle suited to find the chiral crossover transition at small chemical potentials, which may be accessible in heavy-ion collisions at highest energies like ALICE at LHC. An interesting issue that could be clarified using these new experimental data is the relation of chiral crossover transition and chemical freeze-out.

3.3.4 Cumulant ratios along the deconfinement transition

The ratio of the moments c_4 and c_2 has been discussed [EKR06] as a suitable indicator of fluctuations close to the phase transition.[8] The quantity of interest here is the cumulant ratio $R_{4,2}^{\mathrm{q}}$ defined in [EKR06] and given as $R_{4,2}^{\mathrm{q}} = 12\,c_4/c_2$. The PNJL model calculation for this ratio is shown in Fig. 3.11. The dashed curve is found in the mean field limit with $\langle\Phi^*\rangle = \langle\Phi\rangle$ which suppresses one of the two Polyakov loop degrees of freedom. The solid curve is computed with inclusion of corrections beyond mean field and demonstrates the role of $\langle\Phi^* - \Phi\rangle$ being non-zero. According to Ref. [SFR08] the low and high temperature limits for the cumulant ratio are given by

$$R_{4,2}^{\mathrm{q}} \xrightarrow{T\to 0} (3B)^2 \qquad\qquad R_{4,2}^{\mathrm{q}} \xrightarrow{T\to\infty} \frac{6}{\pi^2}\ , \qquad\qquad (3.23)$$

where B is the baryon number carried by the effective degrees of freedom. After taking into account the full dynamics of the Polyakov loop Φ and its complex

---

[8] The expansion coefficient c_2 is related to the quark number susceptibility at $\mu = 0$ by: $\chi_{\mathrm{q}}\big|_{\mu=0} = 2\,c_2\,T^2$.
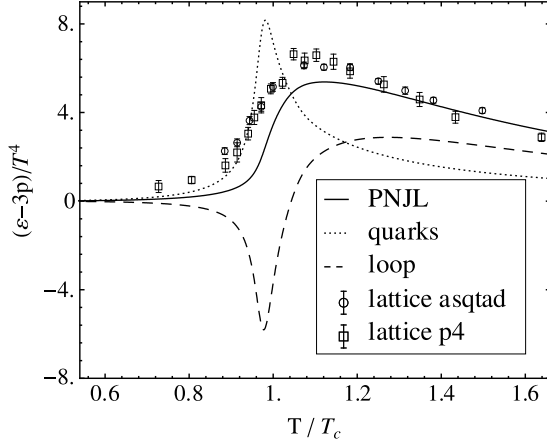
Figure 3.10: Contributions to the inter-action measure from quarks and Polyakov loop, as well as the total PNJL interaction measure for $N_f = 2$. The $N_f = 2+1$ lattice QCD results [Kar08] (with $N_\tau = 8$ for p4-improved and asqtad action) are shown for orientation.
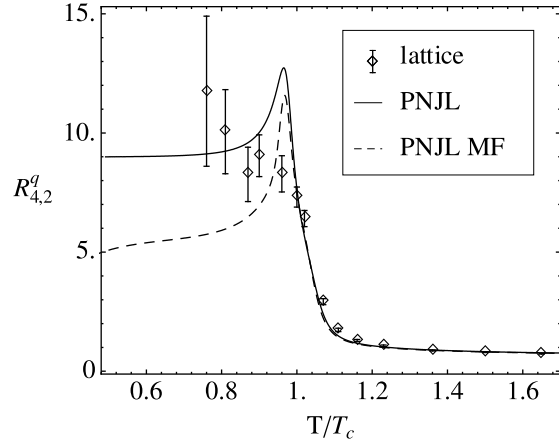
Figure 3.11: The cumulant ratio $R^q_{4,2}$ from the PNJL model in and beyond mean field approximation in comparison with lattice QCD results, with c_2 and c_4 as given in Ref. [A+05].

conjugate Φ^* we reach $B = 1$ at low temperatures. At low temperatures the thermodynamically active degrees of freedom in the PNJL model beyond mean field are compounds with three valence quarks. However, the PNJL model remains a quasi-particle model with quarks, which becomes visible even at low temperature once more detailed quantities like spectral functions are investigated.

At low temperatures the degrees of freedom can only be excited marginally. The partition function of a fermion gas of non-interacting gas can be approximated at low temperatures by the sum of fermion and antifermion contribution: $\mathcal{Z} \propto e^{-(E-\mu)/T} + e^{-(E+\mu)/T} = 2e^{-E/T} \cosh[\mu/T]$. An expansion in μ/T immediately reveals that $R^q_{4,2}$ will assume one. In the presence of Polyakov loop dynamics the first two lowest terms in the approximation of the partition function $\mathcal{Z}$ are suppressed such that $\mathcal{Z} \propto \cosh[3B\,\mu/T]$ resulting in the low temperature limit $(3B)^2$ of $R^q_{4,2}$. At high temperatures it is the prefactors of fourth and second order coefficient of the μ/T-expansion of p/T^4 that determine the high temperature limit.[9] One could add an additional factor of $(3B)^2$ here as well, as Polyakov loop dynamics again would suppress all terms in the partition function not proportional to $e^{3\mu/T}$. At high temperatures we find $3B \approx 1$ (see Fig. 3.11) indicating deconfinement, which is realized because the terms proportional to $\left(e^{\mu/T}\right)^1$ and $\left(e^{\mu/T}\right)^2$ are not suppressed by the Polyakov loop.

If the influence of the Polyakov loop is quenched by the mean field approximation some deconfined quarks remain part of the active degrees of freedom. In mean field approximation $R^q_{4,2} < 9$ at low temperatures as can be seen in Fig. 3.11. In the intermediate temperature regime near the crossover transition the PNJL model

---

[9] $\frac{p}{T^4} \propto \frac{1}{12\pi^2} \left(\frac{\mu}{T}\right)^4 + \frac{1}{6} \left(\frac{\mu}{T}\right)^2 + \frac{7\pi^2}{180}.$

predicts a rather strong peak which is not visible in the lattice QCD data used for comparison. Such a peak cannot be interpreted in the way done before. A value larger than 9 does not imply effective degrees of freedom with a baryon number above 3 as this interpretation was based on expansions in μ/T which is neither a small nor large quantity around the crossover transition. We rather have to go back to the definitions of c_2 and c_4:

$$\frac{c_4}{c_2} = \frac{\left\langle (\delta N_\mathrm{q})^4 \right\rangle - 3 \left\langle (\delta N_\mathrm{q})^2 \right\rangle^2}{\left\langle (\delta N_\mathrm{q})^2 \right\rangle} \quad \text{with} \quad \left\langle (\delta N_\mathrm{q})^2 \right\rangle = \left\langle N_\mathrm{q}^2 \right\rangle - \left\langle N_\mathrm{q} \right\rangle^2 \; . \quad (3.24)$$

A strong increase of $R_{4,2}^\mathrm{q}$ therefore indicates a rise of $\left\langle (\delta N_\mathrm{q})^4 \right\rangle - 3 \left\langle (\delta N_\mathrm{q})^2 \right\rangle^2$ or a decrease of $\left\langle (\delta N_\mathrm{q})^2 \right\rangle$. In terms of an effective potential the increase of the quartic fluctuations relative to the quadratic fluctuations indicates that the quadratic fluctuations are variable in their extend. That is, once the quark density changes we have to expect strong relative changes in the second order term of the effective potential. Such strong relative changes happen once the absolute value of the second order term is close to zero, i.e. the effective potential is dominated by the fourth order term. It is well known that at a second order phase transition (in mean field) the second order term vanishes. Therefore large $R_{4,2}^\mathrm{q}$-values identify regions in the phase diagram close to a second order phase transition. A second order phase transition is realized in the unphysical case of vanishing current quark masses (in the chiral limit) along the restoration of the chiral symmetry and for a critical end point. The relict of this second order phase transition may still be visible at physical current quark masses. The closer we get to the second order phase transition the sharper we expect the structures in $R_{4,2}^\mathrm{q}$ to be. These considerations are equivalent with the observation that large pion masses suppress the peak in $R_{4,2}^\mathrm{q}$ [SFR08]. The authors of Ref. [SFR08] argue on the basis of their Polyakov loop extended quark meson model that this peak increases towards the chiral limit finally exhibiting a cusp in the chiral limit. These considerations also motivate why the lattice data shown in Fig. 3.11 do not peak near the crossover. The used current quark mass of $0.4\,T$ is too large to see relicts of the tricitical point at vanishing quark mass.

While the peak in $R_{4,2}^\mathrm{q}$ indicates the close existence of the chiral tricritical point, the regular parts in $R_{4,2}^\mathrm{q}$ give some indication towards the nature of the active degrees of freedom. The interpretation of the low and high temperature limits in Eq. (3.23) allow to identify the deconfined crossover transition. Thus $R_{4,2}^\mathrm{q}$ is suited to study both crossover transitions of chiral symmetry restauration and deconfinement. The regular parts of $R_{4,2}^\mathrm{q}$ hint towards confinement, while the irregular parts relate to chiral effects. In disrespect of the enormous required effort for this task it would even be possible to study the order of the phase transition by looking for peak- or cusp-like structures. The experimental difficulties, however, will most likely not allow for such an analysis in the near future.

3.3.5   The speed of sound

In the construction of models for the fireball evolution in heavy-ion collisions the speed of sound in medium is of major importance: The PNJL model predicts sig-
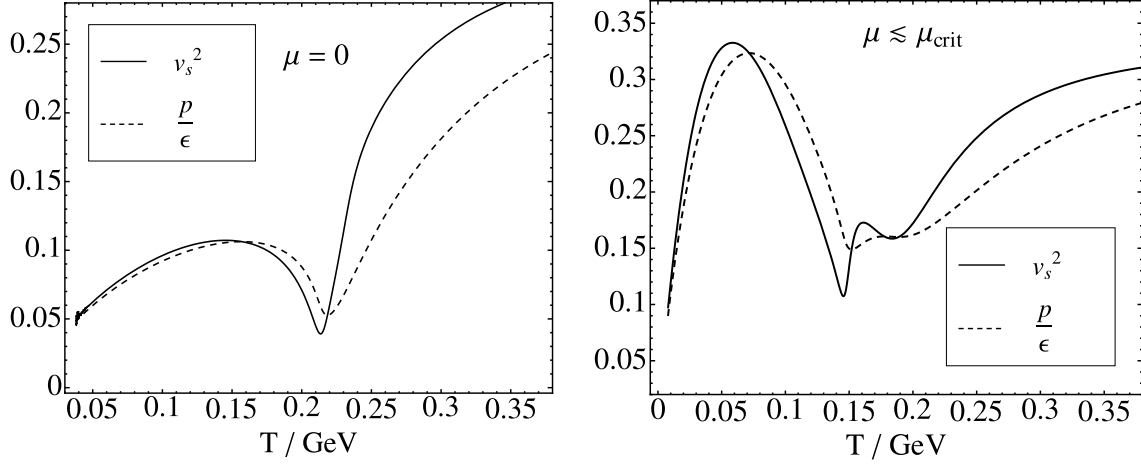
Figure 3.12: The speed of sound (solid) and the ratio of pressure over energy density (dashed) at vanishing chemical potential as function of temperature (left panel). The right panel shows the same quantities at a quark chemical potential slightly below the critical point ($\mu = 0.3\,\mathrm{GeV} \lesssim \mu_{\mathrm{crit}} \simeq 0.31\,\mathrm{GeV}$).

nificant temperature dependence of the speed of sound across the deconfinement crossover transition. The elliptic flow is rather insensitive to the speed of sound. Elliptic flow piles up at very early stages of the fireball evolution, where temperatures are still high such that quarks are light and may be considered weakly interacting resulting in $v_{\mathrm{s}}^2 \approx \frac{1}{3}$ during the relevant early times. In Fig. 3.12 the squared speed of sound in units of the speed of light is plotted as a solid line. The speed of sound v_{s} is defined by

$$v_{\mathrm{s}}^2 = \left.\frac{\partial p}{\partial \varepsilon}\right|_S = \left.\frac{\partial \Omega}{\partial T}\right|_V \Big/ \left. T \frac{\partial^2 \Omega}{\partial T^2}\right|_V \,, \tag{3.25}$$

where the denominator is the specific heat capacity c_V. The specific heat capacity c_V is the main source of this strong temperature dependence. In the chiral limit one expects that the heat capacity diverges at the second order phase transition bringing the speed of sound to zero. This divergence in the specific heat is caused by large susceptibilities which allow for strong energy deposition in diverging fluctuations. The dashed line in Fig. 3.12 gives the size of the ratio of pressure and energy density, $\frac{p}{\varepsilon}$. This quantity corresponds to the speed of sound for an ideal gas. In the panel to the left where the quantities are plotted at vanishing chemical potential $\mu = 0$ both graphs show a pronounced dip near the crossover transition temperature. In the panel to the right the same situation is plotted at a quark chemical potential close to the chemical potential of the critical point $\mu \lesssim \mu_{\mathrm{crit.}}$. Here one can identiy two distinct minima which correspond to the chiral and the deconfinement crossover transitions.

The vanishing of the speed of sound in the chiral limit is part of the critical slowing down at a second order phase transition. The fast evolution and the critical slowing down will prevent the fireball from equilibrating in the vicinity of the critical point. Therefore it is not only the system size that limits the size of possibly observed fluctuations but also the time spent near the critical region. Crudely

approximating the fireball as a homogeniously expanding gas ball, the speed of sound will define some sort of event horizon. If we parametrize this expansion in analogy to the Hubble expansion, we can estimate the maximal correlation length by $\Delta l \approx v_{\mathrm{s}}/H$, where H is the "Hubble"-constant of the litte Big Bang. We can estimate H by $H \approx c/r$, where c is the speed of light and r is the fireball radius. Using the Stefan-Boltzmann energy density $\varepsilon = \left(\frac{8}{15} + \frac{7\,N_{\mathrm{f}}}{20}\right)\pi^2\,T^4$ we estimate the fireball radius: $r \approx \left(\frac{3}{4\pi}\frac{E_{\mathrm{tot}}}{\varepsilon}\right)^{(1/3)} = \frac{1}{\pi}\left(\frac{45}{74}\frac{E_{\mathrm{tot}}}{T^4}\right)^{(1/3)} \approx 19\,\mathrm{fm}$.[10] This allows to estimate the maximal size of a fluctuation that can build up at a given speed of sound: $\Delta l \approx r \times \frac{v_{\mathrm{s}}}{c} \approx 19\,\mathrm{fm}\frac{v_{\mathrm{s}}}{c}$.[11] Using the minimal value in Fig. 3.12 we find $\Delta l \approx 4\,\mathrm{fm}$.

3.4 Phase diagram with and without diquarks

To distinguish different phases in a phase diagram order parameters are needed. I. e. phases are determined as function of certain control parameters; here we concentrate on temperature and quark chemical potential. In case of true phase transitions it is a non-analyticity in the dependence on the order parameter, that indicates a phase transition. The order at which this non-analyticity appears determines the order of the phase transition. In case of QCD where both chiral and deconfinement transition are related to symmetries that are broken not only spontaneously but also explicitly by finite current quark masses the order parameters do not show such non-analytic behaviour. Nevertheless the transition from weak to strong symmetry breaking appears within a small range of the control parameters (here temperature and chemical potential). In this case the transition is classified as rapid crossover. To quantify the position of such a rapid crossover an indicator for the steepness of the change of the approximate order parameter is needed. One class of measures commonly used are susceptibilities which are discussed in detail in Sec. 3.3.3.

The susceptibilities χ_M and χ_Φ serve as indicators for crossover transitions between approximate phases when drawing a phase diagram in the plane of temperature and chemical potential. Several criteria can be used to determine a transition line separating the region of spontaneously broken chiral symmetry from the quark-gluon phase. We use the maxima of the chiral susceptibilities χ_M and of the Polyakov loop susceptibility $\chi_{\mathrm{Re}\,\Phi}$. Alternatively we could use the slopes $\mathrm{d}m/\mathrm{d}T$ and $\mathrm{d}\langle\Phi^* + \Phi\rangle/\mathrm{d}T$ of constituent quark mass and Polyakov loop which act as order parameters in the limiting situations of exact chiral $\mathrm{SU}(2)_{\mathrm{L}} \times \mathrm{SU}(2)_{\mathrm{R}}$ symmetry or $Z(3)$ symmetry, respectively. Fig. 3.13 shows a comparison of crossover transition lines found with the two criteria just mentioned. As both criteria are linked via the quadratic term in the action, all curves finally converge to the same point, the critical point (here in the absence of diquark condensation). A singularity in the second derivative of the action (or equivalently in the propagator) enforces this

---

[10]We have used $N_{\mathrm{f}} = 2$ at $T \approx 200\,\mathrm{MeV}$ and $E_{\mathrm{tot}} = 200\,\mathrm{GeV} \times 197 \times 2$ for a gold on gold collision.

[11]In this estimate correlations grow with total energy i. e. with the system size. For increasing system sizes the pressure gradients will drop leading to a more moderate and longer lasting expansion of the system.

unique intersection point where the specific heat and other quantities show singular behaviour. In the PNJL model this critical point is the remnant of the critical point of the NJL model, i.e. critical behaviour is driven by chiral dynamics. In principle Polyakov loop dynamics could also produce criticality. Here where it is assumed that the Polyakov loop effective potential is independent of the quark chemical potential μ_q this does not happen.

Comparing our Fig. 3.13 with corresponding results in other publications (see Fig. 16 in Ref. [SFR07] and Fig. 4 in Ref. [AAG$^+$08]) one finds that the detailed behaviour of the deconfinement crossover transition line depends sensitively on the parameter choice and regularisation prescription. In the present case of a strong coupling a joint course of chiral and deconfinement crossover line is observed. When the coupling becomes weaker (e.g. due to parameter choice and regularisation prescription as in Refs. [SFR07, AAG$^+$08]) the transition lines may deviate. In any case one should note that such deviations appear at large chemical potentials approaching the typical cutoff scale of the model. Any conclusions drawn at such energy or momentum scales should be handled with care.

At finite current quark mass m_0 the PNJL model produces an approximate coincidence of the peaks in the susceptibilities of the Polyakov loop and the constituent quark mass m, consistent with the pattern observed in Fig. 3.1. The approximate coincidence of the peaks in the chiral and Polyakov loop susceptibilities is demonstated at $\mu = 0$ in Fig. 3.9. The width of the peak in the temperature derivative of the dynamical quark mass $m = m_0 - \sigma$ (shown in the right panel of Fig. 3.9) is widened. This may be explained by the superposition of two peaks. When comparing the left and the right panel of this figure it becomes obvious that these peaks are at the position of the chiral and Polyakov loop crossover. This suggests that the dynamical quark mass $m = m_0 - \sigma$ is significantly influenced by both chiral and Polyakov loop susceptibility.[12]

We now turn to the phase diagram in the (T, μ) plane studying the influence of confinement [RRW07b]. The left panel of Fig. 3.14 shows the phase diagram in the (T, μ)-plane computed using the PNJL model in comparison with the NJL model (the limiting case in which $\Phi \equiv 1$). Of particular interest is the location of the critical endpoint at which the chiral and deconfinement crossover transitions at lower μ turn into a first-order phase transition above some critical μ. In these mean field calculations the position of the transition lines were determined using the position of the local maxima of $d\sigma/dT$ and $d\Phi/dT$. The crossover transition lines fixed by either the susceptibilities of σ and Φ or by maximal changes with temperature, i.e. zeros of $d^2\sigma/dT^2$ or $d^2\Phi/dT^2$, do coincide with the critical point for our PNJL model in the absence of diquarks (see left panel of Fig. 3.15). This is a consequence of the divergences in these quantities at the critical point. However, when including diquarks, a coincidence of critical point and crossover transition line is not guaranteed. In general one finds that the critical endpoint depends sensitively

---

[12]In the present parametrisation of the PNJL model the Polyakov loop susceptibility is that pronounced that it governs also the chiral sector. In Refs. [SFR07, AAG$^+$08] the coupling of the loop sector to the chiral sector seems to be too weak to lead to this forced coincidence of chiral and loop sector.
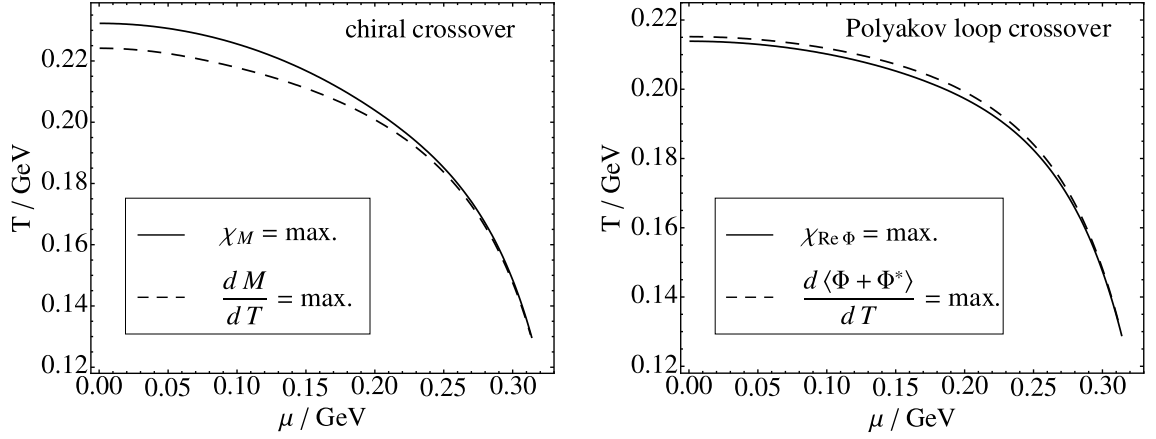
Figure 3.13: Comparison of the transition lines obtained by determination of the maximum in the chiral susceptibility (left panel solid line) and the Polyakov loop susceptibility $\chi_{\mathrm{Re}\,\Phi}$ (right panel solid line) with the transition lines fixed by the maximal change with respect to temperature of constituent quark mass (left panel dashed line) and average of the real part of the Polyakov loop $\frac{1}{2}\langle\Phi+\Phi^*\rangle$ (right panel dashed line). [RHRW08]

on the degrees of freedom involved. From its position in the restricted NJL case this point is shifted to higher T by both, the Polyakov loop effective potential, and by the presence of diquark degrees of freedom. Near the critical endpoint not including diquarks, $\frac{\mathrm{d}\sigma}{\mathrm{d}T}$ diverges together with the chiral susceptibility. This extreme behaviour is not observed in the case with inclusion of diquarks. The region where this critical behaviour would appear is now already located in the diquark dominated phase. Thus there is a qualitative difference of the critical endpoints in these two compared cases: not including diquarks the critical endpoint lies on top of the merging chiral and deconfinement crossover transition lines, while in the case including diquarks the critical endpoint is shifted away from this line. The critical endpoint now lies on the second order transition line bordering the diquark dominated phase (see left panel of Fig. 3.15). I. e. the endpoint is not at the junction of all three transition lines and therefore is not a tricritical point but still a critical point.

Next we use the PNJL model including diquark degrees of freedom to study the dependence of the position of the critical endpoint on the bare (current) quark mass. The right panel of Fig. 3.15 shows phase diagrams in the chiral limit, for current quark masses $m_0 = 5.5\,\mathrm{MeV}$ and $m_0 = 50\,\mathrm{MeV}$. The change of the critical endpoint with varying quark mass mainly reflects the dependence of the critical chemical potential on the quark mass. The presence of the diquark dominated phase appears to stabilise the temperature of the critical endpoint at rather high values.

Generally, the PNJL model exhibits its critical endpoint at a temperature which is significantly higher than the one found with the standard NJL model, i. e. ignoring Polyakov loop dynamics. The reason is that the diquark phase as well as the chiral phase is stabilised by the confinement imitation via the Polyakov loop effective potential. The size of the gap Δ is strongly influenced by the Polyakov loop. The detailed dependence of the gap on the Polyakov loop is displayed in Fig. 3.16. The systematics of this effect becomes evident when the Polyakov loop is held at fixed
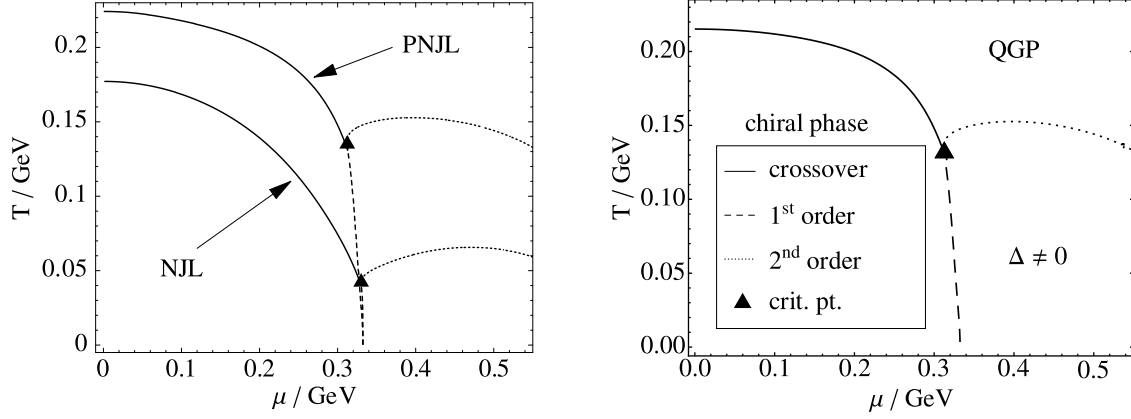
Figure 3.14: Left panel: comparison of the NJL and PNJL phase diagrams in mean field [RRW07b]. Right panel: PNJL phase diagram with the phase diagram including corrections to the order $\beta \leq 1$ [RHRW08]. Solid lines: crossover transition of the susceptibility related to the real part of the Polyakov loop; dashed lines: first order phase transition; dotted lines: second order phase transitions.
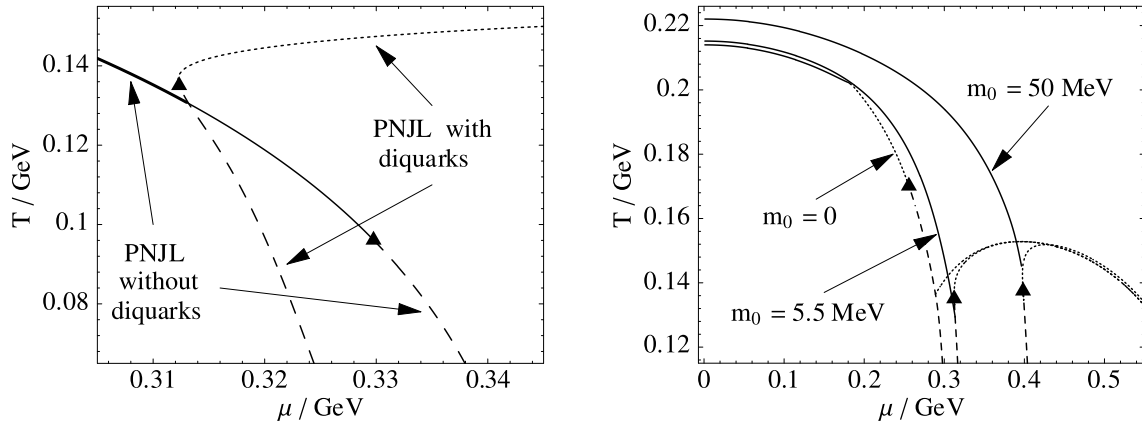
Figure 3.15: Left panel: comparison of the PNJL model in mean field approximation with and without inclusion of diquarks. Right panel: comparison of the phase diagram in mean field approximation at different current quark masses with inclusion of diquark degrees of freedom. (Note the scale on the temperature axis.) [RRW07b].
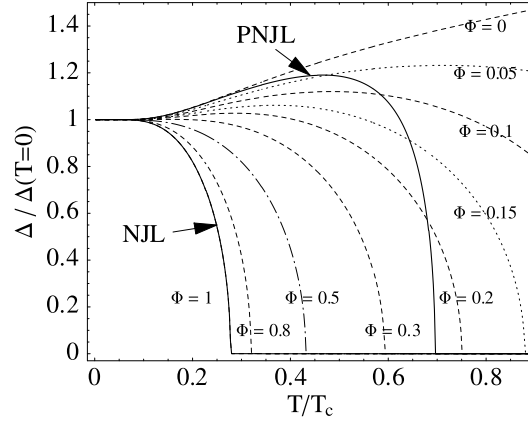
Figure 3.16: Dependence of the gap Δ on the presence of the Polyakov loop. The solid lines are the solutions to the self consistency equations of the NJL and the PNJL model at $\mu = 0.4\,\mathrm{GeV}$. The dashed lines are obtained by enforcing fixed values for the Polyakov loop. Note that the PNJL model with the Polyakov loop fixed at $\Phi = 1$ (deconfinement) coincides with the self consistent solution of the NJL model [RRW07b].

values and varied. The gap resulting from this calculation is then compared to the gap in the PNJL model (with self-consistent determination of Φ) and in the NJL model. The case where the Polyakov loop is fixed to $\Phi = 1$ (i.e. complete deconfinement) coincides with the NJL calculation. The presence of the Polyakov loop restricts the phase space available for quarks in the vicinity of their Fermi surface where Cooper pair condensation takes place. Hence higher temperatures are effectively required to break the pairs. This is the primary reason for the difference in behaviour of the gap Δ when comparing NJL and PNJL results in Fig. 3.16.

A comparison of the phase diagram obtained in mean field approximation (left panel of Fig. 3.14 [RRW07b]) and the phase diagram including corrections to the order $\beta \leq 1$ shown in the right panel of Fig. 3.14 [RHRW08], explicitly approves that corrections to the phase diagram due to the fermion sign problem are indeed small [RRW07b]: the influence of $\mathrm{Im}\,\Omega_0$ and the splitting of $\langle\Phi^*\rangle$ and $\langle\Phi\rangle$ are rather modest.

3.5   Polyakov loop degrees of freedom

With the mean field definition (2.20) the Polyakov loop expectation values $\langle\Phi\rangle$ and $\langle\Phi^*\rangle$ turn out to be equal in this limit, given the reality constraint on Ω_{MF}. It is the corrections from $\mathrm{Im}\,\Omega_0$ induced by the temporal gauge fields which cause the splitting of $\langle\Phi\rangle$ and $\langle\Phi^*\rangle$. The difference $\langle\Phi^*\rangle - \langle\Phi\rangle$ vanishes at zero quark chemical potential μ. It has the same sign as μ, which is in agreement with Ref. [DPZ05]. As can be seen from Fig. 3.17 the difference $\langle\Phi^*\rangle - \langle\Phi\rangle$ is pronounced around the phase transitions. In the upper left panel of Fig. 3.17 the influence of the first order phase transition separating the chiral and the diquark phase at low temperature can be seen as a jump in both $\langle\Phi\rangle$ and $\langle\Phi^*\rangle$. The second order phase transition separating
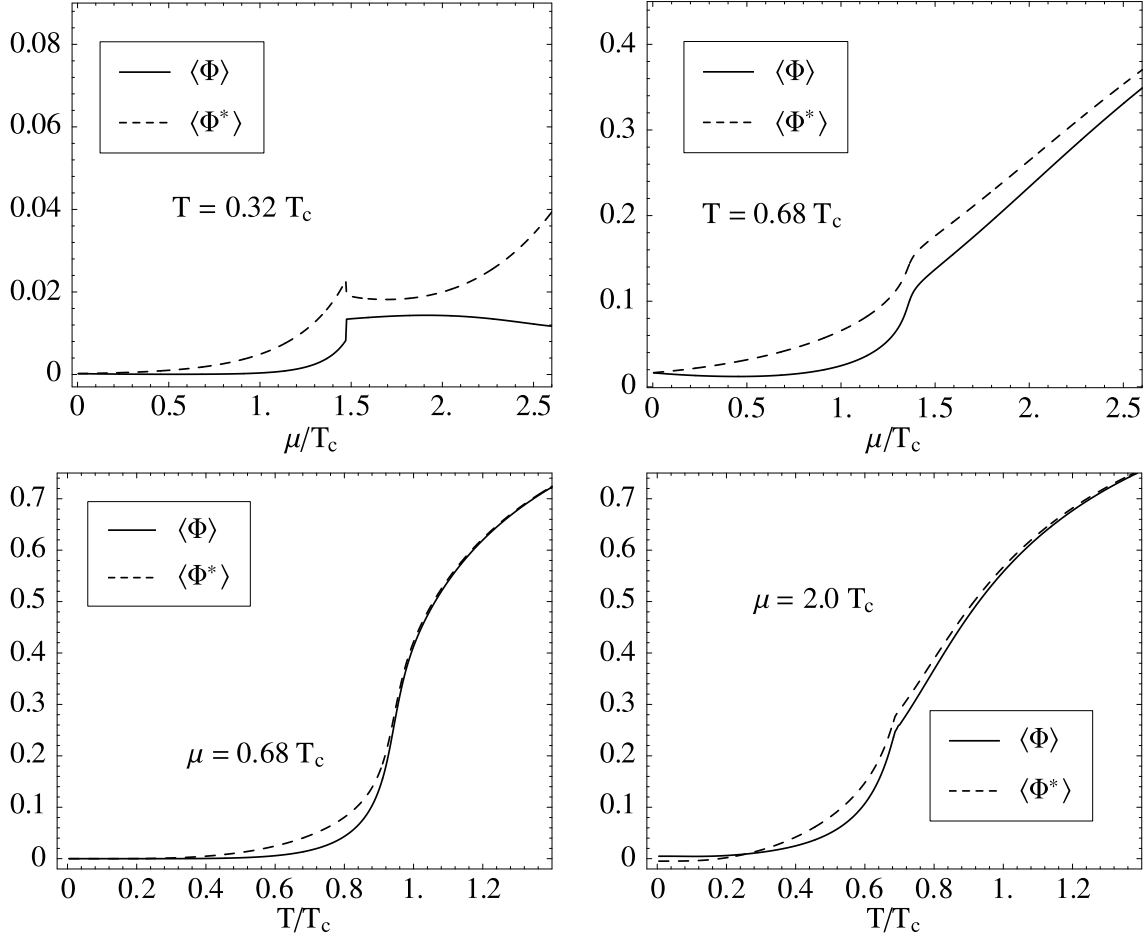
Figure 3.17:   Examples of thermal expectation values of the Polyakov loop $\langle\Phi\rangle$ and its conjugate $\langle\Phi^*\rangle$. In the upper row $\langle\Phi\rangle$ and $\langle\Phi^*\rangle$ are plotted as functions of the chemical potential μ at constant temperature T. Below $\langle\Phi\rangle$ and $\langle\Phi^*\rangle$ are plotted as functions of temperature T at constant chemical potential μ [RHRW08].

the diquark regime from the high temperature quark-gluon phase can be identified as a kink in the lower right panel of Fig. 3.17.

3.6   Isovector degrees of freedom

Up to this section the PNJL model has been considered only in the iso-symmetric case. The influence of confinement on isovector quantities has been studied in Refs. [MMR07, ZL07]. For large isovector chemical potentials $\mu_{\mathrm{I}} = \mu_{\mathrm{u}} - \mu_{\mathrm{d}}$ of the order of the pion mass pion condensation may set in. To study such effects a mean field with the quantum numbers of the pion has to be introduced into the thermodynamic potential. We follow Ref. [ZL07] and add isovector terms to the Lagrangian

$$\delta\mathcal{L}_{\mathrm{PNJL}} = \bar{\psi}\left(\gamma_0\tau_3\mu_{\mathrm{I}} - i\lambda\gamma_5\tau_1\right)\psi \ . \tag{3.26}$$

The quark and Baryon chemical potentials μ, μ_{B} and the isovector chemical potential μ_{I} are connected to the up- and down-quark chemical potentials μ_{u} and μ_{d} via the equations

$$\mu = \frac{\mu_{\mathrm{B}}}{3} = \frac{\mu_{\mathrm{u}} + \mu_{\mathrm{d}}}{2} \qquad \text{and} \qquad \mu_{\mathrm{I}} = \mu_{\mathrm{u}} - \mu_{\mathrm{d}} \ . \tag{3.27}$$

The parameter λ allows to study explicit isovector breaking effects [ZL07], which is not done in this work. We define the chiral up- and down-quark condensates and the pion condensates for π^+, π^- and π^0,

$$\pi^+ = \langle \bar{\psi} i \gamma_5 \tau_+ \psi \rangle \ , \qquad \pi^- = \langle \bar{\psi} i \gamma_5 \tau_- \psi \rangle \ , \qquad \pi^0 = \langle \bar{\psi} i \gamma_5 \tau_0 \psi \rangle \ ,$$
$$\sigma_{\mathrm{u}} = \langle \bar{u} u \rangle \ , \qquad \sigma_{\mathrm{d}} = \langle \bar{d} d \rangle \ , \tag{3.28}$$

where $\tau_{\pm} = (\tau_1 \pm \tau_2)/\sqrt{2}$ and the τ_i are the Pauli matrix in flavour space (see App. C). The flavour structures τ_+, τ_- and τ_0 can be rotated freely under $\mathrm{SU}(N_{\mathrm{f}})$ transformations. It is therefore only necessary to consider one pionic condensate. We choose $\pi = \langle \bar{\psi} i \gamma_5 \tau_1 \psi \rangle$.

After bosonization in the pion channel an additional potential term appears in the thermodynamic potential

$$\delta\Omega = \delta\mathcal{V} = \frac{N^2}{2G} \qquad \text{with} \qquad N = \lambda - G\,\pi = \lambda - G\,\langle \bar{\psi} i \gamma_5 \tau_1 \psi \rangle \ . \tag{3.29}$$

The inverse quark quasiparticle propagator obtains an additional structure

$$\delta\tilde{S}^{-1} = \gamma_0 \tau_3 \,\mu_{\mathrm{I}} - i\gamma_5 \tau_1\,N \ . \tag{3.30}$$

The mean field equations have to be supplemented by

$$\frac{\partial\Omega_{\mathrm{MF}}}{\partial\pi} = \frac{\partial\,\mathrm{Re}\,\Omega_0}{\partial\pi} = 0 \ . \tag{3.31}$$

For simplicity in most studies including isovector condensates, diquark condensation is neglected.[13] This has been done for the current study as well.

In the following subsections the result of Ref. [ZL07] on the additional phases occurring due to the appearance of spontaneous breaking of the isovector symmetry at large isovector chemical potentials is discussed (see Sec. 3.6.1). In analogy to the case with diquark condensation, there exists a critical point. We will study its position in the three dimensional space of temperature, chemical potential and isovector chemical potential. The physical relevance of pion condensates is however strongly criticised [A$^+$08]. In Sec. 3.6.2 and 3.6.3 we abandon finite isovector chemical potentials and concentrate on a Taylor expansion about $\mu_{\mathrm{I}} = 0$, which allows to use lattice QCD data as reference. Even though dealing with a Lagrangian with unbroken isovector symmetry, the PNJL model exhibits finite off diagonal susceptibilities. This phenomenon is discussed in detail in Sec. 3.7.

---

[13]When including both diquark and isovector condensates at the same time it is no longer possible to determine the quasiparticle energies in analytically closed form, complicating the numeric evaluation of the thermodynamic potential and the solution of the mean field equations.

PNJL Phase Diagram
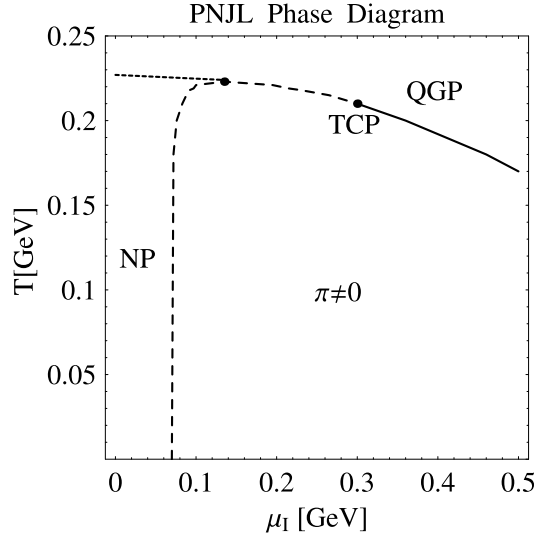
Figure 3.18: The (T, μ_I) phase diagram of the two flavour PNJL model. (NP: normal hadronic phase; QGP: quark-gluon plasma phase) The solid line (dashed line) indicates first order (second order) pion superfluidity phase transitions. The dotted line in the left panel indicates the crossover for deconfinement phase transition. This Figure is taken from Ref. [ZL07] using a different regularisation and parameter set.

3.6.1   Pion condensation

Once the quark chemical potential exceeds the mass of the sigma mode we observe condensation of diquarks. Same is true for the isovector chemical potential. If it reaches the mass of the pion mode we expect pions to condensate. In Ref. [A$^+$08] pion degrees of freedom have been considered under the additional constraint of keeping electric neutrality. According to this work the isovector chemical potential will not exceed such large values at the order of the pion mass, such that pion condensation does not happen in nature. It is nevertheless interesting to study the case of large isovector chemical potentials, not only as the arguments in [A$^+$08] are under debate.

In Fig. 3.18 presented in Ref. [ZL07] the superfluid pion phase is separated from the normal hadronic phase by a second order phase transitions. At large isovector chemical potentials the separation towards the high temperature quark gluon phase is of first order. The position of the critical point in the three dimensional space of temperature T, chemical potential μ and the isovector chemical potential μ_I is visualised in Fig. 3.19 which has been produced making use of the current regularisation prescription and parameter set. We find first order phase transition surfaces at large isovector and quark chemical potentials which are not connected.[14]

---

[14]A possible phase of coinciding diquark and pion condensation has not been considered in this analysis due to technical issues. The simultaneous presence of finite pion and diquark fields requires the numeric determination of the eigenvalues of the inverse quark quasiparticle propagator.
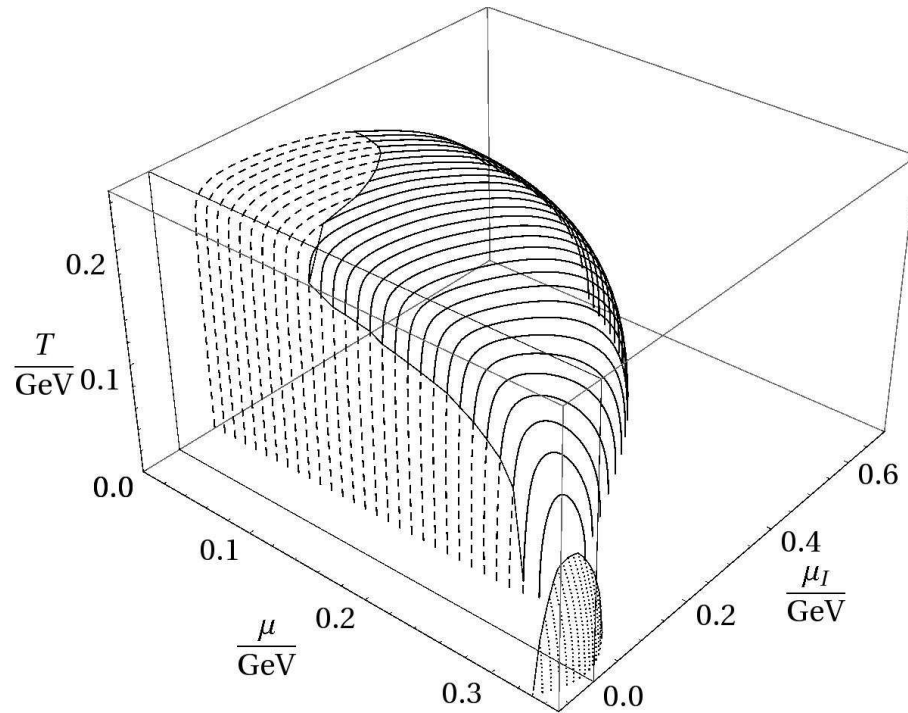
Figure 3.19: The space (T, μ, μ_I) illustrated in a 2D projection. The first order transition separating the pion phase from the quark gluon phase is indicated with solid lines, dashed lines show the region with a second order transition. Pion condensation sets in a isovector chemical potenitals $\mu_I \geq m_\pi$. The first order phase transition at large chemical potentials exists at low isovector chemical potentials (dotted) only. The two first order phase transition surfaces are disconnected.

3.6.2   Off-diagonal isovector susceptibilities

Now we focus on isovector quarknumber susceptibilities. As we are considering an isosymmetric Lagrangian at vanishing isovector chemical potential, we have to expect that up- and down- quark degrees of freedom decouple completely. However, this is only true if there is no degree of freedom that couples to up- and down-quarks simultaneously. This is true in mean field approximation. If we allow for lowest order corrections in the context of the corrections presented in Sec. 2.4.3 and App. B this is no longer true. The principal mechanism at work here is presented in Sec. 3.7.

We define the up-down quark number susceptibility χ_{ud} and the moment of the pressure c_2^{ud}

$$\frac{\chi_{\mathrm{ud}}}{T^2} = \frac{\partial^2 p}{\partial \mu_{\mathrm{u}} \partial \mu_{\mathrm{d}}} \quad \text{and} \quad c_2^{\mathrm{ud}} = \frac{1}{2!} \left. \frac{\partial^2 (\frac{p}{T^4})}{\partial(\frac{\mu_{\mathrm{u}}}{T}) \partial(\frac{\mu_{\mathrm{d}}}{T})} \right|_{\mu_u = \mu_d = 0} = \frac{1}{4} \left(c_2 - c_2^{\mathrm{I}} \right) \ . \quad (3.32)$$

In the same fashion we define the up-up quark number susceptibility χ_{uu} and the moment of the pressure c_2^{uu}

$$\frac{\chi_{\mathrm{uu}}}{T^2} = \frac{\partial^2 p}{\partial \mu_{\mathrm{u}} \partial \mu_{\mathrm{u}}} \quad \text{and} \quad c_2^{\mathrm{uu}} = \frac{1}{2!} \left. \frac{\partial^2 (\frac{p}{T^4})}{\partial(\frac{\mu_{\mathrm{u}}}{T}) \partial(\frac{\mu_{\mathrm{u}}}{T})} \right|_{\mu_u = \mu_u = 0} = \frac{1}{4} \left(c_2 + c_2^{\mathrm{I}} \right) \ .^{[15]} \quad (3.33)$$

Here and in Eq. (3.32) $\mu_{\mathrm{u/d}}$ are the up- and down-quark chemical potentials. Due to the vanishing chemical potentials these quantities can be compared to 2-flavour lattice QCD results [A+05]. In addition we use the nth moment and the nth isovector moment of the pressure which are defined in Ref. [A+05] by

$$c_n = \frac{1}{n!} \left. \frac{\partial^n (\frac{p}{T^4})}{\partial(\frac{\mu}{T})^n} \right|_{\mu = \mu_I = 0} \qquad\qquad c_n^{\mathrm{I}} = \frac{1}{n!} \left. \frac{\partial^n (\frac{p}{T^4})}{\partial(\frac{\mu_{\mathrm{I}}}{T})^2 \partial(\frac{\mu_{\mathrm{I}}}{T})^{(n-2)}} \right|_{\mu = \mu_I = 0} \ . \quad (3.34)$$

If the off diagonal moment of the pressure c_2^{ud} is evaluated in mean field we recover our expectation that it vanishes identically to zero. Including first order corrections we find the situation illustrated in Fig. 3.20 (solid line). The quantity c_2^{ud} is negative and peaks just below the crossover transition temperature T_{c}.

The quantity c_2^{uu} just as c_2 is in astonishingly good agreement with lattice QCD data such that the ratio $c_2^{\mathrm{ud}}/c_2^{\mathrm{uu}}$ shown in Fig. 3.21 (solid line) reproduces lattice results [A+05] to the same extend as the more sensitive quantity c_2^{ud}.

3.6.3   Isovector and charge cumulant ratios

In Sec. 3.3.4 quark (baryon) number cumulants and cumulant ratio have been discussed. As experiments are able to measure charge and baryon number independently, charge number cumulants are worthwhile studying as well. The chemical potentials conjugate to charge density, quark number density and isovector density

---

[15]In the present isosymmetric case up-up and down-down quark number quantities are equivalent.
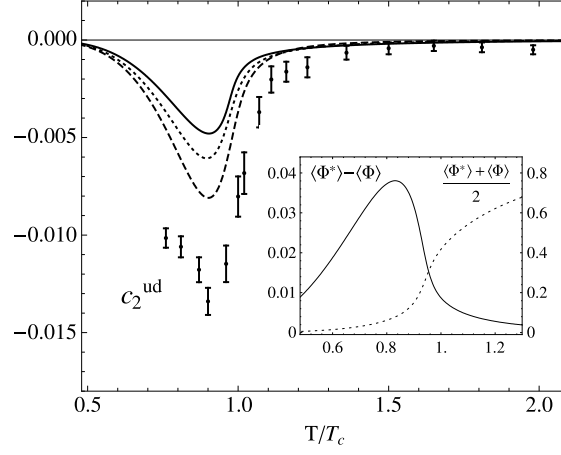
Figure 3.20: Comparison of the PNJL model predictions for c_2^{ud} as function of temperature (solid line) with lattice QCD results [A$^+$05]. The dotted ($a_3 = -6$) and dashed ($a_3 = -12$) lines indicates the model result for a changed Polyakov loop effective potential. The inset illustrates the behaviour of $\langle\Phi^*\rangle - \langle\Phi\rangle$ (solid, left scale) and $\frac{1}{2}(\langle\Phi^*\rangle + \langle\Phi\rangle)$ (dotted, right scale) as predicted by the presented PNJL model at $\mu > 0$. The similarities in the behaviour of $\langle\Phi^*\rangle - \langle\Phi\rangle$ and c_2^{ud} document their joint origin.
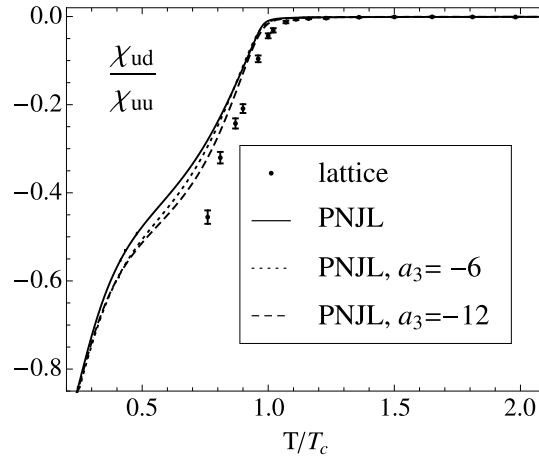
Figure 3.21: The ratio $\frac{\chi_{\mathrm{ud}}}{\chi_{\mathrm{uu}}}$ as function of temperature at $\mu = \mu_{\mathrm{I}} = 0$. The dotted ($a_3 = -6$) and dashed ($a_3 = -12$) lines indicates the model result for a changed Polyakov loop effective potential.

are linearly dependent. This linear dependence can be used to establish the following relation

$$\frac{\partial}{\partial \mu_Q} = \frac{2}{3}\frac{\partial}{\partial \mu_u} - \frac{1}{3}\frac{\partial}{\partial \mu_d} = \frac{1}{6}\frac{\partial}{\partial \mu} + \frac{1}{2}\frac{\partial}{\partial \mu_I} \ . \tag{3.35}$$

This equation allows to connect charge, quark number and isovector cumulants. All of these cumulants are related to fluctuations as given by the following relations

$$d_2^x = \frac{\partial^2(\frac{p}{T^4})}{\partial(\frac{\mu_x}{T})^2} = \frac{1}{VT^3}\langle(\delta N_x)^2\rangle \ , \quad x = \text{q, I, Q and}$$

$$d_4^x = \frac{\partial^4(\frac{p}{T^4})}{\partial(\frac{\mu_x}{T})^4} = \frac{1}{VT^3}\left(\langle(\delta N_x)^4\rangle - 3\langle(\delta N_x)^2\rangle^2\right) \ , \tag{3.36}$$

where $x = \text{q}$ corresponds to quark number density, $x = \text{I}$ to the isovector quark density and $x = \text{Q}$ to charge density. The cumulants are closely linked to the expansion coefficients c_n. To deal with different chemical potentials, the expansion coefficients c_n of p/T^4 in μ/T are generalised to a double Taylor series expansion in μ/T and μ_I/T

$$c_{n,m} = \frac{1}{n!m!}\frac{\partial^{(n+m)}(\frac{p}{T^4})}{\partial(\frac{\mu}{T})^n\partial(\frac{\mu_I}{T})^m} \ . \tag{3.37}$$

Using the relations

$$d_2^Q = \frac{2!}{6^2}c_{2,0} + \frac{2!}{2^2}c_{0,2}$$
$$d_4^Q = \left(\frac{4!}{6^4}c_{4,0} + \frac{4!}{2^4}c_{0,4} + \frac{1}{6^22^2}\binom{4}{2}\right)\left(\langle(\delta N_q)^2(\delta N_I)^2\rangle - 3\langle\delta N_q\delta N_I\rangle^2\right)\right) \tag{3.38}$$

second and fourth charge cumulant have been calculated in Ref. [EKR06] using lattice QCD results for quark number and isovector cumulants. All three cumulants represent an additional benchmark for our model. In particular we compare the ratios of fourth and second moment, which are a measure for the relative strength of density fluctuations. These so-called cumulant ratios are defined by

$$R_{4,2}^I = \frac{d_4^I}{d_2^I} \qquad\qquad R_{4,2}^Q = \frac{d_4^Q}{d_2^Q} \ . \tag{3.39}$$

The comparison of the isovector and the charge density cumulant ratio from the PNJL model to lattice QCD results is shown in Fig. 3.22. As discussed in Sec. 3.3.4 the low temperature limit of the quark number cumulant ratio, which is $9 = (3B)^2$, is an indication for confinement. In nature we expect that only the lightest mesons, namely the pions, contribute to $R_{4,2}^Q$ producing the low temperature limit of unity as all charged degrees of freedom carry one unit of charge. The high temperature limit is $\frac{34}{15\pi^2}$ [EKR06]. The charge cumulant ratio $R_{4,2}^Q$ is in principle also accessible by heavy-ion experiments (see discussion in Sec. 3.3.4).[16] The absence of the strong peak in the lattice data may be understood when considering the large explicit chiral symmetry breaking by the large implemented current quark mass of $m_0 =$

---

[16]The isovector cumulant ratio $R_{4,2}^I$ can be derived from quark number and charge cumulant ratios.
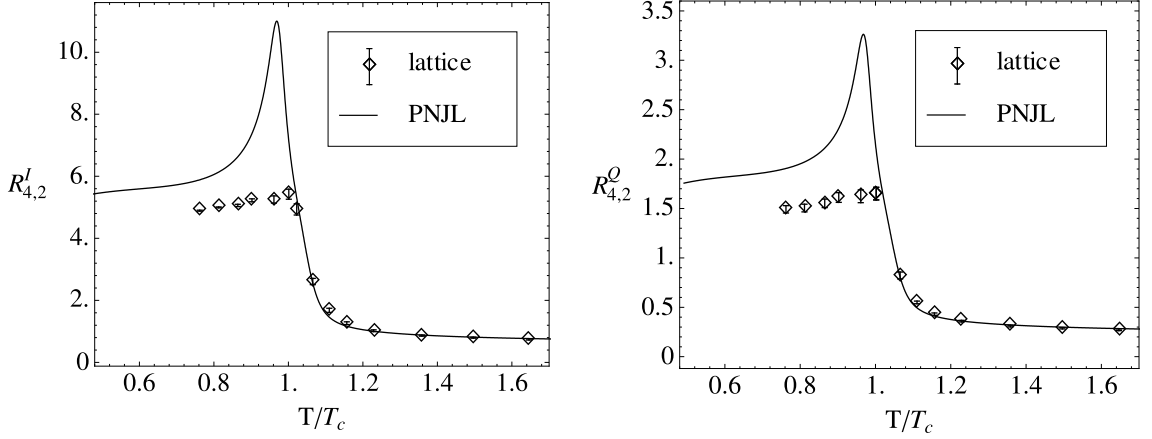
Figure 3.22: Comparison of the cumulant ratios $R^{\mathrm{I}}_{4,2}$ and $R^{\mathrm{Q}}_{4,2}$ obtained in the PNJL model with results shown in Ref. [EKR06].

$0.4\,T$, as this peak is a remnant of the second order phase transition in the chiral limit. The deviation of the PNJL result from lattice data at temperatures below the deconfinement crossover document shortcomings of the description of hadrons and mesons in the PNJL model. This weakness of the PNJL is more articulate in isovector and charge cumulant ratio than in the quark number cumulant ratio.

3.7 Isovector susceptibilities

In this section we present a general mechanism that is able to explain how the PNJL model in its current isosymmetric formulation can produce off diagonal susceptibilities χ_{ud} and expansion coefficients c^{ud}_2 at $\mu_{\mathrm{I}} = 0$. The key to the mechanism presented is an additional degree of freedom that couples to both up- and down-quark densities equally. As it will turn out, Polyakov loop degrees of freedom may act as such an intermediary between up- and down-quarks.

For a short investigation of the problem we consider a schematic thermodynamic model with the following partition function

$$\mathcal{Z}^{(0)}(\mu_{\mathrm{u}},\,\mu_{\mathrm{d}}) = \mathcal{Z}_{\mathrm{u}}(\mu_{\mathrm{u}}) \cdot \mathcal{Z}_{\mathrm{d}}(\mu_{\mathrm{d}}) \ . \tag{3.40}$$

In this model up and down quarks are completely decoupled. Using the standard formulae, we derive the pressure, quark densities and quark number susceptibilities:

$$\frac{p^{(0)}}{T^4} = -\frac{\log \mathcal{Z}^{(0)}}{VT^3} \qquad \frac{n^{(0)}_x}{T^3} = \frac{1}{VT^3}\frac{\partial \log \mathcal{Z}^{(0)}}{\partial \frac{\mu_x}{T}} = \frac{1}{VT^3}\frac{\partial \log \mathcal{Z}_x}{\partial(\frac{\mu_x}{T})} \tag{3.41}$$

$$\frac{\chi^{(0)}_{\mathrm{u}x}}{T^2} = \frac{1}{VT^3}\frac{\partial^2 \log \mathcal{Z}^{(0)}}{\partial(\frac{\mu_{\mathrm{u}}}{T})\partial(\frac{\mu_x}{T})} = \frac{1}{VT^3}\delta_{\mathrm{u}x}\frac{\partial^2 \log \mathcal{Z}_{\mathrm{u}}}{\partial(\frac{\mu_{\mathrm{u}}}{T})^2} \ , \tag{3.42}$$

where $\delta_{\mathrm{u}x}$ denotes a Kronecker delta, i.e. the unperturbed off diagonal susceptibility vanishes. To this partition function we add a perturbation $\mathcal{Z}_{\mathrm{I}}(\mu_{\mathrm{u}},\,\mu_{\mathrm{d}},\,\xi)$ such that the total partition function reads

$$\mathcal{Z}(\mu_{\mathrm{u}},\,\mu_{\mathrm{d}},\,\xi) = \mathcal{Z}^{(0)}(\mu_{\mathrm{u}},\,\mu_{\mathrm{d}}) \cdot \mathcal{Z}_{\mathrm{I}}(\mu_{\mathrm{u}},\,\mu_{\mathrm{d}},\,\xi) = \mathcal{Z}_{\mathrm{u}}(\mu_{\mathrm{u}}) \cdot \mathcal{Z}_{\mathrm{d}}(\mu_{\mathrm{d}}) \cdot \mathcal{Z}_{\mathrm{I}}(\mu_{\mathrm{u}},\,\mu_{\mathrm{d}},\,\xi) \ . \tag{3.43}$$

Note that the perturbation (interaction) partition function $\mathcal{Z}_{\mathrm{I}}(\mu_{\mathrm{u}},\, \mu_{\mathrm{d}},\, \xi)$ includes the dependence on an additional degree of freedom, here named ξ. In our model we are free to construct this interaction. We define it such that there is an isosymmetric coupling g of ξ to the quark densities

$$\log \mathcal{Z}_{\mathrm{I}}(\mu_{\mathrm{u}},\, \mu_{\mathrm{d}},\, \xi) = V T^3\, g\, \xi \left(\frac{n_{\mathrm{u}}}{T^3} + \frac{n_{\mathrm{d}}}{T^3} \right)\ . \tag{3.44}$$

We now derive the full susceptibilities

$$\frac{\chi_{\mathrm{u}x}}{T^2} = \frac{\chi_{\mathrm{u}x}^{(0)}}{T^2} - g\, \left(\frac{\mathrm{d}\xi}{\mathrm{d}(\frac{\mu_{\mathrm{u}}}{T})} + \frac{\mathrm{d}\xi}{\mathrm{d}(\frac{\mu_x}{T})} \right) \left(\frac{\chi_{\mathrm{uu}}}{T^2} + \frac{\chi_{\mathrm{ud}}}{T^2} \right)\ . \tag{3.45}$$

Using the fact that $\frac{\mathrm{d}\xi}{\mathrm{d}\mu_{\mathrm{u}}} = \frac{\mathrm{d}\xi}{\mathrm{d}\mu_{\mathrm{d}}} = \frac{1}{2}\frac{\mathrm{d}\xi}{\mathrm{d}\mu}$, we solve for $\frac{\chi_{\mathrm{uu}}}{T^2}$ and $\frac{\chi_{\mathrm{ud}}}{T^2}$ and obtain

$$\frac{\chi_{\mathrm{uu}}}{T^2} = \frac{\chi_{\mathrm{uu}}^{(0)}}{T^2}\, \frac{1 + g\,(\mathrm{d}\xi/\mathrm{d}(\frac{\mu}{T}))}{1 + 2g\,(\mathrm{d}\xi/\mathrm{d}(\frac{\mu}{T}))} \qquad \frac{\chi_{\mathrm{ud}}}{T^2} = \frac{\chi_{\mathrm{uu}}^{(0)}}{T^2}\, \frac{-g\,(\mathrm{d}\xi/\mathrm{d}(\frac{\mu}{T}))}{1 + 2g\,(\mathrm{d}\xi/\mathrm{d}(\frac{\mu}{T}))}\ . \tag{3.46}$$

Eq. (3.46) explains non-vanishing off diagonal flavour susceptibilities χ_{ud} in the presence of an additional degree of freedom, here named ξ, that couples to both up- an down-quark densities in an isosymmetric way. From Eq. (3.46) it may be seen that a necessary condition for non-vanishing χ_{ud} is that ξ has a finite derivative with respect to the quark chemical potential μ, i. e. ξ has to be charge conjugation odd and density sensitive.

This approach can also be reversed: if there is a field that reacts to density or chemical potential at lowest order and satisfies a mean field equation, i. e. if

$$\frac{\mathrm{d}\xi}{\mathrm{d}\mu} \neq 0 \qquad\qquad \text{and} \qquad\qquad \frac{\partial \Omega}{\partial \xi} = 0\ , \tag{3.47}$$

we find

$$\frac{\mathrm{d}}{\mathrm{d}\mu} \left(\frac{\partial \Omega}{\partial \xi} \right) = 0 = \left[\frac{\partial^2 \Omega}{\partial \xi^2} \right] \frac{\mathrm{d}\xi}{\mathrm{d}\mu} + \frac{\partial^2 \Omega}{\partial \mu \partial \xi} \quad \Rightarrow \quad \frac{\mathrm{d}\xi}{\mathrm{d}\mu} = - \left[\frac{\partial^2 \Omega}{\partial \xi^2} \right]^{-1} \frac{\partial^2 \Omega}{\partial \mu \partial \xi}\ . \tag{3.48}$$

Using the inequality in (3.47) this implies that

$$\frac{\partial^2 \Omega}{\partial \mu \partial \xi} \neq 0\ . \tag{3.49}$$

Thus a Taylor series of Ω in ξ and μ necessarily contains a term of the form

$$\delta\Omega = \frac{\partial^2 \Omega}{\partial \mu \partial \xi}\, \mu\, \xi = -g\, n_0\, \mu\, \xi\ , \quad \text{with } g\, n_0 = -\frac{\partial^2 \Omega}{\partial \mu \partial \xi}\ . \tag{3.50}$$

Using Eq. (3.44) the constant n_0 (at $\mu = 0$) evaluates to $n_0 = T\, \chi_0$, where χ_0 is the quark number susceptibility at $\mu = 0$.

For small g the denominators in Eq. (3.46) may be simplified by setting them equal to one. With Eqs. (3.48) and (3.50) and $n_0/T^3 = \chi_0/T^2 = 2\chi_{\mathrm{uu}}^{(0)}/T^2$ we find

$$\chi_{\mathrm{ud}} = -\frac{1}{2} \frac{\partial^2 \Omega}{\partial \mu \partial \xi} \left[\frac{\partial^2 \Omega}{\partial \xi^2} \right]^{-1} \frac{\partial^2 \Omega}{\partial \mu \partial \xi}\ , \tag{3.51}$$

manifestly featuring the negative sign of χ_{ud}. Eq. (3.51) reveals a close relation of the ξ-susceptibilty $[\partial^2\Omega/\partial\xi^2]^{-1}$ and χ_{ud}.

Using the fact that the quark density n vanishes at $\mu = 0$ the quark density n can be expressed as $n = n_0(\mu/T) + \cdots$ (at $\mu = 0$). A Legendre transformation of the thermodynamic potential Ω produces the free energy density f

$$f = \Omega + n\,\mu\ . \tag{3.52}$$

Using Eq. (3.50) we find

$$\delta f = g\,n_0\,\mu\,\xi + \frac{\mathrm{d}\xi}{\mathrm{d}(\frac{\mu}{T})}n_0\,\mu^2 + \cdots = g\,\underbrace{(n_{\mathrm{u}} + n_{\mathrm{d}})}_{n}\,\xi + \frac{\mathrm{d}\xi}{\mathrm{d}(\frac{\mu}{T})}\frac{n^2\,T^2}{n_0} + \cdots \tag{3.53}$$

The lowest term in n and ξ is $g = -n_0^{-1}\,\partial^2\Omega/(\partial\mu\partial\xi)$. If we derive the free energy f around $\mu_{\mathrm{u}} = \mu_{\mathrm{d}} = 0$ from the assumptions above, the free energy f can be written in the following form

$$f = f_0 + \frac{1}{2}\begin{bmatrix} \xi \\ n_{\mathrm{u}} \\ n_{\mathrm{d}} \end{bmatrix}^T \begin{bmatrix} a & b & b \\ b & c & 0 \\ b & 0 & c \end{bmatrix} \begin{bmatrix} \xi \\ n_{\mathrm{u}} \\ n_{\mathrm{d}} \end{bmatrix}\ , \tag{3.54}$$

where the first order terms vanish due to the requirement that the free energy is minimal. With $n_x \propto \mu_x$ we conclude that $b = g/2$. Evaluating the eigenvectors of the matrix in Eq. (3.54) one finds that if $a \neq c$ increasing $n = n_{\mathrm{u}} + n_{\mathrm{d}}$ has to be accompanied with a change of ξ to conserve the minimal value of the free energy. Considering the eigenvalues[17] of this matrix it can also be concluded, that for this matrix to remain positively definite, the following conditions have to be met:

$$\frac{g^2}{2} = 2\,b^2 > a\,c \qquad\qquad a > 0 \qquad\qquad c > 0\ . \tag{3.55}$$

The first inequality states that large coupling constants g of the quark densities to the field ξ lead to unphysical susceptibilities. Considering the isosymmetric eigenvectors the one corresponding to the smaller eigenvalue, $\frac{1}{2}(a + c - \sqrt{(a-c)^2 + 8b^2})$, determines the behaviour of ξ around $\mu = 0$. By virtue of the eigenvectors, quark density and quark chemical potential on the one hand and the field ξ on the other hand have the same (opposite) sign if $b > 0$ ($b < 0$).

Comparing the functional forms of the thermal expectation values of the imaginary part Polyakov loop $\frac{1}{2}\langle\Phi^* - \Phi\rangle = \Phi^-$ (see inset of Fig. 3.20) and the off diagonal expansion coefficient c_2^{ud} a striking coincidence is observed. If we consider the quantity $\mathrm{d}\Phi^-/\mathrm{d}\mu$ at vanishing chemical potential and consider its quotient with c_2^{ud} we find the behaviour shown in Fig. 3.23. The pronounced extrema in both c_2^{ud} and $\mathrm{d}\Phi^-/\mathrm{d}\mu$ compensate.

To consolidate the study of the PNJL model behaviour the Polyakov loop effective potential has been modified. The lattice QCD results, that have been used as

---

[17]The eigenvalues evaluate to: $\lambda_1 = c$ and $\lambda_{2,3} = \frac{1}{2}(a + c \pm \sqrt{(a-c)^2 + 8b^2})$. The corresponding eigenvectors are $v_1 = (0,\,1,\,-1)^T$ and $v_{2,3} = (\lambda_{2,3} - c,\,b,\,b)^T$.

a guidance in the adjustment of the Polyakov loop effective potential, constrain the potential at temperatures around $T_0 = 270\,\text{MeV}$ and above. The region where the Polyakov loop effective potential interferes with the chiral crossover in the PNJL model is much lower. Thus the potential used in Refs. [RRW07b, RHRW08] may be supplemented by an additional higher order term term in the polynomial ansatz of the coefficient $a(T)$ in Eq. (2.16). The coefficient a_3 of the additional term $a_3\,(T_0/T)^3$ has been fixed to the values -6 and -12. The remaining parameters in the Polyakov loop effective potential have been readjusted to optimize the agreement with lattice data in $N_\text{f} = 0$. The result of this proceedure is given in Tab. 3.1. The χ^2 in these fits does not increase significantly by this biased modification of the potential. The behaviour of the potential around T_c changes however. This has the consequence that first of all T_c varies slightly while the flavour off diagonal quantity c_2^ud is altered quite significantly as illustrated in Fig. 3.20. The ratio of c_2^ud and $\text{d}\Phi^-/\text{d}\mu$ is almost flat around T_c and remains almost unaffected by changes to the potential. The changes to the Polyakov loop effective potential are changes to the stiffness of the potential in Φ^--direction around T_c. In the presented toy model this corresponds to a change of the parameter a in Eq. (3.54). As the Polyakov loop effective potential is constraint by lattice QCD data [B$^+$96, KKPZ02] around T_0 and above, it is legitimate to modify the effective potential without losing physical relevance. We argue that it is therefore possible to extract information about an Polyakov loop effective potential from flavour off diagonal quantities.

From Eq. (3.46) we can derive the isovector coupling stength of the field Φ^- and the flavoured quark densities $n_\text{u/d}$

$$g = -\frac{2\,c_2^\text{ud}}{c_2}\left[\frac{\text{d}\Phi^-}{\text{d}(\mu/T)}\right]^{-1} . \tag{3.56}$$

It is interesting to note that the quasi universal quantity plotted in Fig. 3.23 reappears in this formula with the prefactor $-2/c_2$. In Fig. 3.24 the logarithm of the coupling constant g has been plotted. The overall view to the left indicates that the coupling decreases towards the crossover transition exponentially. The detailed graph in the right panel of Fig. 3.23 focuses on the behaviour above the crossover temperature T_c. With increasing temperature the coupling constant g decreases approximately $\propto T^{-1}$. This qualitative behaviour seems to be in agreement with lattice data within their errors.

The extraction of this information on the Polyakov loop effective potential can however only work if the presented mechanism is in fact at work in QCD as it is in the presented model. Even under this assumption it is expected, however, that the flavour off diagonal susceptibility χ_ud depends on $1/N_\text{c}$ (pion) corrections. The unknown size of the $1/N_\text{c}$ contributions complicates to extract quantitative information about an Polyakov loop effective potential. The presented PNJL calculation does not include $1/N_\text{c}$-corrections, which are in principle included in lattice QCD. One has to note that Ref. [A$^+$05] which have been used for reference in Fig. 3.20 reports on calculations implementing rather large current quark mass of $0.4\,T$. This large current quark mass implies heavy pions which strongly suppresses meson loops (i. e. $1/N_\text{c}$-corrections). We conclude that for a quantitative extraction of information
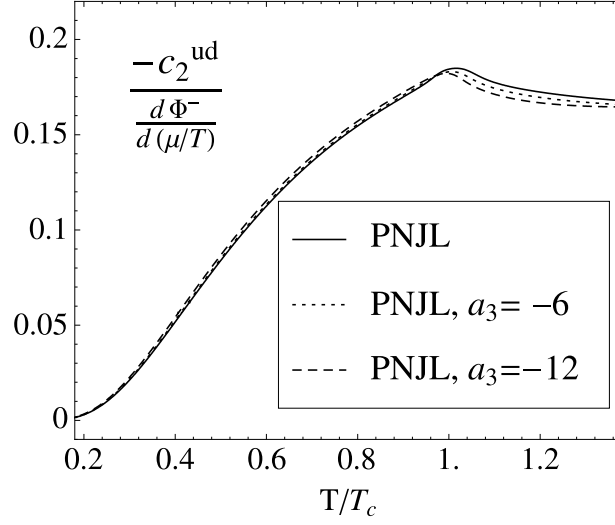
Figure 3.23: The ratio of c_2^{ud} and $\mathrm{d}\Phi^-/\mathrm{d}\mu$ as a function of temperature at vanishing chemical potential. The rather flat behaviour demonstrates that the peaks in c_2^{ud} and $\mathrm{d}\Phi^-/\mathrm{d}\mu$ are shaped very much alike indicating the close relation of the two quantities. The ratio has been plotted for different Polyakov loop effective potentials (see Tab. 3.1). The plotted ratio is almost universal even though the peaks of c_2^{ud} and $\mathrm{d}\Phi^-/\mathrm{d}\mu$ are quite distinct. This almost universal behaviour hints towards the mechanism outlined in Sec. 3.7.

a_0	a_1	a_2	a_3	b_3	χ^2/χ_0^2
	-2.47	15.2	0	-1.75	1.0
$\frac{16\pi^2}{45}$	-3.70	16.2	-6	-1.08	1.3
	-6.06	20.6	-12	-0.66	1.9

Table 3.1: Supplementing $a(T)$ by an additional summand $a_3\,(T_0/T)^3$ and readjusting a_1, a_2 and b_3 increases χ^2. The overall quality of the reproduction of the lattice data in pure gluonic theory [B+96, KKPZ02] has to be judged by χ^2/χ_0^2. Using this new parametrisation changes the stiffness of the Polyakov effective potential at temperatures just below T_{c} increasing the mixing of up and down quark number.

from lattice data it is in order to use more recent lattice data with lower current quark masses [C+08, GG08]. As these more recent results are obtained including strange quarks a reasonable comparison will have to be performed using a $2 + 1$-flavour PNJL model.
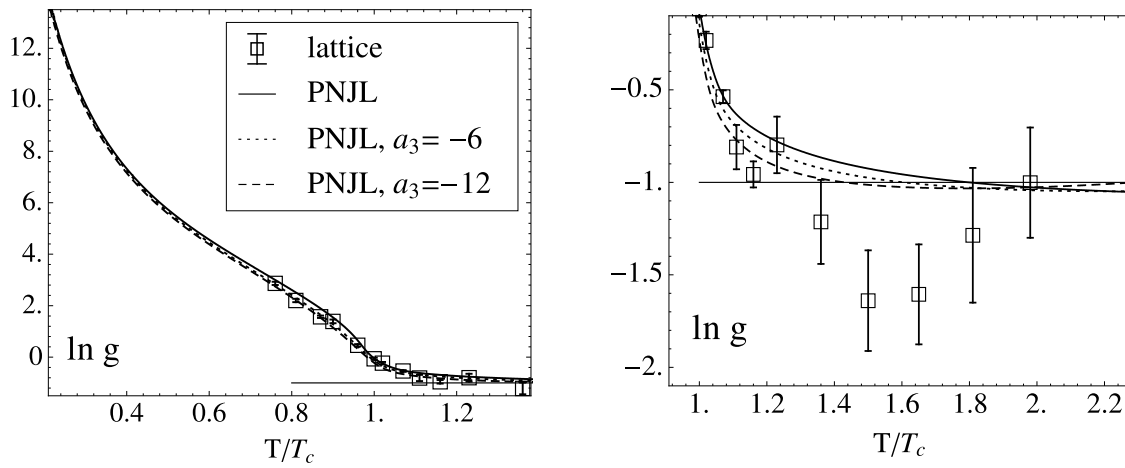
Figure 3.24: The proposed coupling g of Φ^- to the flavoured quark densities $n_{u/d}$ has been extracted using Eq. (3.56) from the PNJL model for three different Polyakov loop potential parametrizations. The numeric values employed in these parametrisations are listed in Tab. 3.1. The outcome is compared to lattice points obtained from data in Refs. [A+05, Dör06].

Chapter 4

Conclusion and Outlook

The investigation of the QCD phases in this work is based on an assumption albeit widely accepted: QCD at scales of the order of Λ_{QCD} and below is governed by spontaneous chiral symmetry breaking and confinement. The work presented here and other NJL based model rely on the correct modelling of spontaneous chiral symmetry breaking in QCD. The standard NJL approach only respects leading order chiral effects. Due to the non-renormalisability of the NJL model the regularisation proceedure has to be part of the model. This does not allow to implement the running of quark masses and coupling characteristic of QCD. Further higher loop corrections suffer from this non-renormalisability as well. Higher loop contributions ($1/N_{\mathrm{c}}$-corrections) involve higher powers of the four-quark coupling G and further divergent loop integrals. The subtraction of the infinities in each of these divergent integrals should be done using physical input. For the one-loop integrals it is the properties of the pion that anchor the regularisation in physical properties. If mesonic contributions involving higher loop integrals shall be estimated these infinities cannot be fixed to physical input. The arbitraryness in the subtraction of the divergences destroys the predictive power of such calculations. While it is possible to consider contributions originating in the meson pole consistently, pressure generated in resonant interactions of mesons with quark-antiquark pairs involve divergent loop integrals and cannot be determined unambiguously.

Despite these shortcomings of local NJL model, they are able to reproduce the observed meson spectrum of QCD to high accuracy by implementing spontaneous chiral symmetry breaking at leading order. Considering Polyakov loop extended NJL (PNJL) models it may be concluded that spontaneous chiral symmetry breaking as the leading chiral effect is deeply involved in QCD dynamics generating pressure. As shown by these PNJL models spontaneous chiral symmetry breaking is also complexly intertwined with confinement. Confinement effects are implemented by Polyakov loop effective potentials. If higher accuracy in the description of QCD dynamics is needed, mesonic pressure contributions play an essential role below the crossover transition temperature. More accurate description can be accomplished by generalising the local PNJL approach to non-local quark coupling terms [SFR07, AAG+08, GDGS06, BBRV08, HRCW09]. Such calculations reveal that pressure contributions originating in resonant meson to quark-antiquark interac-

tions are small. Therefore the astonishing agreement with lattice data observed in local PNJL models [RTW06, RRTW07, RRW07b, RHRW08] remains in non-local calculations. Much larger uncertainties in the comparison of model and lattice QCD calculation originate in systematic errors of available lattice calculations. Due to lacking computing power, data is very noisy at low temperatures requiring to normalise the pressure at temperatures of approximately $0.5\,T_c$. Even though small compared to the crossover temperature such temperatures are still rather large in terms of the pion mass, leading to uncertainties at the order of mesonic pressure contributions (see discussion in Ref. [RHRW08]).

Besides spontaneous chiral symmetry breaking confinement exerts mayor influence on the QCD pressure. There are two ways how confinement plays into the QCD equation of state. Firstly it is the pressure from freely propagating gluons in the high temperature and high density phase of QCD. Secondly it is the influence of confinement on the quark pressure. The ratio of the asymptotic high temperature pressures generated by free quark and gluon degrees of freedom is $\frac{N_c \cdot N_f \cdot N_{\text{spin}}}{(N_c^2 - 1) \cdot N_{\text{spin}}} \times \frac{p_{\text{SB}}^{\text{fermion}}}{p_{\text{SB}}^{\text{boson}}} = \frac{12}{16} \times \frac{7}{8} \approx 0.66$ (for $N_f = 2$). This indicates that both effects are equally relevant. This is the reason why the extension of the NJL model by a Polyakov loop effective potential is essential in the description of QCD thermodynamics. To find a quantitatively reliable parametrisation of the Polyakov loop effective potential, lattice QCD calculations without quarks have been exploited. In the absence of quarks, i.e. for infinitely heavy quarks, the Z(3) centre symmetry of $SU(3)_c$ is exact. Thus there must not exist an explicit Z(3) symmetry breaking term in this effective potential once $\langle \Phi^* \rangle = \langle \Phi \rangle = 0$.

Even though the ansatz (2.15) only includes Polyakov loop degrees of freedom, it works very well at crossover temperatures and far above. However Polyakov loop degrees of freedom are not able to describe the dynamics of gluons at very high temperatures. Transverse gluon degrees of freedom will start to dominate the generation of pressure. Even though the Polyakov loop effective potential produces reasonable quantitative results, it implements the wrong physics at high temperatures. The region where Polyakov loop degrees of freedom as constant temporal background fields are appropriate to describe gluon dynamics is where spatial correlation lengths are larger than the inverse temperature.[1] A better implementation of the Polyakov loop effective potential relies on the strong coupling expansion [Fuk08a].

Coupling the Polyakov loop effective potential to the quark sector via minimal substitution produces an equation of state that agrees with full QCD lattice calculations to an astonishing accuracy. Even though the PNJL model is able to model the equation of state correctly, there are aspects of confinement in this model description that cannot fully satisfy. The good reproduction of the equation of state is due to the suppression of the quark degrees of freedom below the crossover temperature. This suppression is caused by a formal decrease of the effective quark temperature. The reduced effective temperature of the quarks does only influence the relationship

---

[1]Lattice QCD calculations found that the spatial correlation length of the field strength λ is of the order of $\lambda \approx 0.25\,\text{fm} \approx (0.8\,\text{GeV})^{-1} > T_c^{-1}$. In the region where $\lambda > T^{-1}$ the dimensionality is effectively reduced from 4 to 3.

of quarks and mesons quantitatively and not qualitatively. This is why unphysical decays of mesons into quark-antiquark pairs are not suppressed [H$^+$07] to the extent it is happening in QCD. Again NJL models show weaknesses as soon as applied beyond leading order in the $1/N_\mathrm{c}$-expansion. Here non-local generalisations could bring some improvement.

One central part of this thesis is the proper description of Polyakov loop degrees of freedom coupled to quarks using the minimal coupling scheme. One of the successes of the presented formalism is the description of the behaviour of the thermal expectation values of the Polyakov loop and its complex conjugate $\langle \Phi^* \rangle$ and $\langle \Phi \rangle$. It has been shown that up to the used order of approximation the calculated values of $\langle \Phi^* \rangle$ and $\langle \Phi \rangle$ (and other thermal expectation values) do maximise the partition function. As parts of these Polyakov loop degrees of freedom cannot be separated from the appearance of the fermion sign problem, this requires to constrain all mean fields such that their physical meaning is maintained. In the context of isovector quantities and the low temperature limit of cumulant ratios it became obvious that the pure mean field treatment (imposing constraints like formost $\langle \Phi^* \rangle = \langle \Phi \rangle$) is not appropriate for quark models coupled to Polyakov effective potentials. Perturbative corrections to the mean field approximation represent a possible systematic treatment of the fermion sign problem in the PNJL model. At the same time this approach allows for a clear separation of bare fields and thermal expectation values. The saddle point approximation, which is an alternative way to deal with the fermion sign problem, directly jumps to thermal expectation values, which destroys this clear separation of mean field from fluctuational contributions. The approach advocated here uses a perturbative expansion in spatially and temporally constant fields to recover the dynamics of the Polyakov loop entering the model through complex contributions of the action. Mesonic quark-antiquark loops involving physics beyond constant fields are treated in random phase approximation (RPA) of the corresponding correlation functions.

One of the questions currently of hightest interest is the issue of a critical point in the QCD phase diagram. Many model calculations and lattice QCD approaches predict its existence, however, both ways to address QCD are not completely decisive on this. The possibility to remove the critical point from the PNJL phase diagram by introduction of a repulsive vector coupling term has been shown in Ref. [Fuk08a]. Lattice QCD calculations studying the extension of the Columbia plot to non-zero chemical potential [dFP08] also question the existence of the critical end point.

In the experimental search for the critical end point, fluctuations are key quantities. As both the critical end point as well as the chiral phase transition in the chiral limit are second order phase transitions, one expects fluctuations to diverge at these points. Critical analysis of the chiral tricritical point (in the chiral limit) indicate that physical quark masses are in its critical region. Therefore fluctuations are suitable measures for the chiral crossover. The rapidly changing amplitude of the fluctuations allows to determine the position of the critical endpoint. We have studied susceptibilities in the PNJL model supporting the idea of locating the critical end point using fluctuations. The experimental accomplishment of this task will however require huge effort. As the system size in heavy-ion collisions is finite, the

growth of fluctuations in the critical region is limited. The fast evolution of the fire ball also restricts the time spent in the critical region. In combination with the critical slowing down, which has been observed in this PNJL analysis in the reduction of the speed of sound near the chiral crossover transition, the size of fluctuations building up while passing through the critical region is additionally limited. To maximise the size of the observable fluctuations, it is most promising to use the full detector acceptance to select a fixed volume in phase space for this measurement of fluctuations. The way to create large statistics is to assume the equivalence of many successive heavy-ion collisions. The observed fluctuations are then considered on the so-called event-by-event basis, requiring to bin successive events by the number of participants (or impact parameter).

Quantities sensitive to changes in fluctuations are cumulants and cumulant ratios such as $R_{4,2} = d_4/d_2$ proposed in Ref. [SFR08]. Close to the tricritical point at small current quark masses, a peak in the cumulant ratios $R_{4,2}$ is expected along chiral symmetry restauration. As this peak has to be understood as part of the critical region of the tricritical point in the chiral limit, it will be strongly current quark mass and pion mass dependent. In accordance with this interpretation of this peak Ref. [SFR08] reports a reduction of the peak height with increasing pion mass also seen in this PNJL analysis of the chiral crossover transition. On the other hand the regular parts of the cumulant ratios $R_{4,2} = d_4/d_2$ are determined by the number of degrees of freedom that can be accessed thermodynamically. Thus the absolute value of the regular parts of the cumulant ratios allow to distinguish confined and deconfined matter. In case of the quark number cumulant ratio the PNJL model is in very good agreement with lattice QCD results, when respecting the considerations on large pion masses given above. The extraction of the isovector cumulant ratio from the PNJL model gives a handle on the charge cumulant ratio possibly accessible in heavy-ion collision experiments in the future.

The inclusion of fluctuating temporal gauge background fields allows for differences in Polyakov loop expectation values $\langle \Phi \rangle$ and $\langle \Phi^* \rangle$. The accessibility of the degree of freedom $\Phi^- = \frac{1}{2} \langle \Phi^* - \Phi \rangle$ modifies the model's reaction on isovector chemical potentials. Even though the model has been formulated symmetrically for up- and down- quarks finite up-down quark susceptibilities are observed. It is the coupling of both up- and down- quark densities to Φ^- that allows one quark density to influence the other by changing the mean field value Φ^-. The possibility of different expectation values $\langle \Phi^* \rangle$ and $\langle \Phi \rangle$ therefore may induce an effective isovector coupling strength. In principle this isovector coupling strength which has been evaluated in the presented PNJL model may also be non-vanishing in full QCD. At finite quark densities non-vanishing off diagonal susceptibilities χ_{ud} do not imply explicit isospin breaking, even though the differences in the measured quark masses of heavy quarks suggest that also the light quark masses may differ. The effects generated by the presented mechanism may be overruled by effects of dynamic pionic degrees of freedom. Nevertheless the comparison of isovector quantities with lattice QCD calculations does in principle allow for a more accurate determination of the coefficients in the Polyakov loop effective potential. Missing pion contributions to the equation of state in the local PNJL model prohibit this extraction of information

from lattice QCD. On the other hand the contributions of pion correlations are also strongly suppressed on the lattice QCD side. The available data for $N_{\mathrm{f}} = 2$ flavours unfortunately features a rather high current quark mass of $0.4\,T$ [A$^+$05]. The current data with smaller explicit chiral symmetry breaking are however produced including strange quarks [C$^+$08]. Trustworthy procedures to extract $1/N_{\mathrm{c}}$-corrections in the PNJL model and access to lattice QCD data at more realistic pion masses are necessary to refine the information on the Polyakov loop effective potential using flavour off diagonal susceptibilities.

In view of the enormous difference between the simplicity of the PNJL model and the complexity of full QCD it is stunning how QCD is modelled by PNJL calculations. Already at mean field level thermodynamic quantities are reproduced to astonishingly high accuracy. Moreover the approach of extending the NJL model by a Polyakov loop effective potential by minimally coupling the NJL sector to temporal gauge background fields causes the so-called fermion sign problem. A strict mean field treatment which only allows variations of fields within a physically meaningful range cannot deal with all effects generated by this fermion sign problem. The present work introduces a treatment of this problem in the PNJL model which permits to evaluate the differences in $\langle \Phi \rangle$ and $\langle \Phi^* \rangle$ in agreement with complementary model studies [DPZ05] and lattice QCD [Dör06]. It is this degree of freedom, $\Phi^- = \frac{1}{2}\langle \Phi^* - \Phi \rangle$, that induces a finite isovector coupling, also observed in lattice QCD calculations [A$^+$05]. The very good agreement of PNJL calculations with QCD, as far as we know it, will hopefully serve as a true guidance in the experimental search of the position of a possible critical end point in the QCD phase diagram. There are PNJL approaches to QCD that improve on several issues of the presented PNJL calculation. Many of the unphysical features of the PNJL mesons can be avoided using non-local approaches to the PNJL model [GDGS06, HRCW09]. To keep up with current lattice QCD simulations it will be necessary to extend this two-flavour study by explicit implementation of strangeness.

Appendix A

Pion mass and decay constant

A.1 Evaluation of pion mass and pion decay constant

Meson propagators are the correlation of two fields at different space-time which can be derived from the effective action by differentiation:

$$S_\pi^{-1}(x, y) = \frac{\delta}{\delta\pi(x)} \frac{\delta}{\delta\pi(y)} \mathcal{S}_{\text{eff}} \ . \tag{A.1}$$

We apply the formulae $\partial_x \operatorname{tr} \log[M^{-1}] = \operatorname{tr}[M \, \partial_x M^{-1}]$ and $\partial_x M^{-1} = -M \, \partial_x M^{-1} \, M$ to derive

$$S_\pi^{-1}(p, q) = -\widetilde{\operatorname{Tr}} \left[S(p) \, \delta_\pi S^{-1} \, S(q) \, \delta_\pi S^{-1} \right] + \frac{1}{G} = \left[\text{\tiny∝ = = = = •} \right]^{-1} \tag{A.2}$$

$$= 2N_{\text{c}}N_{\text{f}} \, N_{\text{M}}(p^2) \, I_2(p^2) - \frac{1}{G} \frac{m_0}{M} \tag{A.3}$$

where the spatial dependence has been replaced by a momentum dependence, and the derivative $\delta_\pi S^{-1}$ is a constant structure representing the meson quantum numbers (in the pion case: $\delta_\pi S^{-1} = i \, \gamma_5 \tau_{\pm,3}$). The polynomial $N_{\text{M}}(p^2)$ depends on the quantum numbers of the considered meson. For pions we find $N_{\text{M}}(p^2) = p^2$, for the sigma meson we find $N_{\text{M}}(p^2) = p^2 - 4M^2$. Another way of deriving the meson propagator is to write down a recursive equation:

$$\text{\tiny∝ = = = = •} = \frac{1}{1 - \text{\tiny⊸◯•}} \ , \tag{A.4}$$

where the filled vertex implies the multiplication with the coupling strength G, while the empty vertex excludes this factor G. We can now identify the meson mass m_{M} and the quark-meson coupling $g_{\text{M}qq}$ performing a Taylor expansion in $q^2 = -s$:

$$\text{\tiny∝ = = = = •} = \frac{g_{\text{M}qq}^2}{q^2 - m_{\text{M}}^2} \tag{A.5}$$

$$\Rightarrow \frac{\partial \left[\text{\tiny∝ = = = = •} \right]^{-1}}{\partial q^2} \bigg|_{q^2 = m_{\text{M}}^2} = g_{\text{M}qq}^{-2} \qquad -g_{\text{M}qq}^2 \left[\text{\tiny∝ = = = = •} \right]^{-1} \big|_{q^2 = 0} = m_{\text{M}}^2 \tag{A.6}$$

For the pion this reads

$$\Rightarrow 2N_{\mathrm{c}}N_{\mathrm{f}}I_2(m_\pi^2) = g_{\pi qq}^{-2} \qquad \text{and} \qquad g_{\pi qq}^2 \frac{1}{G}\frac{m_0}{M} = m_\pi^2 \ . \tag{A.7}$$

The pion decay constant is defined as the matrix element given in Eq. (1.14), connecting the vacuum to the pion wave function. In the NJL framework the axial current A_a^μ is discribed by the structure $i\gamma^\mu\gamma_5\frac{\tau_a}{2}$ and the vertex Γ connecting two quarks to the pion $\pi_b(p)$ is $\Gamma = ig_{\pi qq}\gamma_5\tau_b$. The pion decay constant therefore can be evaluated using

$$\langle\Omega|A_a^\mu(x)|\pi_b(p)\rangle = i\,f_\pi\,p^\mu\delta_{ab}e^{-ip\cdot x} = i\gamma^\mu\gamma_5\frac{\tau_a}{2} \;\overset{\Gamma}{\bigcirc}\!\!= \; _{p,\,b} \ . \tag{A.8}$$

The loop graph to the right can be translated into a trace and integration over all loop momenta. Making use of the cyclic invariance of the trace, γ^μ inside the trace in Eq. Eq. (A.8) can be eliminated and replaced by p^μ in front of the trace, allowing to rewritte Eq. (A.8) using the integral I_2 defined in Eq. (2.14):

$$f_\pi\,p^\mu = -2N_{\mathrm{c}}N_{\mathrm{f}}\,g_{\pi qq}\,M\,p^\mu\,I_2(p^2) \ , \tag{A.9}$$

where we have set $a = b$ and $x = 0$. The quark pion coupling contant $g_{\pi qq}$ is eliminated from Eq. (A.9) using the first relation in Eq. (A.7).

$$f_\pi^2 = 2\,N_{\mathrm{c}}N_{\mathrm{f}}\,M^2\,I_2(0) \ . \tag{A.10}$$

Combining the two equations in Eq. (A.7) to eliminate the quark pion coupling contant $g_{\pi qq}$ produces a relation for the pion mass:

$$m_\pi^2 = \frac{m_0}{M}\frac{1}{2G\,N_{\mathrm{c}}N_{\mathrm{f}}\,I_2(m_\pi^2)} \tag{A.11}$$

Multiplication of Eqs. (A.10) and (A.11) eliminates the integral I_2 if we use the simplification that $I_2(m_\pi^2) \approx I_2(0)$, which holds true near the chiral limit. This manipulation returns the 2-flavour NJL Gell-Mann-Oakes-Renner (GMOR) relation [GMOR68]:

$$m_\pi^2\,f_\pi^2 = \frac{m_0\,M}{G} = -m_0\,\langle\bar\psi\psi\rangle + O(m_0^2) \ , \tag{A.12}$$

where Eq. (2.10) has been used, which establishes a direct connection of the constiutent quark mass to the chiral condensate, $M = m_0 - G\,\langle\bar\psi\psi\rangle$, only true in the local 2-flavour NJL framework. Eq. (A.12) is the 2-flavour NJL Gell-Mann-Oakes-Renner (GMOR) relation [GMOR68].

The elimination of the integral $I_2(m_\pi^2)$ from Eqs. (A.7) and (A.10) again using $I_2(m_\pi^2) \approx I_2(0)$ near the chiral limit produces the Goldberger-Treiman relation:

$$f_\pi\,g_{\pi qq} = M \ . \tag{A.13}$$

A.2   Energy of mesonic modes

The derivation of the meson mode self energy at finite temperature and chemical potential can be found in some detail in [HK94]. We would like to repeat some of the calculations and extend them such that the pressure from mesons and $q\bar{q}$ correlations can be evaluated.

We start with the real part following the lines of Ref. [H+07]. We include also the $\vec{q}$-dependence in our calculation. The self energy is derived from the RPA approximation:

$$
\Pi^{XY}(i\omega, \vec{q}) = T \sum_{\omega_n} \int \frac{\mathrm{d}^3 p}{(2\pi)^3} \mathrm{Tr} \left[\Gamma^X \tilde{S}(i\omega_n + \mu, \vec{p}) \Gamma^Y \tilde{S}(i(\omega_n - \omega) + \mu, \vec{p} - \vec{q}) \right]
$$

(A.14)

Here X and Y represent a mesonic current and $\Gamma^{(X/Y)}$ is the corresponding Dirac, flavour and colour structure that connects this current with its quantum numbers to a quark-antiquark loop. The quark propagator is given by $S(i\omega_n, \vec{p}) = -\frac{m + \not{p}}{\omega_n^2 + p^2 + m^2}$ with $\not{p} = i\omega_n \gamma_0 - \vec{\gamma} \cdot \vec{p}$. From now on we will focus on the pseudoscalar isovector channel (i.e. the pionic excitations with $\Gamma^X = \Gamma^Y = \Gamma^P = i\gamma_5 \tau_a$) and the scalar isoscalar channel (i.e. the sigma excitations with $\Gamma^X = \Gamma^Y = \Gamma^S = \mathbb{1}$). As the trace vanishes for different flavour structures in the pion and sigma case, we suppress the index Y and the flavour index a.

$$
\Pi^{\mathrm{P/S}}(i\omega, \vec{q}) = 4N_{\mathrm{f}} \sum_j T \sum_{\omega_n} \int \frac{\mathrm{d}^3 p}{(2\pi)^3} \tilde{N}_j^{\mathrm{P/S}} \Delta(i\omega_n + \mu_j, \vec{p}) \Delta(i(\omega_n - \omega) + \mu_j, \vec{p} - \vec{q})
$$

(A.15)

$$
\tilde{N}_j^P = (\omega_n - i\mu_j)(\omega - \omega_n + i\mu_j) - m^2 - \vec{p} \cdot (\vec{p} - \vec{q})
$$
$$
\tilde{N}_j^S = (\omega_n - i\mu_j)(\omega - \omega_n + i\mu_j) + m^2 - \vec{p} \cdot (\vec{p} - \vec{q})
$$
$$
\Delta(i\omega_n, \vec{p}) = \frac{1}{\omega_n^2 + p^2 + m^2} = \frac{1}{\omega_n^2 + E_p^2} = \sum_{s = \pm 1} \frac{-s}{2E_p} \frac{1}{i\omega_n - sE_p}
$$

(A.16)

Here the colour trace has been written out in form of the sum over all colours j. In addition we use the formal rule $\mu_j \to \mu - iT\phi_j = \mu - iA_j$, which can be derived once the Polyakov loop is in its diagonal representation (in Polyakov gauge). We separate the expression in Eq. (A.15) into partial fractions:

$$
\Pi^{\mathrm{P/S}} = 2N_{\mathrm{f}} \sum_j T \sum_{\omega_n} \int \frac{\mathrm{d}^3 p}{(2\pi)^3} \left(\Delta(i\omega_n + \mu_j, \vec{p}) + \Delta(i(\omega_n - \omega) + \mu_j, \vec{p} - \vec{q}) \right)
$$

(A.17)

$$
+ 2N_{\mathrm{f}} N^{\mathrm{P/S}} \sum_j T \sum_{\omega_n} \int \frac{\mathrm{d}^3 p}{(2\pi)^3} \Delta(i\omega_n + \mu_j, \vec{p}) \Delta(i(\omega_n - \omega) + \mu_j, \vec{p} - \vec{q})
$$

$$
\text{with } N^P = -(\omega^2 + q^2) = s \quad \text{and } N^S = -(\omega^2 + q^2) - 4m^2 = s - 4m^2 .
$$

We shift the arguments in the second term of the integrand in the first line of Eq. (A.17). Applying the correct regularisation, we recover the gap equation for the

constituent quark mass

$$\frac{1}{G}\left(1 - \frac{m_0}{m}\right) = 4N_f \sum_c T \sum_{\omega_n} \int^\Lambda \frac{\mathrm{d}^3 p}{(2\pi)^3} \Delta(i\omega_n + \mu_c, \vec{p}) = 4N_f N_c I_1 \ . \tag{A.18}$$

After performing the Matsubara sum, the integral I_1 can be re-expressed in terms of the Fermi-Dirac distribution. The effect of the Polyakov loop is then taken into account following Ref. [H$^+$07]. The modified Fermi-Dirac distributions $f_\Phi^\pm$ of Ref. [H$^+$07] are introduced to rewrite I_1 as[1]

$$I_1 = \frac{1}{2\pi^2}\left(\int_0^\Lambda p^2 \mathrm{d}p \, \frac{1}{2E_p} \ - \ \int_0^\infty p^2 \mathrm{d}p \, \frac{f_\Phi^+(E_p) + f_\Phi^-(E_p)}{2E_p}\right) \tag{A.19}$$

We define the integral I_2 by rewriting Eq. (A.17) in the following form:

$$\Pi^{\mathrm{P/S}} = 4N_f N_c \, I_1 - 2N_f N_c \, N^{\mathrm{P/S}} \, I_2 \ . \tag{A.20}$$

The Matsubara sum implied in the integral I_2 can be evaluated leaving us with the divergent integral over the three-momentum $\vec{p}$:

$$\begin{aligned}
I_2 = \int^\Lambda \frac{\mathrm{d}^3 p}{(2\pi)^3} \frac{1}{4E_p E_{p-q}} &\left(\frac{1}{i\omega - E_p - E_{p-q}} - \frac{1}{i\omega + E_p + E_{p-q}}\right) + \\
\int \frac{\mathrm{d}^3 p}{(2\pi)^3} \frac{1}{4E_p E_{p-q}} &\left(\frac{-f_\Phi^+(E_p) - f_\Phi^-(E_{p-q})}{i\omega - E_p - E_{p-q}} - \frac{-f_\Phi^-(E_p) - f_\Phi^+(E_{p-q})}{i\omega + E_p + E_{p-q}} \right. \\
&\left. - \frac{f_\Phi^-(E_p) - f_\Phi^-(E_{p-q})}{i\omega + E_p - E_{p-q}} + \frac{f_\Phi^+(E_p) - f_\Phi^+(E_{p-q})}{i\omega - E_p + E_{p-q}}\right) \ .
\end{aligned} \tag{A.21}$$

The divergent part of this integral is treated with a three momentum cutoff at Λ, while the finite parts in line two and three of Eq. (A.21) are integrated over all $\vec{p} \in \mathbb{R}^3$. The separation of finite and divergent parts is derived from the regularisation procedure for the pressure, defined such that the Stefan-Boltzmann limit at high T is reproduced.

We split the quark self energy into real and imaginary part:

$$\mathrm{Re}\,\Pi^{\mathrm{P/S}} = 4N_f N_c \, I_1 - 2N_f N_c \, N^{\mathrm{P/S}} \, \mathrm{Re}[I_2] \tag{A.22}$$

$$\mathrm{Im}\,\Pi^{\mathrm{P/S}} = -2N_f N_c \, N^{\mathrm{P/S}} \, \mathrm{Im}[I_2] \tag{A.23}$$

The real part of I_2 involves the principal value of the momentum space. Here we have shifted the integration variable $\vec{p}$ by $\vec{q}/2$ to obtain a symmetric cutoff behaviour. For the imaginary part this shift is not needed as the imaginary part is finite and therefore is not subject to regularisation.[2] The evaluation of the imaginary part

---

[1]Note that we have defined the Integrals I_1 and I_2 without the prefactor i as done in Ref. [H$^+$07]. Additionally we have implemented a mixed cutoff scheme, regularising only divergent pieces, such that the Stefan-Boltzmann limit for the pressure at asymtotically high temperatures is reached.

[2]The regularisation however destroys the analytic structure of the polarisation function Π. One way to connect real and imaginary parts of Π is to use a Hilbert transformation where the integral over ω is regularised by a sharp cutoff at $\omega^2 = 4\Lambda^2 + 4M^2$ [HK94].

requires the following change of variables:

$$\left(p^2 \mathrm{d}p,\ \mathrm{d}\cos\theta\right) = \left(E_p \mathrm{d}E_p,\ \tfrac{1}{|\vec{q}|}\mathrm{d}\left[\vec{p}\cdot\vec{q}\right]\right) = \left(E_p \mathrm{d}E_p,\ \tfrac{1}{2}|\vec{q}|\,\mathrm{d}\left[E_{p-q}^2 - E_p^2 - q^2\right]\right)$$

$$= \frac{2E_p E_{p-q}}{|\vec{q}|}\left(\mathrm{d}\left[\tfrac{1}{2}\left(E_p + E_{p-q}\right)\right],\ \mathrm{d}\left[\tfrac{1}{2}\left(E_{p-q} - E_p\right)\right]\right)\ . \quad \text{(A.24)}$$

Cauchy's integral theorem

$$\frac{1}{x - x_0 \pm i\varepsilon} = \mp\delta(x - x_0) + \mathcal{P}\frac{1}{x - x_0} \quad\quad \text{(A.25)}$$

is then used where the sign in front of the Feynman ε is always given by the sign of ω leading to an integral that can be given in closed form. Of course, it is crucial to keep track of the limits of integration and the question whether the Dirac deltas do lie inside these limits. For fermions that do not propagate in a Polyakov loop background field we arrive at the following form of the imaginary part of I_2, where we have Wick-rotated back from Euclidean space to Minkowski space substituting $i\omega \to \omega = q_0$

$$\operatorname{Im} I_2 = -\frac{1}{16\pi\,|\vec{q}|}\left(\Theta(s - 4m^2)\left[\Theta(\omega)J_{\text{pair}}^+ + \Theta(-\omega)J_{\text{pair}}^-\right] + \Theta(-s)J_{\text{Landau}}\right) \quad \text{(A.26)}$$

$$J_{\text{pair}}^{\pm} = T\ln\left(\frac{\left[1 - f^{\pm}(E_-)\right]f^{\mp}(E_-)}{\left[1 - f^{\pm}(E_+)\right]f^{\mp}(E_+)}\right)$$

$$J_{\text{Landau}} = T\ln\left(\frac{f^+(E_-)f^-(E_-)}{f^+(-E_+)f^-(-E_+)}\right) = 2\omega + T\ln\left(\frac{f^+(-E_-)f^-(-E_-)}{f^+(E_+)f^-(E_+)}\right)\ .$$

We have used the definitions $E_{\pm} = \frac{\omega}{2} \pm \frac{q}{2}\sqrt{1 - \frac{4m^2}{s}}$ with $s = \omega^2 - q^2$. Note that due to the kinematic ranges the arguments of the Fermi-Dirac distribution functions $f^{\pm}$ in Eq. (A.26) are always positive except for the first expression of the definition of the Landau term J_{Landau}.

In the case of fermions propagating in a Polyakov loop background field the expression for $\operatorname{Im} I_2$ becomes:

$$\operatorname{Im} I_2 = -\frac{1}{16\pi\,|\vec{q}|}\left(\Theta(s - 4m^2)\left[\Theta(\omega)J_{\text{pair}}^+ + \Theta(-\omega)J_{\text{pair}}^-\right] + \Theta(-s)J_{\text{Landau}}\right) \quad \text{(A.27)}$$

$$J_{\text{pair}}^{\pm} = \frac{T}{3}\ln\left(\frac{\tilde{z}_{\Phi}^{\mp}(E_+)\tilde{z}_{\Phi}^{\mp}(-E_+)}{\tilde{z}_{\Phi}^{\mp}(E_-)\tilde{z}_{\Phi}^{\mp}(-E_-)}\right) \qquad J_{\text{Landau}} = \frac{T}{3}\ln\left(\frac{\tilde{z}_{\Phi}^+(E_+)\tilde{z}_{\Phi}^-(E_+)}{\tilde{z}_{\Phi}^+(-E_-)\tilde{z}_{\Phi}^-(-E_-)}\right)$$

$$\text{with}\quad \tilde{z}_{\Phi}^{\pm}(E) = 1 + 3\Phi^* e^{-\frac{E\mp\mu}{T}} + 3\Phi e^{-2\frac{E\mp\mu}{T}} + e^{-3\frac{E\mp\mu}{T}}$$

$$\text{and}\quad z_{\Phi}^{\pm} = \ln[\tilde{z}_{\Phi}^{\pm}] = \operatorname{tr_c}\left[\ln\left(1 + L^{\dagger}e^{-\frac{E\mp\mu}{T}}\right)\right]\ .$$

In a completely deconfined setting where all fields only incorporate trivial colour structures (proportional to unity) Eq. (A.27) translates into Eq. (A.26).

Appendix B

Derivation of corrections to the mean field approximation

This appendix displays some technical details concerning the treatment of fluctuation corrections beyond mean field approximation in the PNJL model (cf. Sec. 2.4.3).

In the following we denote by $\theta = (\theta_i)$ a set of fields which operate as bosonic degrees of freedom in the effective action $\mathcal{S}_{\text{bos}}$. Furthermore, let $\theta_0 = (\langle \sigma \rangle_0, \langle \Delta \rangle_0, \langle \phi_3 \rangle_0, \langle \phi_8 \rangle_0)$ be the set of mean field (expectation) values of these quantities, and introduce deviations from the mean fields by $\xi = (\xi_i) = \theta - \theta_0$.

A frequently used procedure that we follow here, is to expand the effective action in powers of ξ around a properly chosen mean field configuration. The gaussian part of such an expansion of the path integral can be handled analytically. In Sec. 2.4.3 the mean field approximation has been defined such that the (formally) complex action $\mathcal{S}_{\text{bos}}$ produces, to this leading order, a real-valued thermodynamical potential (or pressure), $\Omega_{\text{MF}} = \text{Re}[\Omega_0]$, subject to the mean field equations (2.21). The expansion of $\mathcal{S}_{\text{bos}}$ is then of the generic form

$$\mathcal{S}_{\text{bos}} = \frac{V}{T}\left(\Omega_{\text{MF}} + \omega^{(1)} \cdot \xi + \frac{1}{2}\xi \cdot \omega^{(2)} \cdot \xi \cdots \right), \tag{B.1}$$

where we have introduced the notations $a \cdot b = \sum_i a_i b_i$ and $a \cdot A \cdot b = \sum_{ij} a_i A_{ij} b_j$, with summations extending over all bosonic degrees of freedom. The expansion (B.1) is performed such that the path integral is optimally approximated. This is achieved when the perturbative terms in the expansion of the action are maximally suppressed. With the thermodynamic weight $e^{-\mathcal{S}} \in \mathbb{C}$ this approximation is optimal near the maximum of $\left|e^{-\mathcal{S}}\right|$. The equations to determine θ_0 are the mean field equations (2.21) (also used in [RRW07b]).

Given the expansion (B.1) in terms of the ξ fields, thermal expectation values incorporate fluctuations around the mean field configuration $\theta_{\text{MF}} \equiv \theta_0$. We refer to these corrections as fluctuations even if the fields themselves (such as the Polyakov loop field variables ϕ_3 and ϕ_8) are constant in space and time.

A perturbative approach is now used to calculate corrections to the mean field solutions. The action $\mathcal{S}_{\text{bos}}$ is split into "large" and "small" parts, $\mathcal{S}_{\text{bos}} = \mathcal{S}_0 + \mathcal{S}_{\text{I}}$, as follows: the "large" part $\mathcal{S}_0$ incorporates the leading mean field terms plus the

additional gaussian part of $O(\xi^2)$ in Eq. (B.1):

$$\mathcal{S}_0 = \frac{V}{T}\left(\mathrm{Re}[\Omega_0] + \frac{1}{2}\xi \cdot \omega^{(2)} \cdot \xi\right) , \tag{B.2}$$

while $\mathcal{S}_\mathrm{I}$ deals with the remaining pieces, in particular with the non-vanishing $\mathrm{Im}[\Omega_0]$. The leading correction of this sort is the term $\delta\mathcal{S}_\mathrm{I} = \frac{V}{T}\omega^{(1)}\cdot\xi$. In the present context we truncate Eq. (B.1) as it stands and keep only this term in $\mathcal{S}_\mathrm{I}$, for the moment.

The thermal expectation values of a given quantity $f(\xi)$ is proportional to

$$\int \mathcal{D}\xi\, f(\xi)\, e^{-\mathcal{S}_\mathrm{bos}} = \int \mathcal{D}\xi\, f(\xi)\, e^{-\mathcal{S}_0}\, e^{-\mathcal{S}_\mathrm{I}} , \tag{B.3}$$

where, for fields constant in space-time, the path integral reduces to

$$\int \mathrm{d}\xi\, f(\xi)\, e^{-\mathcal{S}_0(\xi)}\, e^{-\mathcal{S}_\mathrm{I}(\xi)} = \int \mathrm{d}\xi\, f(\xi)\, e^{-\mathcal{S}_0(\xi)}\, e^{-ik\cdot\xi} , \tag{B.4}$$

with

$$k = \frac{V}{iT}\omega^{(1)} = \frac{V}{T}\,\mathrm{Im}\,\omega^{(1)} . \tag{B.5}$$

A perturbative expansion of $f(\xi)$ about $\xi = 0$ (i. e. about $\theta = \theta_\mathrm{MF}$) in powers of ξ involves integrals of the form

$$\int \mathrm{d}\xi\, \xi^n\, e^{-\mathcal{S}_0(\xi)}\, e^{-ik\cdot\xi} = (i\partial_k)^n\, \mathcal{Z}_0(k)\big|_{k=\frac{V}{T}\mathrm{Im}\,\omega^{(1)}} , \tag{B.6}$$

where we have introduced the generating function $\mathcal{Z}_0(k) = \int \mathrm{d}\xi\, e^{-\mathcal{S}_0(\xi)}\, e^{-ik\cdot\xi}$. Each power of $i\partial_k$ evidently produces a factor $\frac{T}{V}$. At the same time, performing this derivative explicitly on $\mathcal{Z}_0(k)$, with $\mathcal{S}_0(\xi)$ specified in Eq. (B.2), produces a factor

$$\delta = i\frac{T}{V}\left[\omega^{(2)}\right]^{-1}\cdot k = \left[\omega^{(2)}\right]^{-1}\cdot\omega^{(1)} , \tag{B.7}$$

which is independent of $\frac{T}{V}$.

Hence there are two small quantities at hand to establish a perturbative expansion: $\frac{T}{V}$ and δ. The smallness of $\frac{T}{V}$ is given here as we are interested in the thermodynamic limit. The size of δ, however, is controlled by the action itself. Whether the expansion in δ is justified or not depends on the model and must be examined accordingly. The explicit calculations presented in the main body of this work shows that in the present version of the PNJL model the expansion in δ is indeed a good approximation.

We are now in a position to write down the thermal expectation value of a generic function f as an expansion in powers of $\frac{T}{V}$ and δ. We proceed here with establishing Feynman diagrams for this perturbative approach. We write generically

$$Z = \frac{1}{\mathcal{N}}\int \mathcal{D}\xi\, e^{-\mathcal{S}_\mathrm{bos}} = \frac{1}{\mathcal{N}}\int \mathcal{D}\xi\, \sum_{l=0}^{\infty}\frac{1}{l!}\left(-\mathcal{S}_\mathrm{I}\right)^l\, e^{-\mathcal{S}_0} . \tag{B.8}$$

If corrections to the partition function of the PNJL model are to be calculated, the $\mathcal{S}_0$ part of the action only comprises zeroth and second order terms, while the "small" part $\mathcal{S}_\mathrm{I}$ is identified with all other orders. The first order term acts as a source term. We establish the following Feynman rules:

$$
\begin{aligned}
j \;{\times}{-} &= -\frac{\partial \mathcal{S}_\mathrm{bos}}{\partial \xi_j}
& j \;{\longrightarrow}\; k &= + \left[\frac{\partial^2 \mathcal{S}_\mathrm{bos}}{\partial \xi_j \partial \xi_k} \right]^{-1} \\[2mm]
\overset{k}{\underset{j}{\diagdown}}{-}\, l &= -\frac{\partial^3 \mathcal{S}_\mathrm{bos}}{\partial \xi_j \partial \xi_k \partial \xi_l}
& \overset{l}{\underset{j\,\ \ \ k}{\big|}} m &= -\frac{\partial^4 \mathcal{S}_\mathrm{bos}}{\partial \xi_j \partial \xi_k \partial \xi_l \partial \xi_m} \qquad \text{(B.9)}\\
\vdots & & \vdots &
\end{aligned}
$$

In perturbation theory it can be shown that only connected diagrams contribute to the partition function, i. e.

$$
Z_\mathrm{I} = \langle e^{-\mathcal{S}_\mathrm{I}} \rangle_0 = \sum_{l=0}^{\infty} \frac{1}{l!} \langle (-\mathcal{S}_\mathrm{I})^l \rangle_0 = \exp\left\{ \sum_{n=1}^{\infty} \frac{1}{n!} \langle (-\mathcal{S}_\mathrm{I})^n \rangle_{0c} \right\}, \qquad \text{(B.10)}
$$

where $\langle \cdots \rangle_0$ denotes the expectation value with respect to the unperturbed action, and $\langle \cdots \rangle_{0c}$ is the expectation value of the connected diagrams with respect to this unperturbed action. Note that here the corrections depicted by the Feynman diagrams are corrections to the negative action, $-\mathcal{S}$, as the partition function was defined by $Z = e^{-\mathcal{S}_\mathrm{eff.}}$. The corrections therefore need to be subtracted from the mean field result of the action $\mathcal{S}_\mathrm{MF}$.

For the thermal expectation values of f we write

$$
\langle f \rangle = \frac{\langle f\, e^{-\mathcal{S}_\mathrm{I}} \rangle_0}{\langle e^{-\mathcal{S}_\mathrm{I}} \rangle_0} = \frac{1}{\langle e^{-\mathcal{S}_\mathrm{I}} \rangle_0} \sum_{l=0}^{\infty} \frac{1}{l!} \langle f\, (-\mathcal{S}_\mathrm{I})^l \rangle_0 . \qquad \text{(B.11)}
$$

Here each term under the sum can be written in terms of connected expectation values

$$
\langle f\, (-\mathcal{S}_\mathrm{I})^l \rangle_0 = \sum_{a_1, a_2 \cdots,\, a_n,\, m=0}^{\infty} \frac{l!}{a_1! a_2! (2!)^{a_2} \cdots (a_n!)(n!)^{a_n} m!} \langle (-\mathcal{S}_\mathrm{I}) \rangle_{0c}^{a_1} \langle (-\mathcal{S}_\mathrm{I})^2 \rangle_{0c}^{a_2} \cdots
$$
$$
\cdots \langle f\, (-\mathcal{S}_\mathrm{I})^m \rangle_{0c}\, \delta_{\nu, l} \ , \quad \text{(B.12)}
$$

where $\nu = a_1 + 2a_2 + \cdots + na_n + m$. Substituting back in Eq. (B.11) gives

$$
\langle f\, e^{-\mathcal{S}_\mathrm{I}} \rangle_0 = \exp\left\{ \sum_{n=1}^{\infty} \frac{1}{n!} \langle (-\mathcal{S}_\mathrm{I})^n \rangle_{0c} \right\} \times \sum_{m=0}^{\infty} \frac{1}{m!} \langle f\, (-\mathcal{S}_\mathrm{I})^m \rangle_{0c} . \qquad \text{(B.13)}
$$

Using Eq. (B.10) we find the final result

$$
\langle f \rangle = \frac{\langle f\, e^{-\mathcal{S}_\mathrm{I}} \rangle_0}{\langle e^{-\mathcal{S}_\mathrm{I}} \rangle_0} = \sum_{n=0}^{\infty} \frac{1}{n!} \langle f\, (-\mathcal{S}_\mathrm{I})^n \rangle_{0c} . \qquad \text{(B.14)}
$$

In terms of Feynman diagrams Eq. (B.14) can be translated into all those connected diagrams that contain exactly one insertion coming from the function f. The Feynman rules for the insertions of f are

$$
\begin{array}{ll}
j \;\circ\!\!-\!\!- \;=\; \dfrac{\partial f}{\partial \xi_j} & \qquad \underset{j}{\!-\!\!-\!\!\circ\!\!-\!\!-}\underset{k}{} \;=\; \dfrac{\partial^2 f}{\partial \xi_j \partial \xi_k}
\end{array}
$$

$$
\begin{array}{ll}
\overset{k}{\underset{j}{\diagdown\!\!\circ\!\!-\!\! l}} \;=\; \dfrac{\partial^3 f}{\partial \xi_j \partial \xi_k \partial \xi_l} & \qquad \underset{j}{\overset{l}{\vert}}\!\!\circ\!\!\underset{k}{\vert}\; m \;=\; \dfrac{\partial^4 f}{\partial \xi_j \partial \xi_k \partial \xi_l \partial \xi_m}
\end{array}
\tag{B.15}
$$

$$
\vdots \qquad\qquad\qquad\qquad \vdots
$$

What is needed to use these rules systematically is a scheme that orders all possible diagrams according to their importance in powers of the small parameters $\frac{T}{V}$ and δ. The lowest order corrections in $\frac{T}{V}$ and δ are shown in Table B.1.

The formalism allows to determine susceptibilities involving a quantity g, $\chi_g = [V(\langle g^2 \rangle - \langle g \rangle^2)]^{1/2}$. All that needs to be done is to apply the previously developed formalism to the function g^2. In Table B.1 the Feynman rules and multiplicity factors are written down for the evaluation of $\langle f \rangle$. In a second step f is replaced by g^2. In this step the product rule of differentiation has to be applied producing additional prefactors. In this procedure it will happen that vertices of f with $m = 2, 3, \ldots$ or more legs will split into two vertices with $m_1 + m_2 = m$ legs. The lowest orders of the expression are shown in Table B.2. The contributions of order $\left(\frac{T}{V}\right)^0$ cancel. In this framework susceptibilities scale with $V^{\frac{1}{2}}$ as expected. Additionally, it becomes obvious from Table B.2 that there are no mean field contributions to susceptibilities in the sense that $\langle (g - \langle g \rangle_{\mathrm{MF}})^2 \rangle_{\mathrm{MF}} = \langle g^2 \rangle_{\mathrm{MF}} - \langle g \rangle_{\mathrm{MF}}^2 = g_{\mathrm{MF}}^2 - g_{\mathrm{MF}}^2 = 0$. In the framework of mean field calculations, susceptibilities are usually evaluated by inverting the second derivative of the mean field action with respect to the fields. This is seen in the present framework as well: the entry for $\alpha = 1$ and $\beta = 0$ in Table B.2 produces exactly this expression.
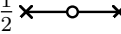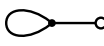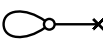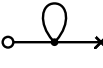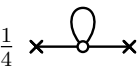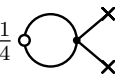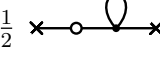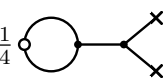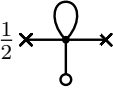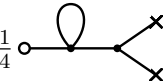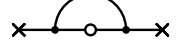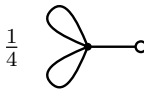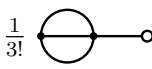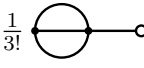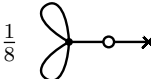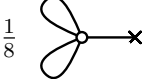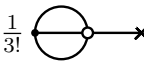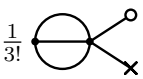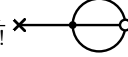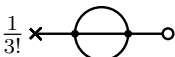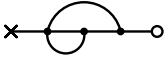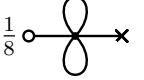
Table B.1: The Feynman graphs contributing to $\langle f \rangle$, ordered in $\left(\frac{T}{V}\right)^{\alpha}$ and δ^{β} with multiplicity factors.
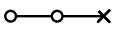
	$\beta = 0$	$\beta = 1$	
$\alpha = 0$	—	—	
$\alpha = 1$	$\frac{1}{2} \times 2$ ○—○	$\frac{1}{2} \times 4$ ○—○—✕	$+ \quad \frac{1}{2} \times 2$ ⟨—✕

Table B.2: The lowest order Feynman graphs contributing to χ_g^2. The vertices depicted as a circle are now the contributions of g, defined analogously to the contributions of f in Eq. (B.15). The prefactors are the product of the multiplicity factors of the original Feynman graphs and the factors arising from the differentiation.

Appendix C

Conventions

This appendix shall facilitate the combined study of this present work and other publications by summarizing some notations and conventions as they are used in the current work.

Traces

- The separate trace over *Dirac*, *color* or *flavor* indices is denoted explicitly as $\text{tr}_{\text{Dirac}} = \text{tr}_{\text{d}}$, tr_{c} or tr_{f}.

- The trace over *Dirac*, *color* and *flavor* indices is denoted as $\text{Tr} = \text{tr}_{\text{d}}\text{tr}_{\text{c}}\text{tr}_{\text{f}}$

- In analogy the determinant over *Dirac*, *color* or *flavor* indices is denoted Det (in contrast to det)

- A functional trace with an additional trace over *Dirac*, *color* and *flavor* indices is denoted as

$$\widetilde{\text{Tr}}\,\hat{\mathcal{O}} = \int \frac{\mathrm{d}^4 p}{(2\pi)^4} \text{Tr}\,\langle p|\hat{\mathcal{O}}|p\rangle = \int \mathrm{d}^4 x\,\text{Tr}\,\langle x|\hat{\mathcal{O}}|x\rangle$$

Polyakov loops

- The Polyakov loop L is defined by Eq. (1.29) as an operator in colour space.

- The normalized trace of the Polyakov loop L is a scalar quantity and defined by $\Phi = \frac{1}{N_{\text{c}}}\text{tr}_{\text{c}}\,[L]$. Both normalized trace Φ and the Polyakov loop L itself are referred to as the Polyakov loop, as it is usually done in the literature.

- The thermal expectation value of real and imaginary parts of the traced Polyakov loop Φ is denoted as $\Phi^+ = \langle\text{Re}\,\Phi\rangle = \frac{1}{2}\langle\Phi + \Phi^*\rangle$ and $\Phi^- = -\langle\text{Im}\,\Phi\rangle = \frac{1}{2}\langle\Phi^* - \Phi\rangle$.

Notations of $\mathrm{SU}(N)$ structures

- The generators of $\mathrm{SU}(N)$ are denoted τ_a with $a = 1, \ldots, N^2 - 1$. In the special case $\mathrm{SU}(3)_\mathrm{c}$ the generators are sometimes denoted λ_a.

- The generators are normalized such that $\mathrm{tr}\,[\tau_a \tau_b] = 2\delta_{ab}$.

- The $N \times N$ unity matrix is denoted $\mathbb{1}$.

- The generators are supplemented by $\tau_0 = \sqrt{2/N}\,\mathbb{1}$.

- In $\mathrm{SU}(2)$ we define the ladder generators $\tau^\pm = (\tau^1 \pm \tau^2)/\sqrt{2}$

- In case of the colour group where $N = N_\mathrm{c} = 3$ the Gell-Mann matrices λ_i are chosen as an explicit representation of the $SU(3)_\mathrm{c}$ generators.

Classification of the order of phase transitions

- An nth order phase transition appears once an nth derivative of the thermodynamic potential (or the partition function) with respect to some thermodynamic quantity is discontinuous.

- A crossover transition is not a phase transition in the strict sense. There is no discontinuous behaviour of the thermodynamic potential what so ever. If there exists a symmetry that corresponds to the crossover transition, it is broken on both sides of the transition line.

Isovector densities and chemical potentials

$$\mu = \frac{\mu_\mathrm{u} + \mu_\mathrm{d}}{2} = \frac{\mu_\mathrm{B}}{3} \qquad \mu_\mathrm{I} = \frac{\mu_\mathrm{u} - \mu_\mathrm{d}}{2} \tag{C.1}$$

$$\frac{\partial}{\partial \mu_Q} = \frac{2}{3}\frac{\partial}{\partial \mu_\mathrm{u}} - \frac{1}{3}\frac{\partial}{\partial \mu_\mathrm{d}} = \frac{1}{6}\frac{\partial}{\partial \mu} + \frac{1}{2}\frac{\partial}{\partial \mu_\mathrm{I}} \tag{C.2}$$

$$n_\mathrm{q} = n_\mathrm{u} + n_\mathrm{d} \tag{C.3}$$

Chiral condensates

$$\langle \bar{\psi}\psi \rangle = \frac{\sigma}{G} = \frac{\sigma_u + \sigma_d}{G} = \langle \bar{u}u \rangle + \langle \bar{d}d \rangle \tag{C.4}$$

List of Symbols

p	: pressure	μ	: chemical potential
Ω	: thermodynamic potential density	μ_{I}	: isovector chemical potential
ε	: energy density	μ_{B}	: baryon chemical potential
s	: entropy density	$\mu_{\mathrm{u/d}}$	: up/down quark chemical pot.
n_{B}	: baryon number density	$\mathcal{L}$	: Lagrangian density
n_{I}	: isovector quark number density	$\mathcal{H}$	: Hamilton denity
n_{q}	: quark number density	$\mathcal{Z}$	: partition function
$n_{\mathrm{u/d}}$	: up/down quark number density	$\mathcal{S}$	: action
χ	: susceptibility	ψ	: fermion field
χ_{ud}	: up/down quark number susc.	$\mathcal{C}$	: charge conjugation operator
v_{s}	: speed of sound	Γ	: generic operator structure
c_n	: expansion coefficient of p/T^4	γ_x	: Dirac structures
$R_{4,2}$	: cumulant ratio	$\tilde{S}$	: quark propagator
T	: temperature	$f^{\pm}$	: Fermi Dirac distrubution
β	: inverse temperature	$f_{\Phi}^{\pm}$	: modified FD distrubution
m_{π}	: pion mass	N	: pionic mean field
f_{π}	: pion decay constant	Δ	: diquark mean field
$g_{\pi qq}$	: pion to quark coupling const.	$A_{3/8}^4$	: temporal gauge background field
M, m	: constituent quark mass	$\phi_{3/8}^4$	: Polyakov loop parametrizations
m_0	: current quark mass	$\langle\cdots\rangle$	: (thermal) expectation value
Φ	: Polyakov loop	G	: NJL coupling strength
ϕ	: generic field	H	: NJL diquark coupling strength
σ	: sigma field	N_{c}	: number of colours
π	: pion field	N_{f}	: number of flavours
ξ	: in Sec. B: shifted boson field	ξ	: in Sec. 3.7: generic boson field
$|0\rangle$	: Wigner-Weyl vacuum state	$|\Omega\rangle$	: Nambu-Goldstone vacuum state

List of Figures

List of Tables

Index

Q

R

S

T

W

Bibliography

[A⁺05]   C. R. Allton et al. *Thermodynamics of two flavor QCD to sixth order in quark chemical potential.* Phys. Rev. D71:054508, 2005.

[A⁺07a]   B. I. Abelev et al. *Mass, quark-number, and $s_{NN}^{1/2}$ dependence of the second and fourth flow harmonics in ultra-relativistic nucleus nucleus collisions.* Phys. Rev. C75:054906, 2007.

[A⁺07b]   A. Adare et al. *Scaling properties of azimuthal anisotropy in Au + Au and Cu + Cu collisions at $s_{NN}^{1/2} = 200\,\mathrm{GeV}$.* Phys. Rev. Lett. 98:162301, 2007.

[A⁺08]   H. Abuki et al. *Electrical neutrality and pion modes in the two flavor PNJL model.* Phys. Rev. D78:014002, 2008.

[AAG⁺08]   H. Abuki, R. Anglani, R. Gatto, G. Nardulli, and M. Ruggieri. *Chiral crossover, deconfinement and quarkyonic matter within a Nambu-Jona Lasinio model with the Polyakov loop.* Phys. Rev. D78:034034, 2008.

[ABMS06]   A. Andronic, P. Braun-Munzinger, and J. Stachel. *Hadron production in central nucleus nucleus collisions at chemical freeze-out.* Nucl. Phys. A772:167–199, 2006.

[AEF⁺06]   Y. Aoki, G. Endrodi, Z. Fodor, S. D. Katz, and K. K. Szabo. *The order of the quantum chromodynamics transition predicted by the Standard Model of particle physics.* Nature 443:675–678, 2006.

[AFKS06a]   Y. Aoki, Z. Fodor, S. D. Katz, and K. K. Szabo. *The equation of state in lattice QCD: With physical quark masses towards the continuum limit.* JHEP 01:089, 2006.

[AFKS06b]   Y. Aoki, Z. Fodor, S. D. Katz, and K. K. Szabo. *The QCD transition temperature: Results with physical masses in the continuum limit.* Phys. Lett. B643:46–54, 2006.

[AL73]   E. S. Abers and B. W. Lee. *Gauge theories.* Phys. Rept. 9:1–141, 1973.

[Alf03]   M. G. Alford. *QCD at high density / temperature.* Nucl. Phys. Proc. Suppl. 117:65–82, 2003.

[ARW99]   M. G. Alford, K. Rajagopal, and F. Wilczek. *Color-flavor locking and chiral symmetry breaking in high density QCD.* Nucl. Phys. B537:443–458, 1999.

[B+90]   F. R. Brown et al. *On the existence of a phase transition for QCD with three light quarks.* Phys. Rev. Lett. 65:2491–2494, 1990.

[B+96]   G. Boyd et al. *Thermodynamics of SU(3) lattice gauge theory.* Nucl. Phys. B469:419–444, 1996.

[B+98]   S. A. Bass et al. *Microscopic models for ultrarelativistic heavy-ion collisions.* Prog. Part. Nucl. Phys. 41:255–369, 1998.

[B+99]   M. Bleicher et al. *Relativistic hadron hadron collisions in the ultra-relativistic quantum molecular dynamics model.* J. Phys. G25:1859–1896, 1999.

[BBRV08]   D. Blaschke, M. Buballa, A. E. Radzhabov, and M. K. Volkov. *Effects of mesonic correlations in the QCD phase transition.* Yad. Fiz. 71:2012–2018, 2008.

[BBV98]   G. S. Bali, N. Brambilla, and A. Vairo. *A lattice determination of QCD field strength correlators.* Phys. Lett. B421:265–272, 1998.

[BH99]   G. Baym and H. Heiselberg. *Event-by-event fluctuations in ultrarelativistic heavy-ion collisions.* Phys. Lett. B469:7–11, 1999.

[BJK00]   M. Bleicher, S. Jeon, and V. Koch. *Event-by-event fluctuations of the charged particle ratio from non-equilibrium transport theory.* Phys. Rev. C62:061902, 2000.

[BK08]   M. Bluhm and B. Kämpfer. *Flavor diagonal and off-diagonal susceptibilities in a quasiparticle model of the quark-gluon plasma.* Phys. Rev. D77:114016, 2008.

[BMRS04]   P. Braun-Munzinger, K. Redlich, and J. Stachel. Particle production in heavy ion collisions. In R. C. Hwa and X.-N. Wang, editors, *Quark-Gluon Plasma*, page 491ff, 2004.

[Bub05]   M. Buballa. *NJL model analysis of quark matter at large density.* Phys. Rept. 407:205–376, 2005.

[C+06]   M. Cheng et al. *The transition temperature in QCD.* Phys. Rev. D74:054507, 2006.

[C+08]   M. Cheng et al. *The QCD Equation of State with almost physical quark masses.* Phys. Rev. D77:014511, 2008.

[CJJ+74]   A. Chodos, R. L. Jaffe, K. Johnson, Charles B. Thorn, and V. F. Weisskopf. *A new extended model of hadrons.* Phys. Rev. D9:3471–3495, 1974.

[CJJT74] A. Chodos, R. L. Jaffe, K. Johnson, and Charles B. Thorn. *Baryon structure in the bag theory.* Phys. Rev. D10:2599, 1974.

[CRS09] P. Castorina, K. Redlich, and H. Satz. *The Phase Diagram of Hadronic Matter.* Eur. Phys. J. C59:67–73, 2009.

[DDGM03] M. D'Elia, A. Di Giacomo, and E. Meggiolaro. *Gauge-invariant field-strength correlators in pure Yang- Mills and full QCD at finite temperature.* Phys. Rev. D67:114504, 2003.

[dFP08] Philippe de Forcrand and Owe Philipsen. *The chiral critical point of $N_{\mathrm{f}} = 3$ QCD at finite density to the order $(\mu/T)^4$.* JHEP 11:012, 2008.

[DJJK75] T. A. DeGrand, R. L. Jaffe, K. Johnson, and J. E. Kiskis. *Masses and other parameters of the light hadrons.* Phys. Rev. D12:2060, 1975.

[DPZ05] A. Dumitru, R. D. Pisarski, and D. Zschiesche. *Dense quarks, and the fermion sign problem, in a SU(N) matrix model.* Phys. Rev. D72:065008, 2005.

[Dör06] M. Döring. *Screening of heavy quarks and hadrons at finite temperature and density.* 2006. Ph. D. thesis, Universität Bielefeld.

[Eji08] Shinji Ejiri. *Canonical partition function and finite density phase transition in lattice QCD.* Phys. Rev. D78:074507, 2008.

[EKR06] S. Ejiri, F. Karsch, and K. Redlich. *Hadronic fluctuations at the QCD phase transition.* Phys. Lett. B633:275–282, 2006.

[FMT⁺98] C. Ford, U. G. Mitreuter, T. Tok, A. Wipf, and J. M. Pawlowski. *Monopoles, Polyakov loops, and gauge fixing on the torus.* Annals Phys. 269:26–50, 1998.

[Fuk04] K. Fukushima. *Chiral effective model with the Polyakov loop.* Phys. Lett. B591:277–284, 2004.

[Fuk08a] K. Fukushima. *Critical surface in hot and dense QCD with the vector interaction.* arXiv:0809.3080 [hep-ph], 2008.

[Fuk08b] K. Fukushima. *Phase diagrams in the three-flavor Nambu–Jona-Lasinio model with the Polyakov loop.* Phys. Rev. D77:114028, 2008.

[GDGS06] D. Gomez Dumm, A. G. Grunfeld, and N. N. Scoccola. *On covariant nonlocal chiral quark models with separable interactions.* Phys. Rev. D74:054026, 2006.

[GG08] R. V. Gavai and S. Gupta. *QCD at finite chemical potential with six time slices.* arXiv:0806.2233 [hep-lat], 2008.

[GMMR06] S. K. Ghosh, T. K. Mukherjee, M. G. Mustafa, and R. Ray. *Suscepti-bilities and speed of sound from PNJL model.* Phys. Rev. D73:114007, 2006.

[GMOR68] M. Gell-Mann, R. J. Oakes, and B. Renner. *Behavior of current diver-gences under $SU(3) \times SU(3)$.* Phys. Rev. 175:2195–2199, 1968.

[GO85] A. Gocksch and M. Ogilvie. *Finite temperature deconfinement and chiral symmetry restauration at strong coupling.* Phys. Rev. D31:877, 1985.

[H$^+$07] H. Hansen et al. *Mesonic correlation functions at finite temperature and density in the Nambu-Jona-Lasinio model with a Polyakov loop.* Phys. Rev. D75:065004, 2007.

[HF04] Y. Hatta and K. Fukushima. *Linking the chiral and deconfinement phase transitions.* Phys. Rev. D69:097502, 2004.

[HI03] Y. Hatta and T. Ikeda. *Universality, the QCD critical / tricritical point and the quark number susceptibility.* Phys. Rev. D67:014028, 2003.

[HJS$^+$98] A. M. Halasz, A. D. Jackson, R. E. Shrock, M. A. Stephanov, and J. J. M. Verbaarschot. *On the phase diagram of QCD.* Phys. Rev. D58:096007, 1998.

[HK84] T. Hatsuda and T. Kunihiro. *Possible critical phenomena associated with the chiral symmetry breaking.* Phys. Lett. B145:7–10, 1984.

[HK94] T. Hatsuda and T. Kunihiro. *QCD phenomenology based on a chiral effective Lagrangian.* Phys. Rept. 247:221–367, 1994.

[HKZV94] J. Hüfner, S. P. Klevansky, P. Zhuang, and H. Voss. *Thermodynamics of a quark plasma beyond the mean field: A generalized Beth-Uhlenbeck approach.* Annals Phys. 234:225–244, 1994.

[HRCW09] T. Hell, S. Rößner, M. Cristoforetti, and W. Weise. *Dynamics and ther-modynamics of a non-local PNJL model with running coupling.* Phys. Rev. D79:014022, 2009.

[HTYB06] T. Hatsuda, M. Tachibana, N. Yamamoto, and G. Baym. *New critical point induced by the axial anomaly in dense QCD.* Phys. Rev. Lett. 97:122001, 2006.

[Kar08] F. Karsch. *Equation of state and more from lattice regularized QCD.* J. Phys. G35:104096, 2008.

[KKPZ02] O. Kaczmarek, F. Karsch, P. Petreczky, and F. Zantow. *Heavy quark-antiquark free energy and the renormalized Polyakov loop.* Phys. Lett. B543:41–47, 2002.

[Kle92]   S. P. Klevansky. *The Nambu-Jona-Lasinio model of quantum chromo-dynamics.* Rev. Mod. Phys. 64:649–708, 1992.

[KLP00]   F. Karsch, E. Laermann, and A. Peikert. *The pressure in 2, 2+1 and 3 flavour QCD.* Phys. Lett. B478:447–455, 2000.

[KLVW90]   S. Klimt, M. Lutz, U. Vogl, and W. Weise. *Generalized SU(3) Nambu-Jona-Lasinio Model. Part. 1. Mesonic modes.* Nucl. Phys. A516:429–468, 1990.

[Koc08]   V. Koch. *Correlations and fluctuations: status and perspectives.* J. Phys. G35:104030, 2008.

[KZ05]   O. Kaczmarek and F. Zantow. *Static quark-antiquark interactions in zero and finite temperature QCD. I: Heavy quark free energies, running coupling and quarkonium binding.* Phys. Rev. D71:114510, 2005.

[LB]   M. Le Bellac. *Thermal field theory.* Cambridge, United Kingdom: Cambridge University Press (1996) 256 p.

[LH98]   P. Levai and U. W. Heinz. *Massive gluons and quarks and the equation of state obtained from SU(3) lattice QCD.* Phys. Rev. C57:1879–1890, 1998.

[Lom06]   M. P. Lombardo. *Lattice QCD at finite density: Imaginary chemical potential.* PoS CPOD2006:003, 2006.

[McL08]   L. McLerran. *Quarkyonic matter and the phase diagram of QCD.* arXiv:0808.1057 [hep-ph], 2008.

[MMR07]   S. Mukherjee, M. G. Mustafa, and R. Ray. *Thermodynamics of the PNJL model with nonzero baryon and isospin chemical potentials.* Phys. Rev. D75:094015, 2007.

[MO96]   P. N. Meisinger and M. C. Ogilvie. *Chiral symmetry restoration and Z_N symmetry.* Phys. Lett. B379:163–168, 1996.

[MOM04]   P. N. Meisinger, M. C. Ogilvie, and T. R. Miller. *Gluon quasiparticles and the Polyakov loop.* Phys. Lett. B585:149–154, 2004.

[NJL61a]   Y. Nambu and G. Jona-Lasinio. *Dynamical model of elementary particles based on an analogy with superconductivity. I.* Phys. Rev. 122:345–358, 1961.

[NJL61b]   Y. Nambu and G. Jona-Lasinio. *Dynamical model of elementary particles based on an analogy with superconductivity. II.* Phys. Rev. 124:246–254, 1961.

[PKS02]   A. Peshier, B. Kämpfer, and G. Soff. *From QCD lattice calculations to the equation of state of quark matter.* Phys. Rev. D66:094003, 2002.

[Pol78]   A. M. Polyakov. *Thermal properties of gauge fields and quark liberation.* Phys. Lett. B72:477–480, 1978.

[PS]   M. E. Peskin and D. V. Schroeder. *An introduction to quantum field theory.* Reading, USA: Addison-Wesley (1995) 842 p.

[PW84]   R. D. Pisarski and F. Wilczek. *Remarks on the chiral phase transition in chromodynamics.* Phys. Rev. D29:338–341, 1984.

[Raj99]   K. Rajagopal. *Mapping the QCD phase diagram.* Nucl. Phys. A661:150–161, 1999.

[RHRW08]   S. Rößner, T. Hell, C. Ratti, and W. Weise. *The chiral and deconfinement crossover transitions: PNJL model beyond mean field.* Nucl. Phys. A814:118–143, 2008.

[RR07]   P. Romatschke and U. Romatschke. *Viscosity information from relativistic nuclear collisions: How perfect is the fluid observed at RHIC?* Phys. Rev. Lett. 99:172301, 2007.

[RRTW07]   C. Ratti, S. Rößner, M. A. Thaler, and W. Weise. *Thermodynamics of the PNJL model.* Eur. Phys. J. C49:213–217, 2007.

[RRW07a]   C. Ratti, S. Rößner, and W. Weise. *Quark number susceptibilities: Lattice QCD versus PNJL model.* Phys. Lett. B649:57–60, 2007.

[RRW07b]   S. Rößner, C. Ratti, and W. Weise. *Polyakov loop, diquarks and the two-flavour phase diagram.* Phys. Rev. D75:034007, 2007.

[RTW06]   C. Ratti, M. A. Thaler, and W. Weise. *Phases of QCD: Lattice thermodynamics and a field theoretical model.* Phys. Rev. D73:014019, 2006.

[SFR07]   C. Sasaki, B. Friman, and K. Redlich. *Susceptibilities and the phase structure of a chiral model with Polyakov loops.* Phys. Rev. D75:074013, 2007.

[SFR08]   B. Stokic, B. Friman, and K. Redlich. *Kurtosis and compressibility near the chiral phase transition.* arXiv:0809.3129 [hep-ph], 2008.

[SH08]   H. Song and U. W. Heinz. *Multiplicity scaling in ideal and viscous hydrodynamics.* Phys. Rev. C78:024902, 2008.

[SPW07]   B.-J. Schäfer, J. M. Pawlowski, and J. Wambach. *The phase structure of the Polyakov–quark-meson model.* Phys. Rev. D76:074023, 2007.

[SRS99]   M. A. Stephanov, K. Rajagopal, and E. V. Shuryak. *Event-by-event fluctuations in heavy-ion collisions and the QCD critical point.* Phys. Rev. D60:114028, 1999.

[Ste04]   M. A. Stephanov. *QCD phase diagram and the critical point.* Prog. Theor. Phys. Suppl. 153:139–156, 2004.

[Ste06]   M. A. Stephanov. *QCD phase diagram: An overview.* PoS LAT2006:024, 2006.

[Sus79]   L. Susskind. *Lattice models of quark confinement at high temperature.* Phys. Rev. D20:2610–2618, 1979.

[Sve86]   B. Svetitsky. *Symmetry aspects of finite temperature confinement transitions.* Phys. Rept. 132:1–53, 1986.

[SW01]   R. A. Schneider and W. Weise. *On the quasiparticle description of lattice QCD thermodynamics.* Phys. Rev. C64:055201, 2001.

[SY82]   B. Svetitsky and L. G. Yaffe. *Critical behavior at finite temperature confinement transitions.* Nucl. Phys. B210:423, 1982.

[tH81]   G. 't Hooft. *Topology of the gauge condition and new confinement phases in nonabelian gauge theories.* Nucl. Phys. B190:455, 1981.

[TSW04]   M. A. Thaler, R. A. Schneider, and W. Weise. *Quasiparticle description of hot QCD at finite quark chemical potential.* Phys. Rev. C69:035210, 2004.

[TW]   A. W. Thomas and Wolfram Weise. *The structure of the nucleon.* Berlin, Germany: Wiley-VCH (2001) 389 p.

[VLKW90]   U. Vogl, M. Lutz, S. Klimt, and W. Weise. *Generalized SU(3) Nambu-Jona-Lasinio Model. Part 2. From current to constituent quarks.* Nucl. Phys. A516:469–495, 1990.

[Vol84]   M. K. Volkov. *Meson Lagrangians in a superconductor quark model.* Annals Phys. 157:282–303, 1984.

[VW91]   U. Vogl and W. Weise. *The Nambu and Jona Lasinio model: Its implications for hadrons and nuclei.* Prog. Part. Nucl. Phys. 27:195–272, 1991.

[Wei81]   N. Weiss. *The effective potential for the order parameter of gauge theories at finite temperature.* Phys. Rev. D24:475, 1981.

[Wei82]   N. Weiss. *The Wilson line in finite temperature gauge theories.* Phys. Rev. D25:2667, 1982.

[Wes08]   G. D. Westfall. *Experimental results for fluctuations and correlations as a signature of qcd phase transitions in heavy-ion collisions.* J. Phys. G36:104031, 2008.

[ZL07]   Zhao Zhang and Yu-Xin Liu. *Coupling of pion condensate, chiral condensate and Polyakov loop in an extended NJL model.* Phys. Rev. C75:064910, 2007.

Acknowledgements